CRANFIELD UNIVERSITY

Liang Shao

GNSS PERFORMANCE MODELLING FOR HIGH INTEGRITY AIRCRAFT APPLICATIONS

School of Engineering
Department of Aerospace Engineering

Individual Research Project MSc Thesis
Academic Year: 2011 - 2012

Supervisor: Dr Roberto Sabatini
May 2012

CRANFIELD UNIVERSITY

School of Engineering
MSc by Research

MSc Thesis

Academic Year 2011 - 2012

Liang Shao

GNSS Performance Modelling for High Integrity Aircraft Applications

Supervisor: Dr Roberto Sabatini
May 2012

This thesis is submitted in partial fulfilment of the requirements for the degree of MSc by Research

ABSTRACT

Till recently, no significant attempts have been made of developing Aircraft Based Augmentation System (ABAS) architectures capable of generating integrity signals suitable for safety-critical GNSS applications and no commercial ABAS products are available at present.

The aim of this research is to support the design a system that generates integrity signals suitable for GNSS application. The conceptual design and key mathematical models were recently developed by the Italian Air Force Experimental Flight Test Centre (CSV-RSV) [1, 2]. Such a system, would be able to provide steering information to the pilot, allowing for real-time and continuous integrity monitoring, avoidance of safety/mission-critical flight conditions and fast recovery of the required navigation performance in case of GNSS data losses.

The key elements addressed in this thesis are the development of a CATIA model for military and civil aircraft, supporting antenna obscuration and multipath analysis. This is to allow the ABAS system to generate suitable integrity flags when satellites signals are lost. In order to analyse the GNSS signal loss causes, the GNSS constellation models, the flight dynamics models, fading models, multipath models, Doppler shift models, and GNSS receiver tracking technology previously developed by CSV-RSV, are considered in this research.

Keywords: GNSS, Integrity Flag, Obscuration, Doppler Shift, Multipath, Fading, Receiver Tracking

ACKNOWLEDGEMENTS

I would like to express my sincere appreciation to Dr Roberto Sabatini for his invaluable expertise, advice and encouragement throughout this project, and also Cranfield University and the Italian Air Force Flight Research Centre for supporting and this research.

I would like to express my sincere thanks to Aviation Industry Corporation of China and China Scholarship Council for their supporting on my research at Cranfield University.

Furthermore I would like to thank my workmates from AVIC who provide constructive suggestions and helpful methods.

Finally, I would also thank my parents for their endless love, encouraging and inspiring.

TABLE OF CONTENTS

LIST OF FIGURES

LIST OF TABLES

LIST OF EQUATIONS

LIST OF ABBREVIATIONS

AAL	Aircraft Automatic Landing
ABAS	Avionics Based Augmentation System
ABIA	Avionics Based Integrity Augmentation
ATM	Air Traffic Management
AVIC	Aviation Industry Corporation of China
CNS	Communication, Navigation and Surveillance
CSG	Critical Satellite Geometric
DOP	Dilution Of Precision
ECEF	Earth Centred, Earth Fixed
ENU	East North UP
FCS	Flight Control System
FLL	Frequency Lock Loop
GBAS	Ground Based Augmentation Systems
GDOP	Geometrical Dilution Of Precision
GNSS	Global Navigation Satellite System
GPS	Global Positioning System
HAL	Horizontal Alert Limit
HDOP	Horizontal Dilution Of Precision
HPL	Horizontal Protection Level
IF	Intermediate Frequency
LOS	Line Of Sight
LOs	Local Oscillators
NCO	Numerically controlled oscillator
PLL	Phase Lock Loop
PDOP	Positional Dilution Of Precision
RF	Radio Frequency
RHCP	Right-Hand Circularly Polarized
SNR	Signal to Noise Ratio
SGAAN	Space-Ground-Avionics Augmentation Network
SBAS	Space Based Augmentation Systems
TDOP	Time Dilution Of Precision

TSPI	Space Position Information System
TTA	Time to Alart
VAL	Vertical Alert Limit
VDOP	Vertical Dilution Of Precision
VPL	Vertical Protection Limit

1 INTRODUCTION

1.1 Background

The aim of this research project is to support the development of a novel GNSS integrity augmentation for mission-critical and safety-critical air vehicle applications and for multi-sensor avionics architectures based on GNSS. The supporting rationale for this project is provided below [1, 2]:

- The Aerospace research community has very stringent integrity requirements, especially with mission-critical and safety-critical avionics applications;
- Current and likely future air platforms are equipped with a variety of navigation systems and other sensors. These systems/sensors can be used in a suitable integrated architecture to enhance integrity levels, therefore matching the requirements of mission/safety- critical navigation and lading systems both for military and civil applications;
- The literature search showed that GNSS Avionics Based Integrity Augmentation (ABIA) is a relatively new research topic, especially when applied to Multi-sensor Systems for Aircraft Navigation and Guidance;
- Significant correlation exists between GNSS ABIA and other important areas of current research, including safety critical systems applications like Aircraft Automatic Landing (AAL) and Sense-and-Avoid (SAA).
- A novel and properly conceived technique providing ABIA could have a very significant impact on the aerospace community, with the possibility

of attracting funding from government and industrial organizations (possibly leading to the design and industrialization of an ABIA system);

- An innovative, cost-effective and properly designed ABIA system could have a significant impact on the Air Traffic Management (ATM) Communication, Navigation and Surveillance (CNS) community, with the potential of being selected as a suitable technology for the Future Global Air Traffic Management Network, possibly within the frame of NextGen/SESAR developments (i.e., in association with other ATM/CNS technologies like ABS-B, RNAV and Aeronautical Data Links) [1, 2].

1.2 Research problem and purpose

GNSS systems can provide high accuracy navigation data. However it is certificated only when it is integrated with other navigation system. The reason for that is the integrity instead of accuracy because the GNSS system often influenced by the outer environment [1, 2]

Various strategies have been developed for increasing the levels of integrity of GNSS based navigation/landing systems. Additionally, both Space Based Augmentation Systems (SBAS) and Ground Based Augmentation Systems (GBAS) have been developed in recent years [1, 2]

In the air platforms domain, GNSS augmentation may also take the form of additional information being provided by other avionics systems. In most cases, the additional avionics systems operate via separate principles than the GNSS and, therefore, are not subject to the same sources of error or interference. A system such as this is referred to as an Avionics-Based or Aircraft-Based

Augmentation System (ABAS). The additional sensors may include Inertial Navigation Systems (INS), eLORAN, Automated Celestial Navigation, Dead Reckoning, Radar, Electro-Optical Sensors, etc. Unlike SBAS and GBAS technology, published research on ABAS is limited and mainly concentrates on additional information being blended into the position calculation to increase accuracy and/or continuity of the integrated navigation solutions. Additionally, no significant attempts have been made of developing ABAS architectures capable of generating integrity signals suitable for safety-critical GNSS applications (e.g., aircraft precision approach and landing) and no commercial ABAS products are available at present. Although current and likely future SBAS/GBAS augmentation systems can provide significant improvement of GNSS navigation performance, a properly designed and flight certified ABAS system could play a key role in GNSS Integrity Augmentation for safety-critical applications such as aircraft precision approach and automatic landing. Furthermore, using suitable data link and data processing technologies on the ground, a certified ABAS capability could be a core element of a future GNSS Space-Ground-Avionics Augmentation Network (SGAAN) [1, 2]

The aim of the research is to design a complete GNSS Avionics Based Augmentation System (ABAS) taking advantage of the latest hardware and software integration techniques. A possible architecture of the ABAS system is shown in Figure 1-1.

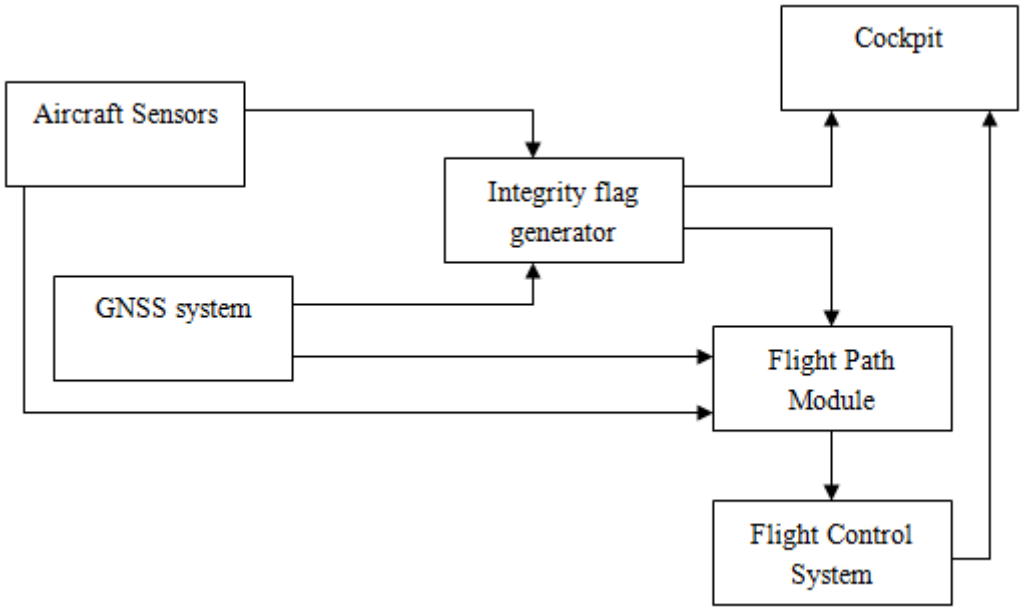

Figure 1-1 Architecture of the ABAS system. Adapted from [1, 2].

Therefore, in this research the aim is to support the design of such an ABAS system, by developing CATIA models of military/civil aircraft to support antenna obscuration and multipath analysis. The conceptual design and key mathematical models were developed by Dr Roberto Sabatini [1, 2] while serving as a Flight Test Engineer in the Italian Air Force Flight Research Centre (CSV-RSV) in collaboration with Cranfield University and Rome University "La Sapienza"). Such a system, would be able to provide steering information to the pilot and, possibly, electronic commands to the aircraft Flight Control System (FCS), allowing for real-time and continuous integrity monitoring, avoidance of safety/mission-critical flight conditions and fast recovery of the required navigation performance in case of GNSS data losses.

The key point of designing such a system is to generate the integrity flag which is consisted with the GNSS data loss causes. To detect that the error is

exceeding a threshold, a monitor function has to be installed within the navigation system. However, the time to alarm (TTA) is also essential to be generated through the integrity flag.

2 LITERATURE REVIEW

2.1 Methodology

Some flight test activities and research have been done .[1] During previous research and flight test activities with various DGSP Time and Space Position Information Systems (TSPI), it was observed that one or more of the following conditions was prone to cause data outages. They are critical bank angle, bad satellite geometric, low signal to noise ratio and multipath effect.

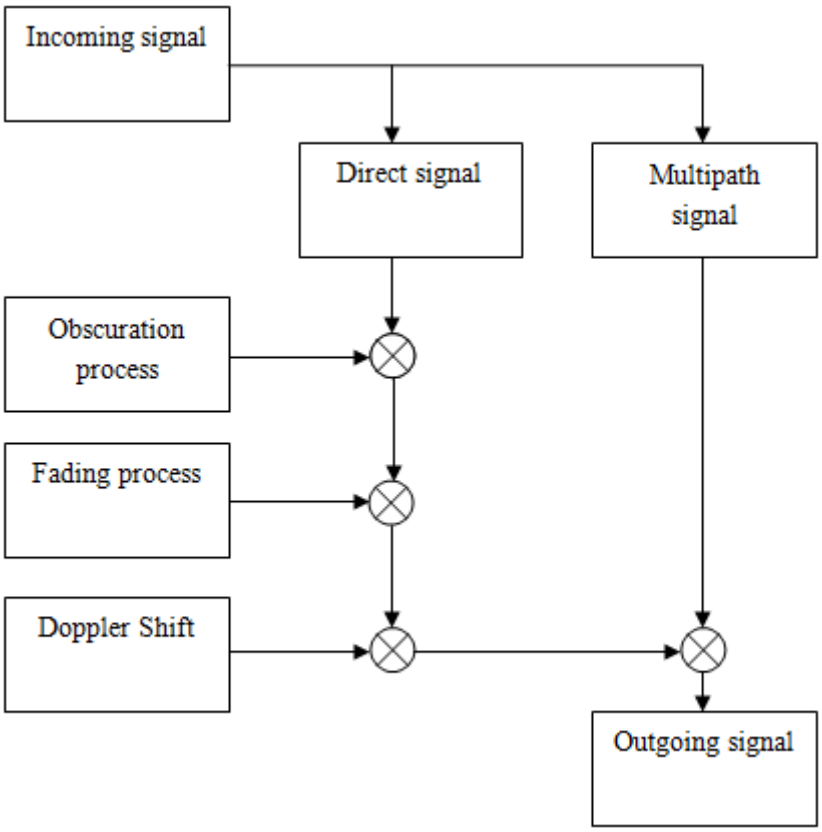

Figure 2-1 GNSS signal channel. Adapted from [2].

In this research the aim is to generate the integrity flag that gives the threshold and time to alert. The integrated navigation system will use the integrity flag to

decide whether the GNSS system or the ABAS will be used. All the factors that cause GNSS signal loss will be considered in this research.

The figure 2-1 shows the GNSS signal channel. It indicates that the obscuration, fading, Doppler Shift and multipath effect will cause GNSS signal loss. So in this research all these models will be built to simulate the integrity flag.

The first step of the research is to built the GNSS Constellation simulation. It will generate the results of the satellites positions in ECEF(Earth Centred, Earth Fixed).In this case we can get the results of the critical satellite geometric (CSG) through calculating the GDOP and PDOP [2].

Due to the manoeuvres of the aircraft, the wing and the fuselage will obscure some satellites signal during the flight. The flight test done shows that the obscuration effect increased during the bank angle is increasing [1, 2]. So in this research the whole obscuration model will be built. Aircraft 3D model and the A/C flight dynamics model are necessary to induce the antenna masking model. Also the simulation of satellite visibility during different flight phase is generated.

In order to generate the integrity flag, the flag that whether the received GNSS signal power strength is strong enough is very important. It will cause the signal loss when the received signal has low power. And there are some factors make contributions to this fading phenomenon. They are known as GNSS antenna gain pattern and the receiver antenna gain pattern, atmospheric effects, inonspheric effects, tropospheric effects and the noise figure [2, 3]. The SNR model will combined all these factors to generate the integrity flag.

GNSS signal has some perturbations which are known as the multipath effects. These effects will influence the received signal power. The multipath signals are consisted of diffractive signal, the wing reflection, the fuselage reflection and ground echo [2, 4]. The multipath model will use the Geometric Ray Tracing method [2, 4].

The Doppler Shift is the change in frequency of a wave for an observer moving relative to the source of the wave. The Doppler shift effects the receiver frequency so that it will affect the antenna to track the GNSS signal carrier phase. Existing research shows that the Doppler Shift influence the acquisition time.[3]

The multipath effect causes phase error and the Doppler shift causes frequency error. Both of the errors make contribution to the false of signal tracking. In order to generate the integrity flag caused by these errors, some research have to be done with the GPS receiver tracking technology.

2.2 Research Objectives

The main objectives of this research are:

1. Take TORNADO aircraft and AIRBUS 320 for example, performing analysis and simulation to identify the combined GNSS/aircraft antenna masking limitations. Using CATIA and CAD to get the 3D view of the TORNADO and A320.
2. Performing analysis and simulation to identify the combined GNSS/aircraft performance limitations at various altitudes and with various flight profiles;

3. Performing simulation to test the multipath, fading, Doppler shift, and GNSS receiver tracking models described in [1, 2];
4. Generate the integrity flag combined with all the models and criteria presented in [1, 2].

All the model simulations will be performed using the Matlab/SIMULINK code developed by CSV-RSV/Cranfield and described in [2]. The following Figure 2-2 shows the integrity flag simulator structure.

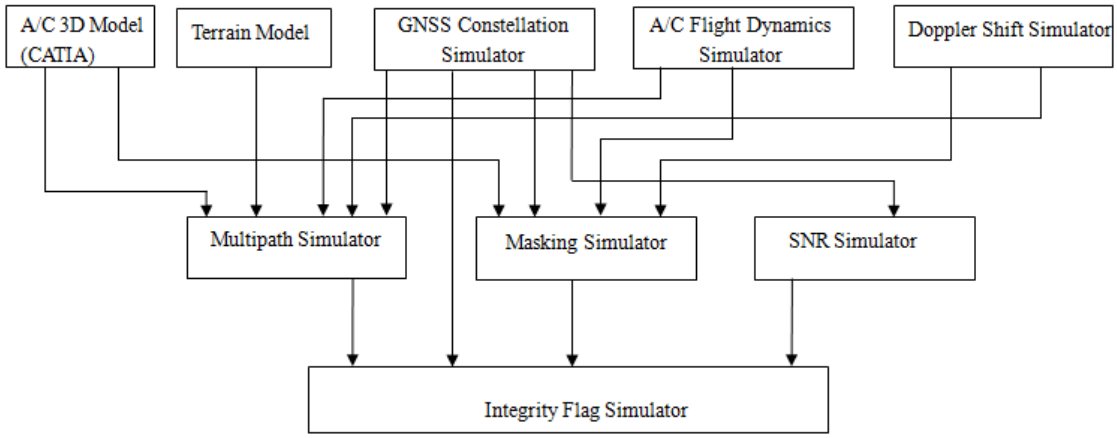

Figure 2-2 Integrity Flag Simulator. Adapted from [2 , 5].

3 GNSS CONSTELLATION

3.1 Introduction

In this research the GNSS constellation (GPS, GALILEO) simulator is implemented in MATLAB. A mathematical model is developed to calculate the satellites position in Earth Centred, Earth Fixed frame (ECEF). It is useful in calculating the satellite visibility. This model also expresses the Pseudo Range as a function of various errors, such as satellite clock error, ionospheric error, and tropospheric error [2, 3]. It will be used to calculate the critical satellite geometric.

GALILEO constellation shares the same theory with GPS. But GALILEO satellite ephemeris data are not available. So in this research, the Walker Delta 56°:27/3/1 constellation is brought in to build the GALILEO constellation. It means that there are 27 satellites in 3 planes inclined at 56 degrees, spanning the 360 degrees around the equator.

3.2 Satellite Position

3.2.1 Ephemeris Data

The simulation is based on data from the NAV-message (Ephemeris/Almanac and Ionospheric data). We built the model reads specified navigation file and return the orbit parameters for all satellites. The specified navigation files are all downloaded from the following website:

Ftp://cddis.gsfc.nasa.gov/../../../gps/data/daily/2011/034/11n/.”

In this transformation model, we can get the outputs of all the satellites ephemeris data:

Table 3-1 Ephemeris Data

No.	Parameter	Definition	Units
1	IODE	Issue of Data, Ephemeris	
2	Crs	sine term, radius correction	m
3	Delta_n	mean motion correction	
4	M0	mean anomaly	rad
5	Cuc	cosine term, argument of lat correction	rad
6	ecc	eccentricity	
7	Cus	sine term, argument of lat correction	rad
8	Sqrt_A	square root of semi-major axis	m
9	Toe	ephemeris time in gps sec of week	s
10	Cic	cosine term, inclination correction	(rad)
11	OMEGA	Right ascension of ascending node	(rad)
12	Cis	sine term, inclination correction	(rad)
13	i0	inclination	(rad)
14	Crc	cosine term, radius correction	(m)
15	omega	argument of perigee	(rad)
16	OMEGA_DOT	right ascension of ascending node, dot	(rad/s)
17	IDOT	inclination dot	(rad/s)

3.2.2 Satellite Position Calculation

The satellites positions are calculated based on the Kepller's laws and so we use the Keplerian anomalies.

The three anomalies are mathematically defined as ([2, 3]):

$$M(t) = M_0 + n \times (t - T_0) \quad \textbf{(3-1)}$$

$$E(t) = M(t) + e \times \sin(E(t)) \quad \textbf{(3-2)}$$

$$\nu_c = \cos\left(\frac{\cos(E(t)) - e}{1 - e \times \cos(E(t))}\right), \nu_{s=}\sin\left(\frac{\sqrt{1-e^2} \times \sin(E(t))}{1 - e \times \cos(E(t))}\right), \nu(t) = \operatorname{atan}\left(\frac{\nu_s}{\nu_c}\right) \quad \textbf{(3-3)}$$

V (t) – true anomaly, E(t) –eccentric anomaly, M(t) – mean anomaly.

The satellites positions and velocity can be calculated from these anomalies. And the satellites ephemeris data performed in the calculations are from the functions in the former chapter 3.2.1.

The mean angular velocity, n, known as mean motion is given by Kepler's 3rd law:

$$n_0 = \sqrt{\frac{\mu}{a^3}} \quad \textbf{(3-4)}$$

Where μ is the value of Earth's universal gravitational parameters

With the GPS Ephemeris correction (Δn)the mean motion is:

$$n = n_0 + \Delta n \quad \textbf{(3-5)}$$

The equation (3-6) is Kepler's Equation for Eccentric Anomaly; it can be solved by iteration, which in this research is solved with the method as Newton-Raphson ([3]):

$$E_m - \frac{E_m - e \times \sin(E_m) - M}{1 - e \times \cos(E_m)}, m = 1, \ldots p \quad \textbf{(3-6)}$$

$$E_0 = M + \frac{e \times \sin(M)}{1 - \sin(M + e) + \sin(M)} \quad \textbf{(3-7)}$$

Where p is a defined number of iterations.

Argument of latitude:

$$\phi(t) = \upsilon(t) + \omega \quad \textbf{(3-8)}$$

The GPS satellite orbit is modelled as a modified elliptical orbit with correction terms.[3]

Argument of Latitude Correction:

$$\delta u = C_{uc}\cos 2\phi + C_{us}\sin 2\phi \quad \textbf{(3-9)}$$

Radius Correction:

$$\delta r = C_{rc}\cos 2\phi + C_{rs}\sin 2\phi \quad \textbf{(3-10)}$$

Inclination Correction:

$$\delta i = C_{ic}\cos 2\phi + C_{is}\sin 2\phi \quad \textbf{(3-11)}$$

where the constants C are transmitted correction sinus and cosine amplitudes.

Then, the corrected argument of latitude, corrected inclination and corrected radius are:[3]

$$u = \phi + \delta u \quad \textbf{(3-12)}$$

$$i_k = i_0 + \frac{di}{dt} \times t + \delta_i \quad \textbf{(3-13)}$$

$$r = a * (1 - e \times \cos(E)) + \delta r \quad \textbf{(3-14)}$$

Due to the earth turn rate and the ascending node right ascension rate, corrected longitude of ascending node is given by:[2]

$$\Omega = \Omega_0 + \left(\dot{\Omega} - \omega_E\right) \times t - \omega_E \times t_{oe} \quad \textbf{(3-15)}$$

The position and velocity vector in the orbital reference frame are ([2]):

$$\underline{r}^0 = r \times \begin{bmatrix} \cos(u) \\ \sin(u) \\ 0 \end{bmatrix} \quad \textbf{(3-16)}$$

$$\dot{\underline{r}}^o = \sqrt{\frac{\mu}{a(1-e^2)}} \times \begin{bmatrix} -\sin(u) \\ \cos(u) + e \\ 0 \end{bmatrix} \quad \textbf{(3-17)}$$

3.3 Pseudo Range

The pseudo range is a distance based on the satellite transmitted and the receiver's reference code, which has been corrected for errors in synchronization between the transmitter's clock and the receiver's clock. With the errors, the equation for calculating the pseudo range is [2, 3]:

$$\rho_i = \rho_{Ti} + c(\delta_i^s - \delta_R) = \rho_{Ti} - c\delta_R + c(\Delta T_i + \Delta I_i + \Delta V_i + \Delta b_i) \quad \textbf{(3-18)}$$

Where:

ΔT_i: Troposphere error

ΔI_i: Ionosphere error

ΔV_i: Relativistic time correction

Δb_i: Satellite bias clock error

In this research only Atmospheric Condition and Clock Drift has been investigated. Ionospheric error, tropospheric error and clock error are described as following.

3.3.1 Ionospheric Error

As GPS satellite signals traverse the ionosphere, they are delayed by an amount proportional to the number of free ions encountered. It is the cause of Ionospheric error.

Klobuchar [3] developed a simple analytical model for ionospheric time delay, which we have used for ionospheric correction model. This form of GPS user ionospheric correction algorithm requires the user's approximate longitude λ_U, geodetic latitude ϕ_U, elevation angle E and azimuth A to each GPS satellite. The calculation proceeds as follows [2, 3]

Calculate the Earth-centred angle ψ

$$\psi = \frac{0.0137}{\mathrm{E} + 0.11} - 0.022 \ (semicircles) \tag{3-19}$$

Compute the subinospheric latitude, ϕ_I

$$\phi_I = \phi_U + \psi \cos A \ (semicircles) \tag{3-20}$$

If $\phi_I \geq 0.416$, then $\phi_I = 0.416$. If $\phi_I \leq 0.416$, then $\phi_I = -0.416$.

Compute the subionospheric longitude λ_I

$$\lambda_I = \lambda_U + \left(\psi \frac{\sin A}{\cos \phi_I}\right) \ (semicircles) \tag{3-21}$$

ϕ_m, which means geomagnetic latitude, can be calculated by :

$$\phi_m = \phi_I + 0.064 \cos(\lambda_I - 1.617) \ (semicircles) \tag{3-22}$$

On subionospheric point , the local time can be calculated by :

$$t = 4.32 \times 10^4 \lambda_I + \mathrm{Time}_{GPS}(\mathrm{Second}) \quad \textbf{(3-23)}$$

If t>86400, then t=t-86400. If t<0, add 86400.

To convert to slant time delay, compute the slant factor,

$$F = 1 + 16(0.53 - E)^3 \quad \textbf{(3-24)}$$

The ionospheric time delay T_{iono} is calculated by first computing x:

$$\mathbf{x = \frac{2\pi(t - 50400)}{\sum_{n=0}^{3} \beta_n \phi_m^n}} \quad \textbf{(3-25)}$$

If PER< 72000 then PER=72000.

If $|x| > 1.57$, then

$$T_{iono} = F \times (5 \times 10^{-9}) \quad \textbf{(3-26)}$$

Otherwise

$$T_{iono} = F \times \left[5 \times 10^{-9} + \sum_{n=0}^{3} \alpha_n \phi_m^n \times (1 - \frac{x^2}{2} + \frac{x^4}{24})\right] \quad \textbf{(3-27)}$$

3.3.2 Tropospheric Error

The primary purpose of the tropospheric analysis system is to estimate wet tropospheric delays that can be converted into integrated water vapour and thereby serve as a valuable input into numerical weather and climate models. For this reason, Hopfield model [3] is devoted to tropospheric delay modelling and estimation. In this model troposphere delay are divided into two parts: the “Dry” component and the “Wet” atmosphere component. The zenith delay caused by dry component is calculated by [2, 3]

$$K_d = 1.55208E-4 \times P_{amb} \times (40136 + 148.72 \times T_{amb})/(T_{amb} + 273.16) \quad \textbf{(3-28)}$$

Where T_{amb} is ambient temperature and P_{amb} is ambient air pressure. The zenith delay caused by wet component is calculated by [3]

$$K_w = -0.282 \times \frac{P_{vap}}{(T_{amb} + 273.16)} + 8307.2 \times \frac{P_{vap}}{(T_{amb} + 273.16)^2} \quad \textbf{(3-29)}$$

The zenith delay and the elevation angle E can used to obtain the SV's tropospheric delay correction [3]:

$$\Delta T = \frac{K_d}{\sin(\sqrt{El^2 + 1.904E-3})} + \frac{K_w}{\sin(\sqrt{El^2 + 0.6854E-3})} \ (\text{Meter}) \quad \textbf{(3-30)}$$

Where El is the SV's elevation in Rad.

3.3.3 Satellite Clock Error

The user receiver needs to correct the GPS satellite clock errors. The user receiver must have an accurate representation of GPS system time at the time of transmission for GPS signal it receiving from satellite i. the satellite clock correction Δt_{sv} is obtained using coefficients broadcast from the satellite after being uploaded by the GPS control segment. The control segment actually uploads several different sets of coefficient to the satellite, of which each set is valid over a given time period. The data sets are then transmitted in the downlink DataStream to the users in the appropriate time intervals. These corrections represent a second order polynomial in time. [2, 3]

The GPS time needed to solve for user position is $t = t_{sv} - \Delta t_{sv}$ where t_{sv} the SV pseudorandom noise code phase is time at the time of transmission and is

easily determined by the GPS receiver. The satellite clock correction term is approximated by a polynomial

$$\Delta t_{sv} = af_0 + af_1(t - t_{oc}) + af_2(t - t_{oc})^2 + \Delta t_R - T_{gd} \quad \textbf{(3-31)}$$

Where af_0, af_1 and af_2 are the polynomial correction coefficient related to phase error, frequency error, and change rate of frequency error; the relativistic correction is Δt_R; t_{oc} is a reference time for clock correction and T_{gd} is group delay.

Relativistic correction must be computed by the user. A first order effect described in the GPS gives the relativistic correction for an Earth-centred, Earth-fixed (ECEF) observer and a GPS satellite of eccentricity e. This relativistic correction varies as the sine of the satellite eccentric anomaly E_k as follows:

$$\Delta t_R = Fe\sqrt{A}\sin(E_k) \quad \textbf{(3-32)}$$

Where

F:-4.442807633E-10s/m.

E_k: eccentric anomaly of the satellite orbit

A: semi major axis of the satellite orbit

4 OBSCURATION

4.1 Introduction

Due to the manoeuvres of the aircraft, the wing and the fuselage will obscure some satellites signal during the flight.

The Figure 4-1 below show the GNSS satellite obscuration simulator structure. The aircraft 3D model and the A/C flight dynamics model are built for the analysis of antenna masking. And the satellite visibility are generated during different flight phase when combing the 3D model, A/C flight dynamics model and the GNSS constellation simulator.

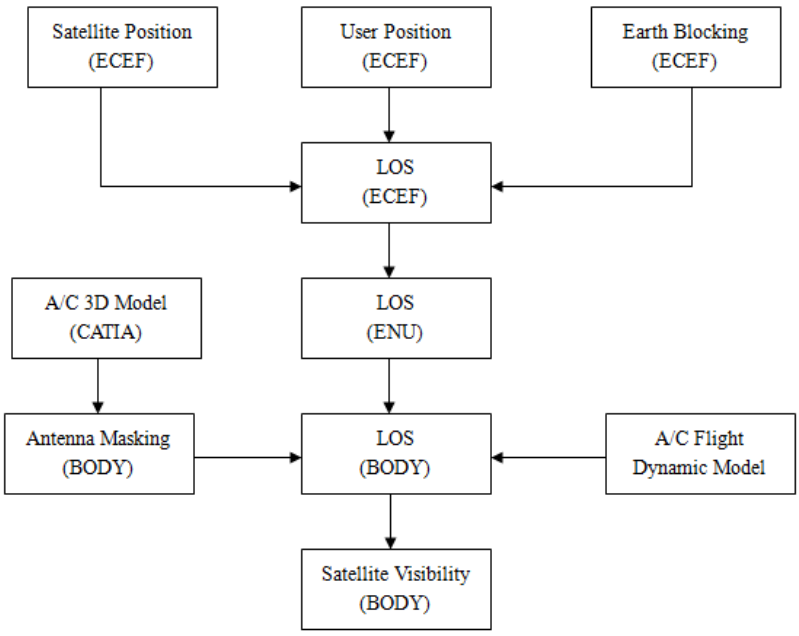

Figure 4-1 GNSS satellite obscuration simulator. Adapted from [2].

In this chapter the antenna masking due to the fuselage and wing and tails are simulated. The simulation results show the both the upper antenna and lower

antenna in a military aircraft TORNADO masking matrix when concerning about the change of pitch angle, roll angle and yaw angle. Also the simulation results of satellite visibility during different flight phase are generated.

4.2 Aircraft 3D Model

In this research there are two cases: military aircraft, TORNADO is chosen； Large civil aircraft, AIRBUS 320. Both of them are drawn in CATIA to get the 3D models.

3D model can be used to generate the antenna masking due to the obscuration of wing and fuselage and tails. They are also useful in calculating the satellite visibility during different flight phase combined with the GNSS constellation simulator. 3D models will be used in the simulation of multipath when calculating the wing reflection and fuselage reflection via geometrical optics method.

4.2.1 TORNADO

4.2.1.1 TORNADO CATIA Model

The following Figure 4-2 shows 2D drawing of TORNADO.[6] It is useful to get the outline of the TORNADO when drawing it in CATIA.

And also some main parameters are very essential to draw the CATIA model. Some of them are listed in the following Table 4-1 [5, 7].

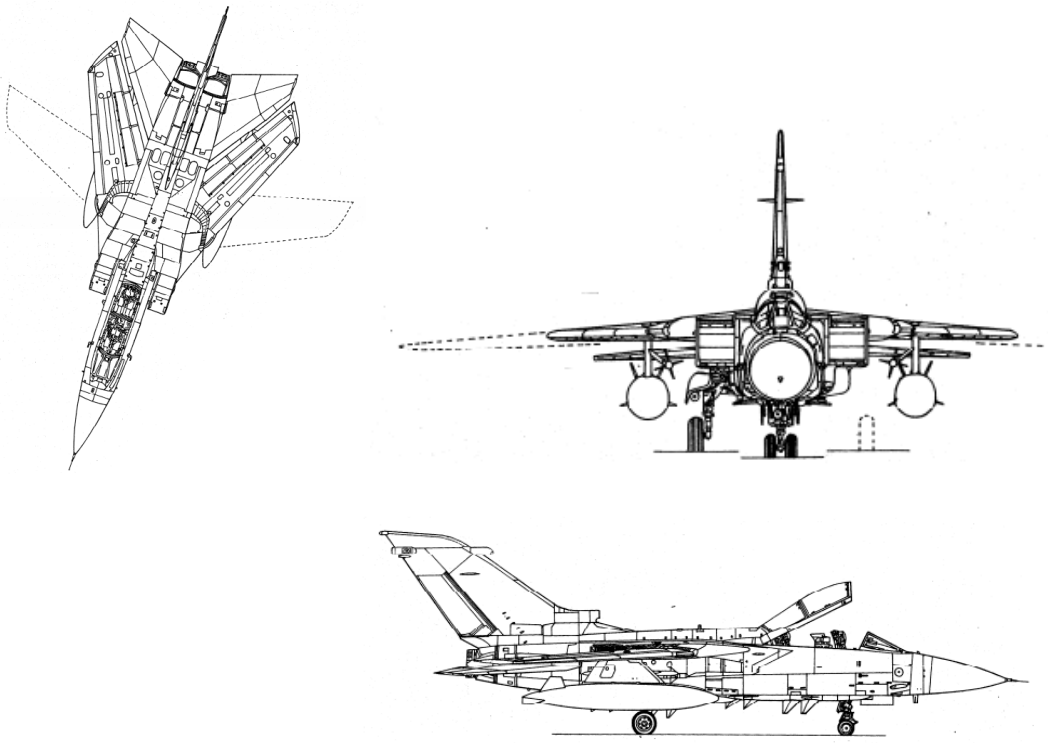

Figure 4-2 TORNADO 2D figure [5, 6].

Table 4-1 TORNADO parameters [5, 7]

	Parameters
Length	16.72 m (54 ft 10 in)
Wingspan	13.91 m at 25° wing sweep, 8.60 m at 67° wing sweep (45.6 ft / 28.2 ft)
Height	5.95 m (19.5 ft)
Wing area	26.6 m² (286 ft²)

From the 2D figure and the parameters, the Tornado Fighter 3D model is drawn by CATIA. It can be seen in the figure 4-3 below.

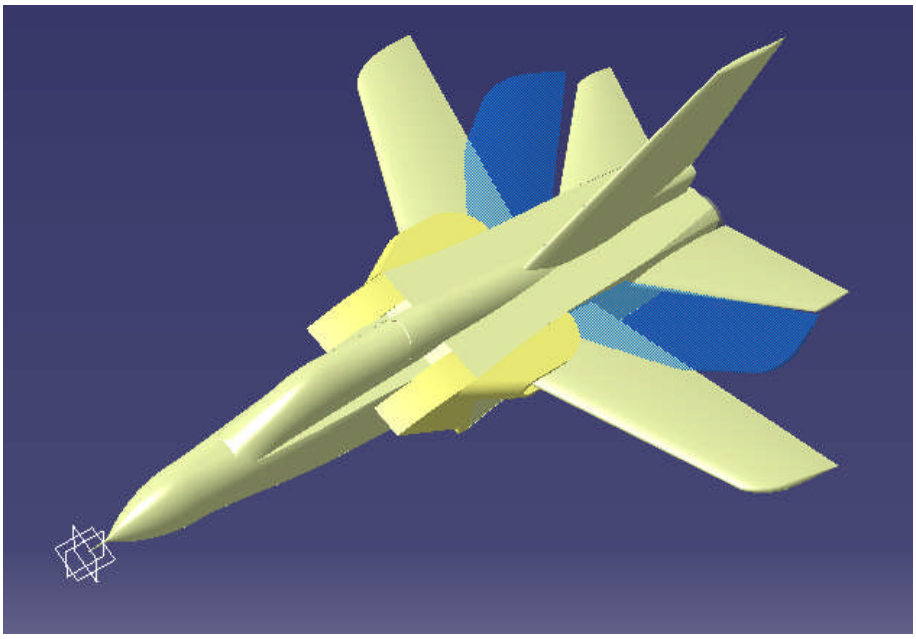

Figure 4-3 TORNADO 3D CATIA model [2].

4.2.1.2 TORNADO antenna location

When calculating the antenna masking matrix and the satellite visibility, the location of antenna is essential. Using the 3D TORNADO CATIA model, the position of the receiver antenna can be located.

For the military aircraft there are both the upper antenna on the top of the fuselage and the lower antenna on the back of the fuselage. Take TORNADO for example, the upper antenna is 1.5m behind the cockpit. [1] And the antenna is assumed to be 5cm high. The lower antenna is right below the upper antenna and is located in the back of the fuselage. All can be seen in the Figure 4-4 below.

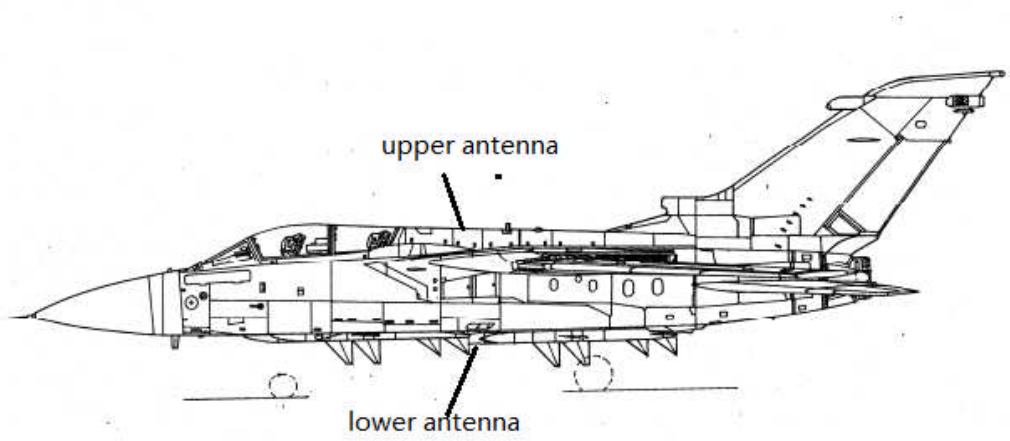

Figure 4-4 3D Tornado antenna position [2, 5]

From the Figure 4-4 we notice that the antenna position is not the same with the centre of mass. When calculating the satellite visibility, the line of sight (LOS) should be measured in the antenna frame. Then the transformation from body-frame to antenna frame is the following equation [2, 5]:

$$\mathrm{F_{antenna}} = \mathrm{F_{body}} + \mathrm{T_{body}^{antenna}}\ (\mathrm{m}) \tag{4-1}$$

Using the TORNADO 3D CATIA model the upper antenna to body frame transformation can be measured in equation [2, 5]:

$$\mathrm{T_{body}^{upper}} = \begin{bmatrix} -0.88 \\ 0 \\ -0.74 \end{bmatrix} (\mathrm{m}) \tag{4-2}$$

And the lower antenna to body frame transformation is measured in equation [2,5]:

$$\mathrm{T_{body}^{lower}} = \begin{bmatrix} -0.88 \\ 0 \\ 2.13 \end{bmatrix} (\mathrm{m}) \tag{4-3}$$

4.2.2 Airbus 320

4.2.2.1 A320 3D CATIA Model

In order to draw the 3D view of AIRBUS 320, the following figure provides the parameters needed. [2, 8]

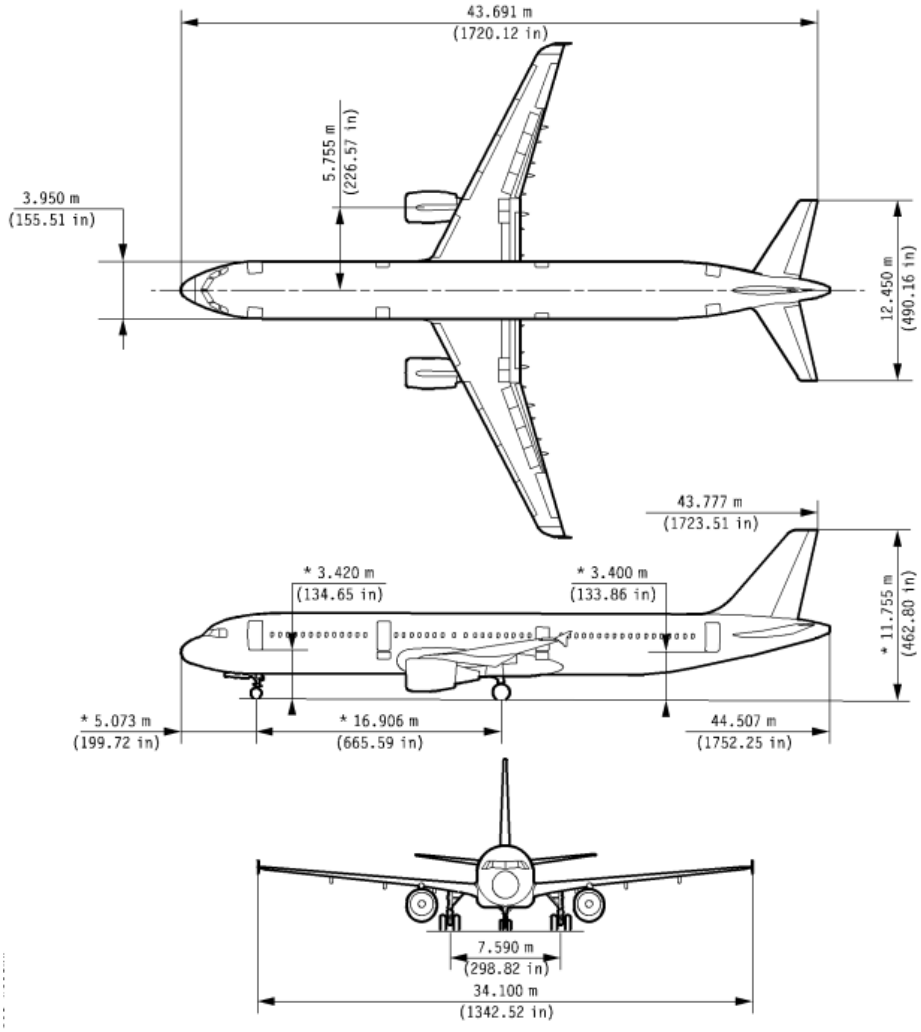

Figure 4-5 A320 2D geometric model

Then the A320 3D model is finished in CATIA. It can be seen in the following Figure 4-6.

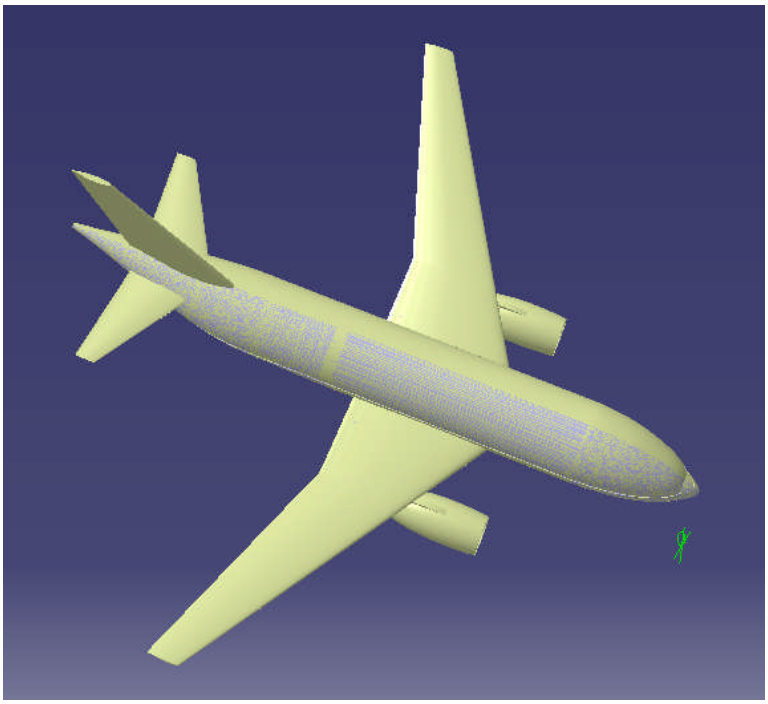

Figure 4-6 3D A320 CATIA model [2].

4.2.2.2 A320 antenna location

When calculating the A320 antenna masking matrix and the satellite visibility, the location of antenna is essential. Using the 3D A320 CATIA model, the position of the receiver antenna can be located.

For the civil aircraft there is only a receiver antenna on the top of the fuselage. Take A320 for example, from the Figure 4-7[8], the GPS antenna is 10.2m behind the nose on the top on the fuselage. And the antenna is assumed to be 5cm high.

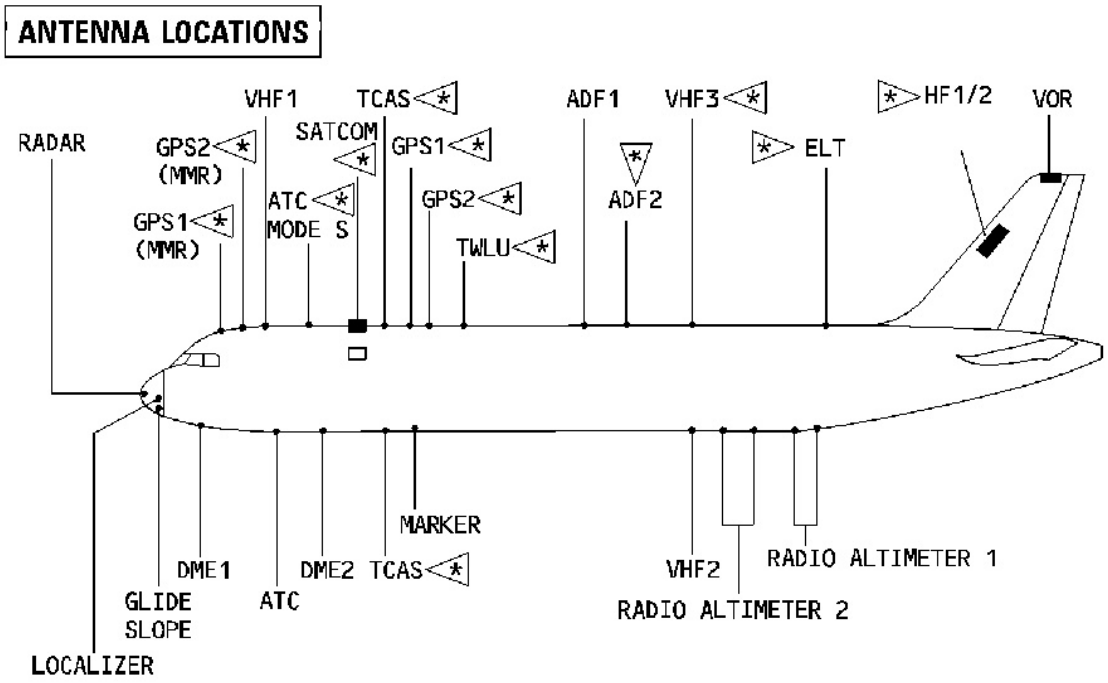

Figure 4-7 A320 antenna location [8]

From the figure 4-7 we notice that the antenna position is not the same with the centre of mass. When calculating the satellite visibility, it should from the antenna frame. Then the transformation from body-frame to antenna frame is the following equation [2]:

$$\mathrm{F}_{\mathrm{antenna}} = \mathrm{F}_{\mathrm{body}} + \mathrm{T}_{\mathrm{body}}^{\mathrm{antenna}} \ (\mathrm{m}) \tag{4-4}$$

Using the A320 CATIA model the antenna to body frame transformation can be measured in equation [2]:

$$\mathrm{T}_{\mathrm{body}}^{\mathrm{antenna}} = \begin{bmatrix} -10.63 \\ 0 \\ -3.4 \end{bmatrix} (\mathrm{m}) \tag{4-5}$$

4.3 Flight Trajectory

4.3.1 Introduction

In this research the TORNADO and A320 are two cases to perform the simulation of the A/C flight dynamics model. The flight dynamics model is a 3-DOF model with variable mass due to the fuel consumption.

As the results of the simulations, the position and velocity of the aircraft can be generated. Also the pitch angle, yaw angle and the roll angle are the outputs. From these outputs we can generate the flight trajectory.

The simulations are to be done in 6 different phases: taxi, climb, cruise, turn and climb, turn and descend, landing.

The following symbols will be used in the flight dynamics equations.

Table 4-2 Flight dynamics symbols

	Parameters
a_c	acceleration vector of aeroplane mass centre
C_D	drag coefficient
C_L	lift coefficient
D	aerodynamic drag
G	acceleration due to gravity
h	height, altitude
L	lift
m	mass of aeroplane
S	wing area
T	thrust
s_{sfc}	specific fuel consumption
t	time

Table 4-2 Flight dynamics symbols (continued)

	Parameters
V	speed of aeroplane, true airspeed
W	weight of aeroplane
x,y,z	coordinates of aeroplane mass centre
α	incidence, angle between chord line and free stream wind direction
Δh	altitude increase during turn manoeuvre
ρ	density of air
γ	angle of flight path, path angle in the vertical plane
ϕ	angle of bank
Ψ	angle of yaw, path angle in the horizontal plane
Ω	rate of turn, $\Omega = d\psi/dt$

4.3.2 Taxi

In the taxi phase, the aircraft is speed up on the land and the pitch, roll and yaw angle is considered to be 0 deg. The mass is decreasing due to the fuel consumption. And the 3-DOF model equations are the following [2, 5]:

$$m * \frac{dV}{dt} = T - D \quad \textbf{(4-6)}$$

$$0 = L - mg + N \quad \textbf{(4-7)}$$

$$L = 0.5\rho V^2 C_L S \quad \textbf{(4-8)}$$

$$D = 0.5\rho V^2 C_D S \quad \textbf{(4-9)}$$

$$m = m_0 - s_{sfc} * t \quad \textbf{(4-10)}$$

4.3.3 Climb

In the climb phase, the aircraft flight trajectory is straight up to the sky with a certain pitch angle and its roll and yaw angle are considered to be 0 deg. The velocity is not constant in this phase. The mass is decreasing due to the fuel consumption. And the 3-DOF model equations are the following [2, 5]:

$$m * \frac{dV}{dt} = T * \cos\alpha - D - mg * \sin\gamma \quad \textbf{(4-11)}$$

$$m * V * \frac{d\gamma}{dt} = L + T * \sin\alpha - mg * \cos\gamma \quad \textbf{(4-12)}$$

$$L = 0.5\rho V^2 C_L S \quad \textbf{(4-13)}$$

$$D = 0.5\rho V^2 C_D S \quad \textbf{(4-14)}$$

$$m = m_0 - s_{sfc} * t \quad \textbf{(4-15)}$$

4.3.4 Cruise

In the cruise phase, the aircraft flies straight and steady. And its pitch, roll and yaw angle are considered to be 0 deg. The cruise speed is constant in this phase. The mass is decreasing due to the fuel consumption. And the 3-DOF model equations are the following [2, 5]:

$$0 = T * \cos\alpha - D \quad \textbf{(4-16)}$$

$$0 = L + T * \sin\alpha - mg \quad \textbf{(4-17)}$$

$$L = 0.5\rho V^2 C_L S \quad \textbf{(4-18)}$$

$$D = 0.5\rho V^2 C_D S \quad \textbf{(4-19)}$$

$$m = m_0 - s_{sfc} * t \tag{4-20}$$

4.3.5 Turn and Climb

In the turn and climb phase, the aircraft is performing turn manoeuvres. The following figure 4-8 shows this flight phase. And its pitch, roll angle are not steady during the flight while its yaw angle is considered to be constant in this phase. The mass is decreasing due to the fuel consumption. And its 3-DOF model equations are the following [2, 5]:

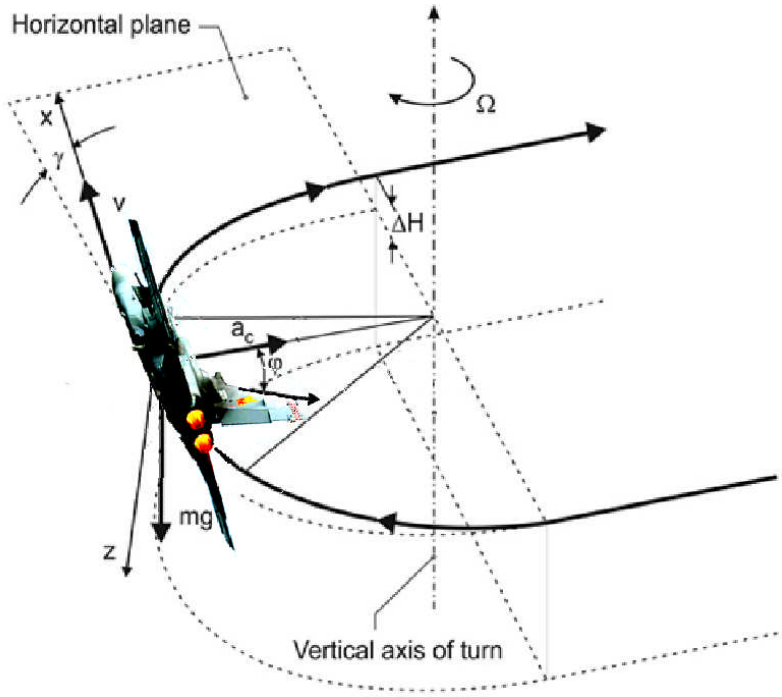

Figure 4-8 Aircraft turn manoeuvres [5].

$$m * \frac{dV}{dt} = T * \cos\alpha - D - mg * \sin\gamma \tag{4-21}$$

$$m * V * \cos\gamma * \frac{d\psi}{dt} = (L + T * \sin\alpha) * \sin\varphi \tag{4-22}$$

$$m * V * \frac{d\gamma}{dt} = (L + T * \sin\alpha) * \cos\varphi - mg * \cos\gamma \quad \textbf{(4-23)}$$

$$\frac{dh}{dt} = V * \sin\gamma \quad \textbf{(4-24)}$$

$$L = 0.5\rho V^2 C_L S \quad \textbf{(4-25)}$$

$$D = 0.5\rho V^2 C_D S \quad \textbf{(4-26)}$$

$$m = m_0 - s_{sfc} * t \quad \textbf{(4-27)}$$

4.3.6 Turn and Descend

In the turn and descend phase, the situations are the same with turn and climb phase. Due to the different thrust the aircraft vertical velocity and pitch angle are different. And its 3-DOF model equations are the following [2, 5]:

$$m * \frac{dV}{dt} = T * \cos\alpha - D - mg * \sin\gamma \quad \textbf{(4-28)}$$

$$m * V * \cos\gamma * \frac{d\psi}{dt} = (L + T * \sin\alpha) * \sin\varphi \quad \textbf{(4-29)}$$

$$m * V * \frac{d\gamma}{dt} = (L + T * \sin\alpha) * \cos\varphi - mg * \cos\gamma \quad \textbf{(4-30)}$$

$$\frac{dh}{dt} = V * \sin\gamma \quad \textbf{(4-31)}$$

$$L = 0.5\rho V^2 C_L S \quad \textbf{(4-32)}$$

$$D = 0.5\rho V^2 C_D S \quad \textbf{(4-33)}$$

$$m = m_0 - s_{sfc} * t \quad \textbf{(4-34)}$$

4.3.7 Landing

In the landing phase, the aircraft flight trajectory is straight down to the ground with a certain pitch angle and its roll and yaw angle are considered to be 0 deg. The velocity is not constant in this phase. The mass is decreasing due to the fuel consumption. And its 3-DOF model equations are the following [2, 5]

$$m * \frac{dV}{dt} = T * \cos\alpha - D - mg * \sin\gamma \quad \textbf{(4-35)}$$

$$m * V * \frac{d\gamma}{dt} = L + T * \sin\alpha - mg * \cos\gamma \quad \textbf{(4-36)}$$

$$L = 0.5\rho V^2 C_L S \quad \textbf{(4-37)}$$

$$D = 0.5\rho V^2 C_D S \quad \textbf{(4-38)}$$

$$m = m_0 - s_{sfc} * t \quad \textbf{(4-39)}$$

4.4 Antenna Masking

Due to the manoeuvres of the aircraft, the wing and the fuselage will obscure some satellites signal during the flight. And the change of pitch angle, yaw angle and roll angle make main contributions to influence the obscuration.

In this research the TORNADO is the antenna masking analysis model. Because the military aircraft has big change of the pitch, yaw and roll angle.

In order to get the masking matrix, the simulation work is done in the CATIA model. Only one of the angle is variable during each measurement.

4.4.1 Pitch Angle Effect

With change of the pitch angle from 0 degree to 180 degree, the antenna elevation and azimuth are measured in the TORNADO CATIA model. The following figure each presents the TORNADO upper antenna masking matrix when the pitch angle is 0 ^{o}, 45 ^{o}, 90 ^{o}, 135 ^{o} and 180^{o}.The blue line shows the masking limitations and the red points represent all the satellites with elevation and azimuth.

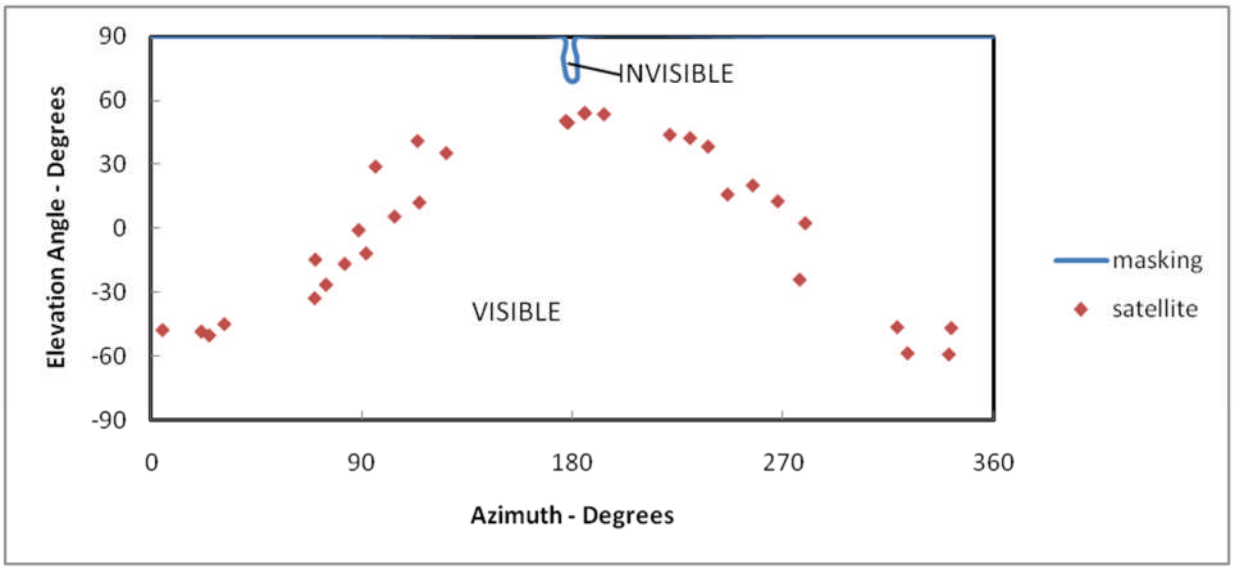

Figure 4-9 upper antenna masking matrix (Pitch angle=0^{0})

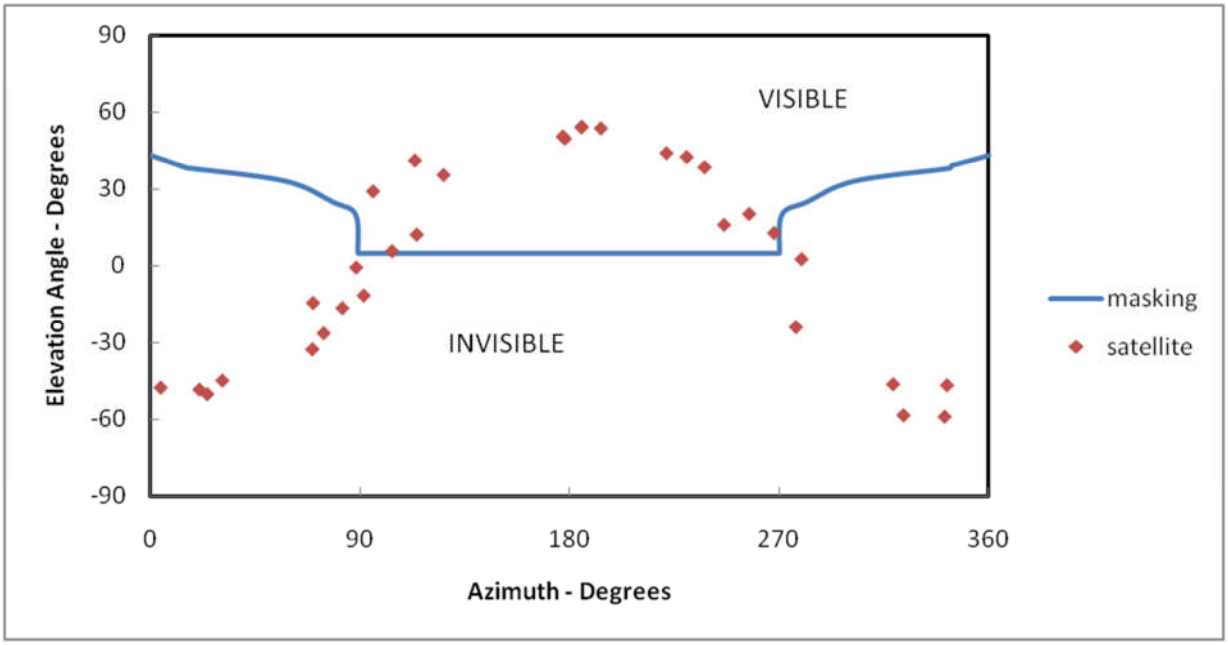

Figure 4-10 upper antenna masking matrix (Pitch angle=45^0)

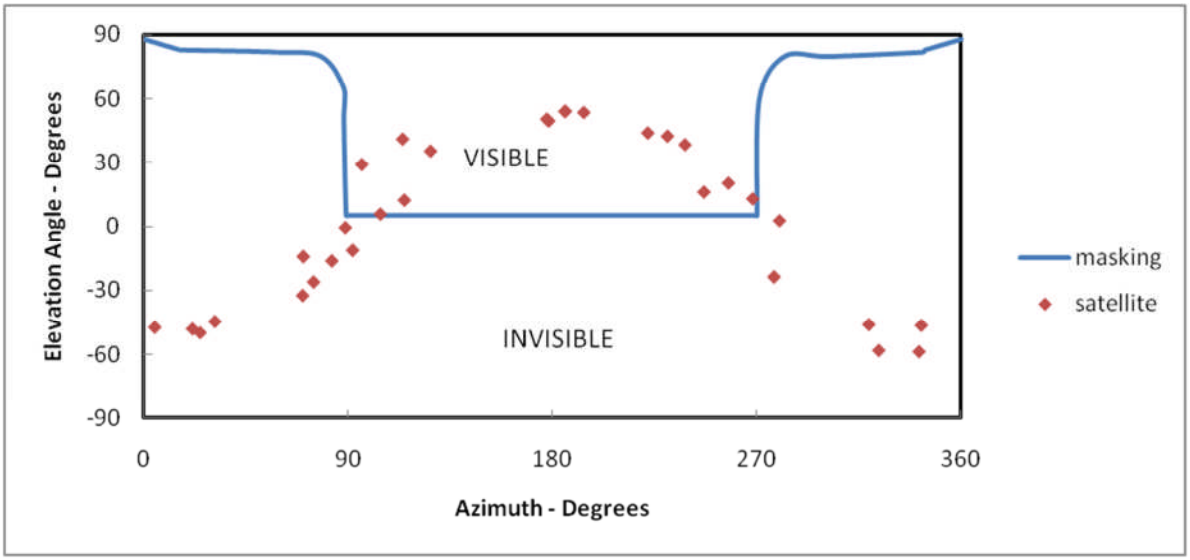

Figure 4-11 upper antenna masking matrix (Pitch angle=90^0)

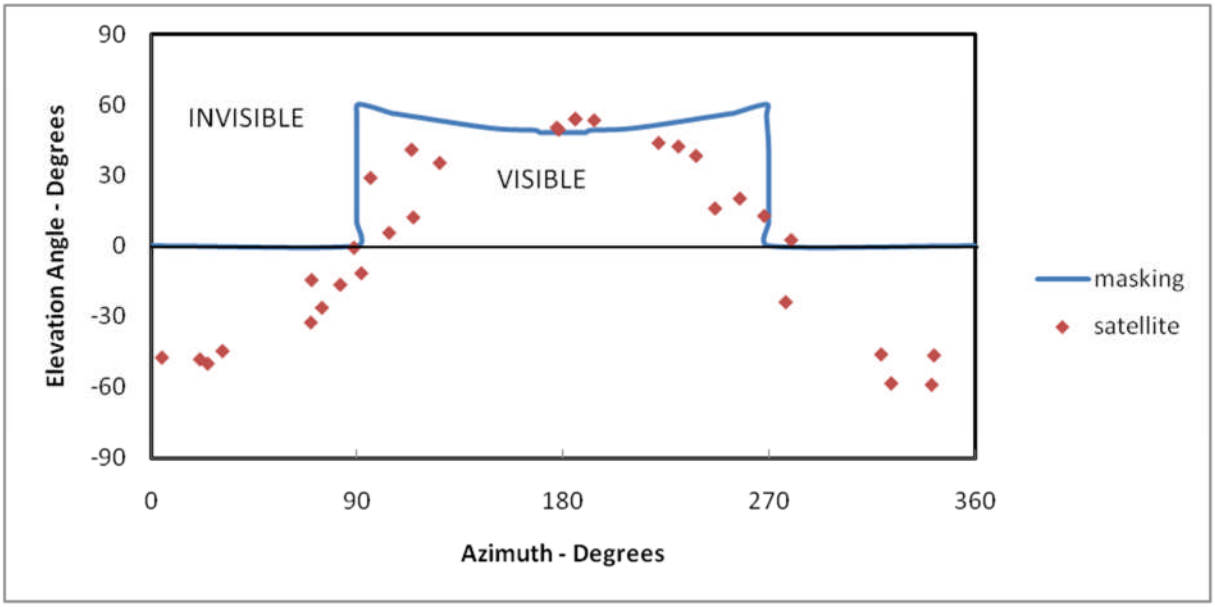

Figure 4-12 upper antenna masking matrix (Pitch angle=135^0)

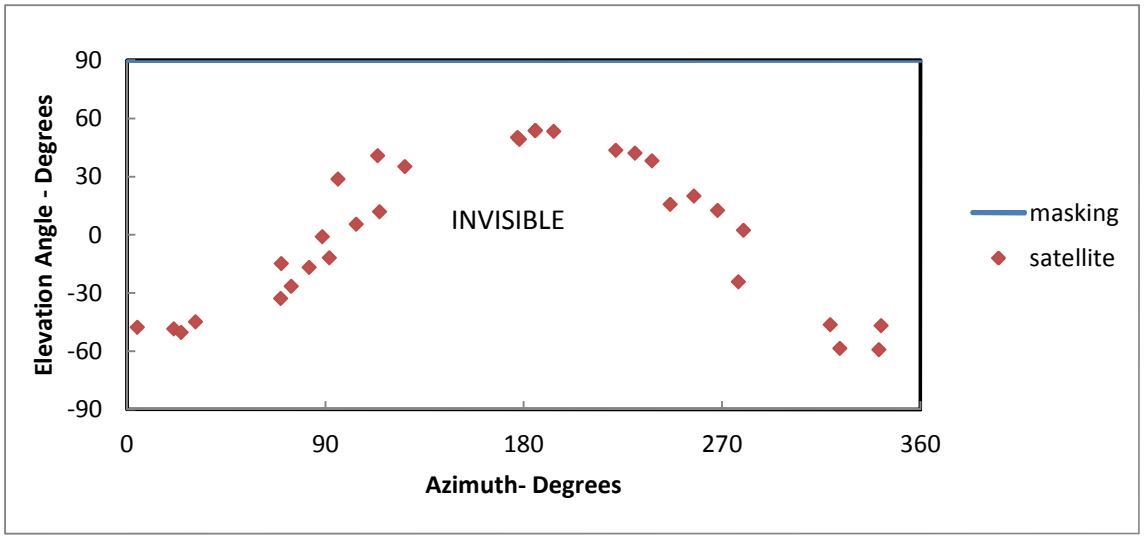

Figure 4-13 upper antenna masking matrix (Pitch angle=180^0)

Figure 4-9 shows the TORNADO upper antenna masking matrix when its pitch angle is 0 deg. The invisible area is due to the tail obscuration.

It is showed in the Figure 4-10,4-11, 4-12 and 4-13 that when the pitch angle changes, the fuselage and wing make contributions to the antenna masking.

And also it can be concluded from these figures when the pitch increases, the upper antenna invisible area is increasing. The integrity flag should generate a pitch angle threshold for the upper antenna.

4.4.2 Roll Angle Effect

With change of the roll angle from 0 degree to 180 degree and the pitch and yaw angle to be set in 0 degree, the antenna elevation and azimuth are measured in the TORNADO CATIA model. The following figures each presents the TORNADO both the upper antenna masking matrix when the roll angle is 0^{o}, 45^{o}, 90^{o}, 135^{o} and 180^{o}.

The blue line shows the masking limitations and the red points represent all the satellites with elevation and azimuth.

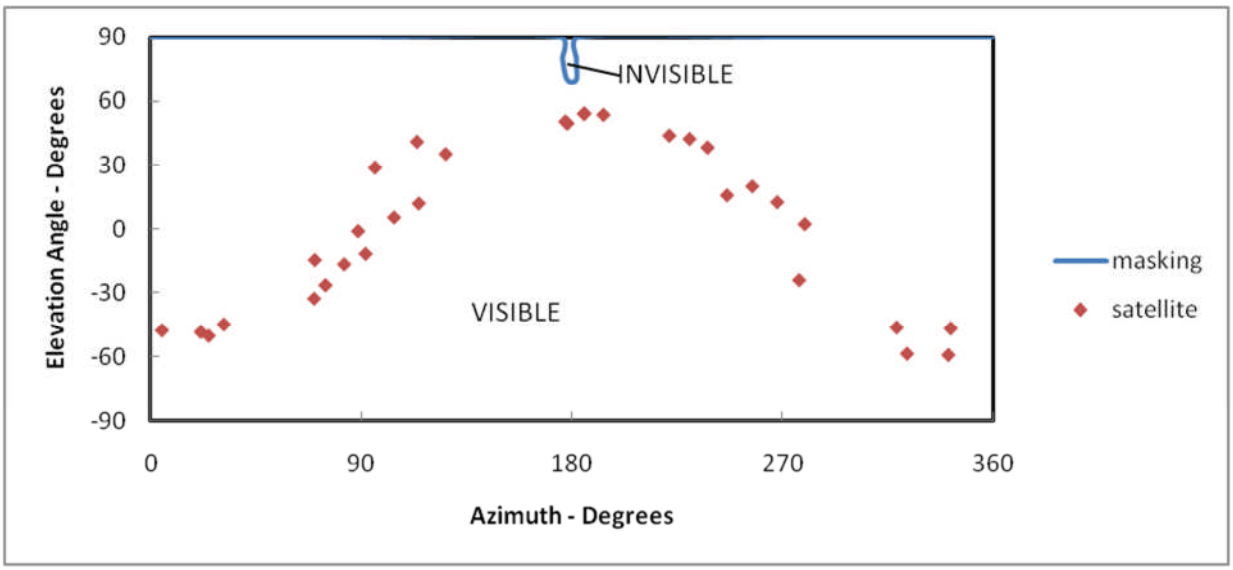

Figure 4-14 upper antenna masking matrix (Roll angle=0^{0})

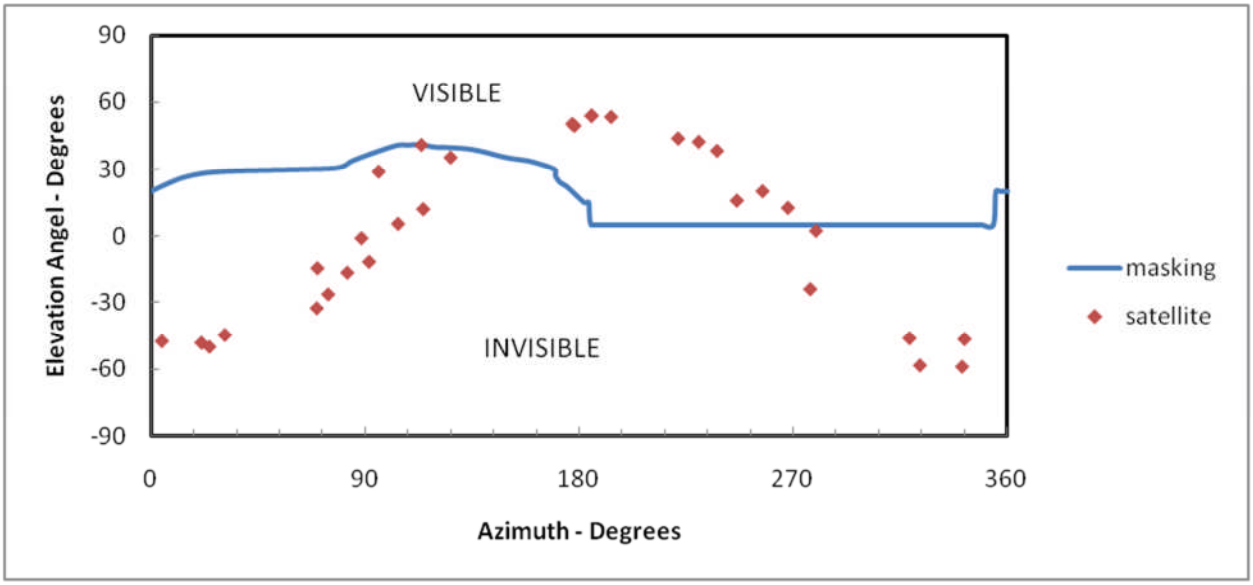

Figure 4-15 upper antenna masking matrix (Roll angle=45^0)

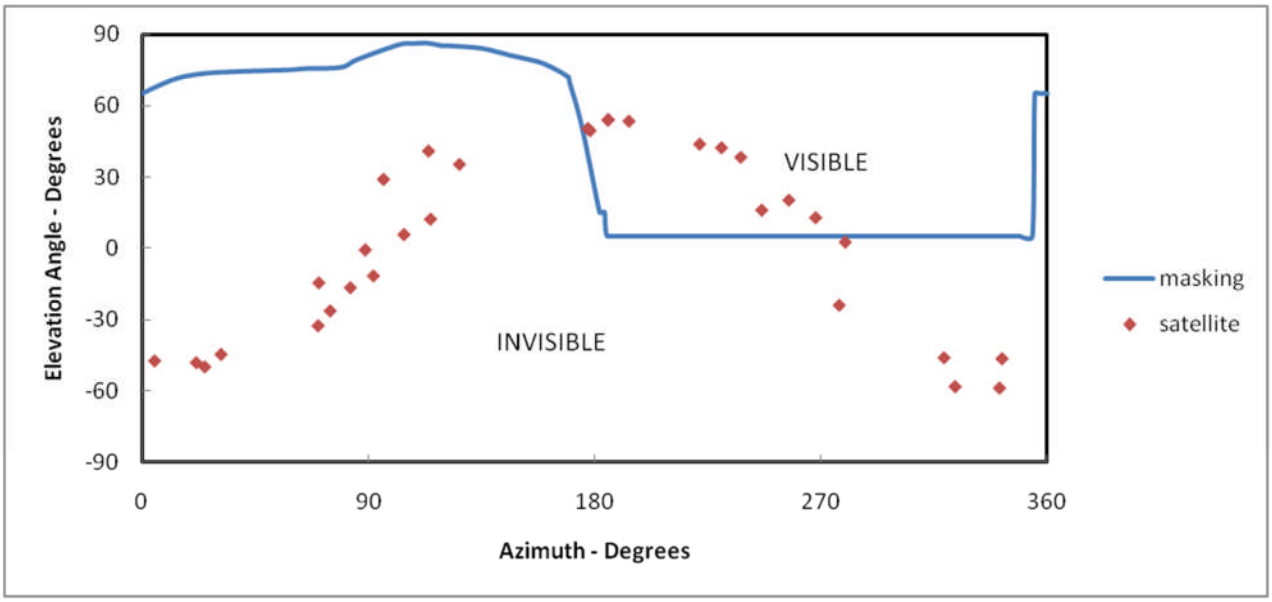

Figure 4-16 upper antenna masking matrix (Roll angle=90^0)

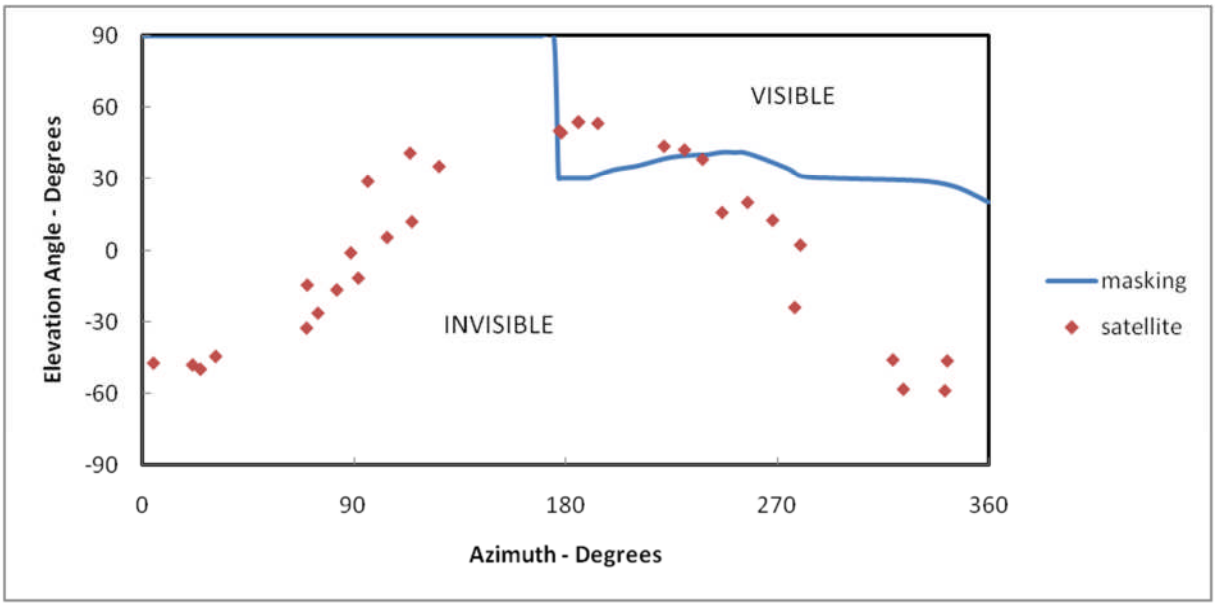

Figure 4-17 upper antenna masking matrix (Roll angle=135^0)

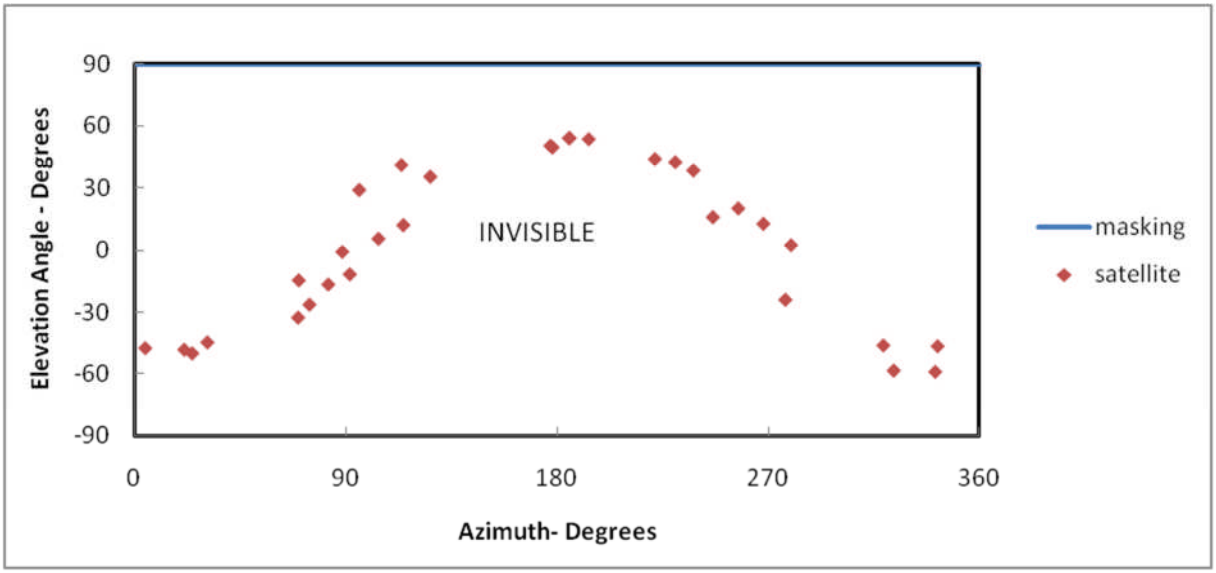

Figure 4-18 upper antenna masking matrix (Roll angle=180^0)

Figure 4-14 shows the TORNADO upper antenna masking matrix when its roll angle is 0 deg. The invisible area is due to the tail obscuration.

It is showed in the Figure 4-15,4-16, 4-17 and 4-18 that when the roll angle changes, one side of the wing makes the most contribution to the antenna

masking. And also it can be concluded from these figures when the roll angle increases, the upper antenna invisible area is increasing. The integrity flag should generate a roll angle threshold for the upper antenna.

4.4.3 Yaw Angle Effect

With change of the yaw angle from 0 degree to 180 degree and the pitch and roll angle to be set in 0 degree, the antenna elevation and azimuth are measured in the TORNADO CATIA model. The following figures each presents the TORNADO both the upper antenna and lower antenna masking matrix when the yaw angle is 0^{o}, 45^{o}, 90^{o}, 135^{o} and 180^{o}.

The blue line shows the masking limitations and the red points represent all the satellites with elevation and azimuth.

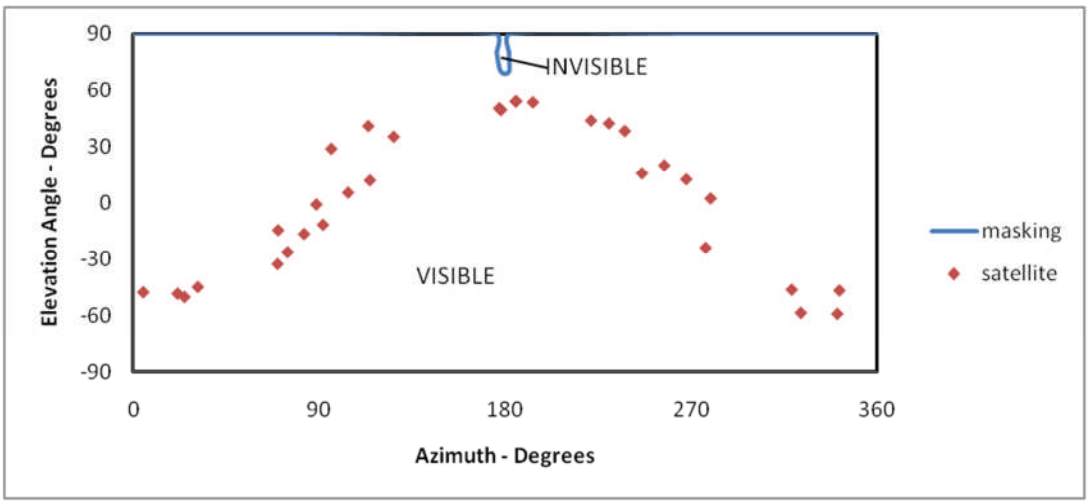

Figure 4-19 upper antenna masking matrix (Yaw angle=0^{0})

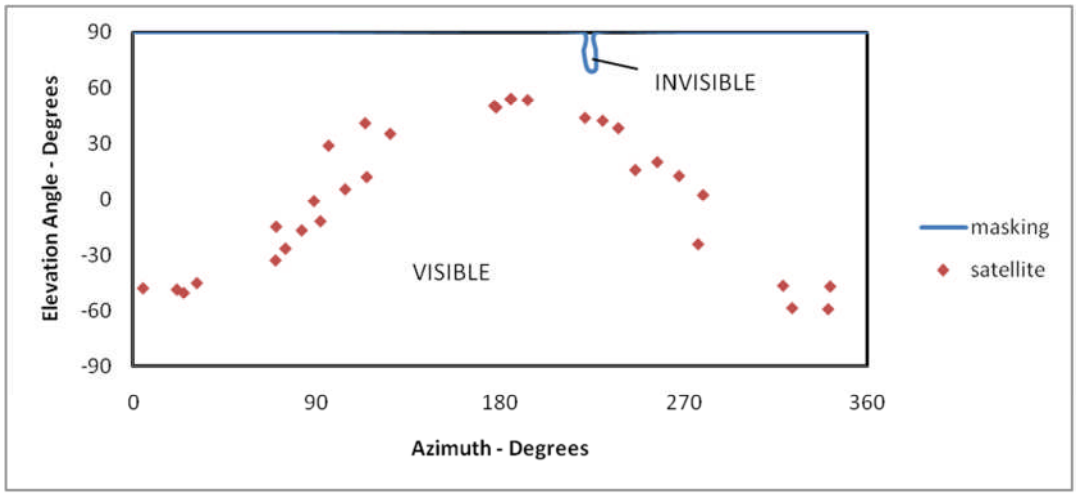

Figure 4-20 upper antenna masking matrix (Yaw angle=45^0)

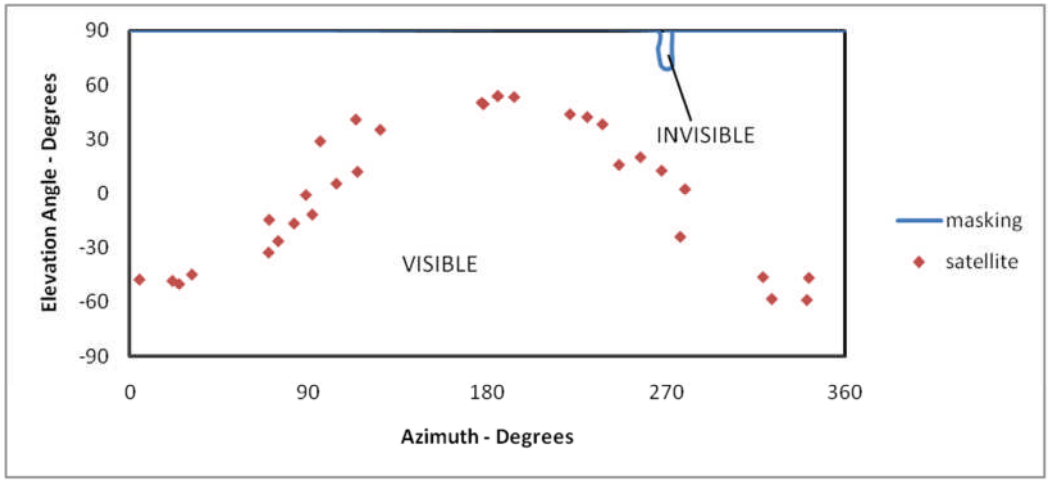

Figure 4-21 upper antenna masking matrix (Yaw angle=90^0)

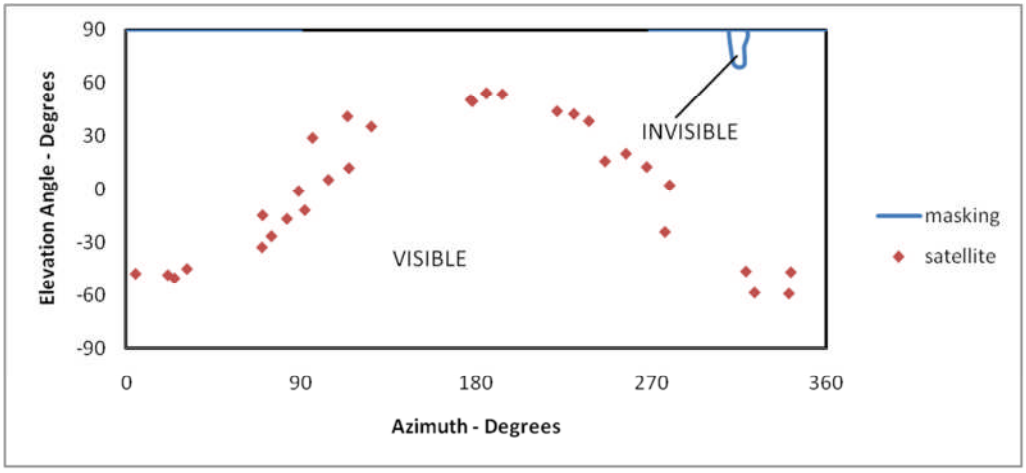

Figure 4-22 upper antenna masking matrix (Yaw angle=135^0)

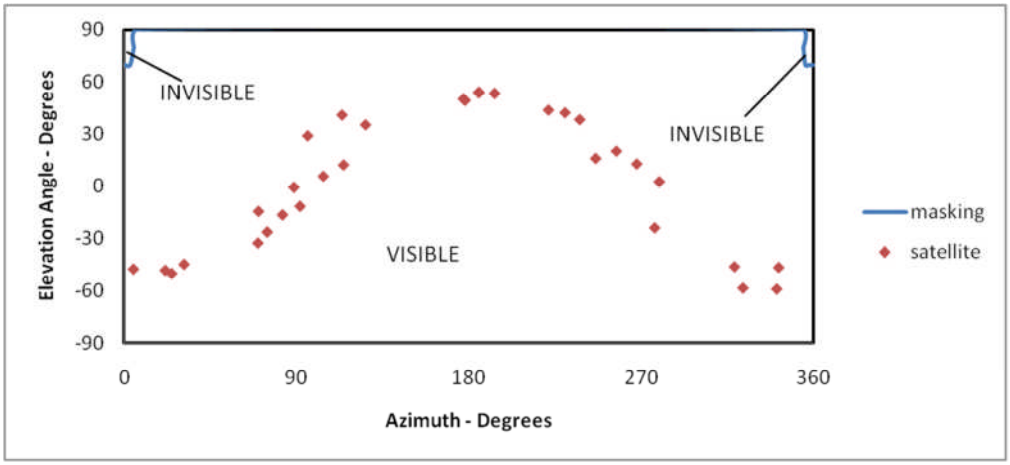

Figure 4-23 upper antenna masking matrix (Yaw angle=180^0)

It is showed in the Figure 4-9,4-10,4-11, 4-12 and 4-13 that when the yaw angle changes, the upper antenna masking matrix changes little. The tail is the only cause of the obscuration.

4.5 Satellite Visibility

4.5.1 Earth Shadow

In the following Figure 4-10 shows that the earth can shadow out the satellite.

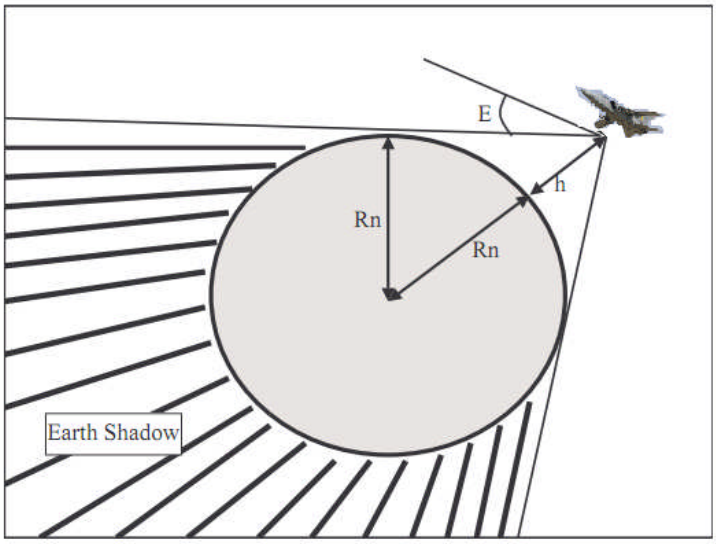

Figure 4-24 Earth shadow

If the elevation between the receiver and satellite is over both the Earth horizon and the receivers elevation mask the satellite is geometrical visible for receiver. The elevation between a receiver and the horizon is approximated through following equation [2, 5]:

$$\mathrm{Elevation}_{\mathrm{sat}}^{\mathrm{horizon}} = \mathrm{acos}\left(\frac{\mathrm{R_n}}{\mathrm{R_n} + \mathrm{h}}\right) \tag{4-40}$$

$$\mathrm{R_n} = \left(\frac{\mathrm{A_{Earth}}}{\sqrt{1 - \mathrm{e}_{\mathrm{Earth}}^2 * \sin^2(\mathrm{lat})}}\right) \tag{4-41}$$

And $\mathrm{R_n}$ is the length of the normal from the ellipsoid surface to its intersection with Z-axes and the attitude of the receiver. h is the length from the same intersection point to the receiver.

$$\mathrm{Elevation}_{\mathrm{sat}}^{\mathrm{horizon}} > 0 degree \tag{4-42}$$

The equation (4-42) shows the situation when the satellite is visible.

4.5.2 ECEF to ENU frame transformation

According to the chapter 3.2, the satellites positions are presented in ECEF frame and the aircraft position is calculated in ENU (East-North-UP) frame in chapter 4.3.But when calculating the satellites visibility and line of sight, they should be in the same ENU frame. So the ECEF to ENU frame transformation matrix is [2]:

$$T_E^N = \begin{bmatrix} -\sin(\lambda) & \cos(\lambda) & 0 \\ -\sin(\varphi) * \cos(\lambda) & -\sin(\varphi) * \sin(\lambda) & \cos(\varphi) \\ \cos(\varphi) * \cos(\lambda) & \cos(\varphi) * \sin(\lambda) & \sin(\varphi) \end{bmatrix} \quad \textbf{(4-43)}$$

Where λ is latitude, φ is longitude.

After getting the results of LOS (line of sight) in ENU frame, the elevation and azimuth can be calculated.

4.5.3 ECEF Frame to Antenna Frame

In order to judge if the satellite is obscured to the antenna, the satellite line of sight with respect to the antenna are necessary.

To get the satellite angles (azimuth, elevation) with respect to the antenna the transformation matrix between ECEF and the antenna must be applied. This transformation is derived using the following equation [2, 5]:

$$T_E^a = T_b^a * T_N^b * T_E^N \quad \textbf{(4-44)}$$

Where T_b^a is the given transformation matrix between the body and the antenna, which is induced in the chapter 3.1. T_N^b is the transformation matrix from ENU to body, and T_E^N matrix (ECEF to ENU) .

$$T_N^b = \begin{bmatrix} \cos(\phi)*\cos(\Psi)+\sin(\phi)*\sin(\gamma)*\sin(\Psi) & -\cos(\phi)*\sin(\Psi)+\sin(\phi)*\sin(\gamma)*\cos(\Psi) & -\sin(\phi)*\cos(\gamma) \\ \cos(\gamma)*\sin(\Psi) & \cos(\gamma)*\cos(\Psi) & \sin(\gamma) \\ \sin(\phi)*\cos(\Psi)-\cos(\phi)*\sin(\gamma)*\sin(\Psi) & -\sin(\phi)*\sin(\Psi)-\cos(\phi)*\sin(\gamma)*\cos(\Psi) & \cos(\phi)*\cos(\gamma) \end{bmatrix} \quad \textbf{(4-45)}$$

Where γ is pitch angle, ϕ is roll angle and Ψ is yaw angle.

4.5.4 Antenna Gain Pattern

The below Figure 4-25 [10] shows the receiver antenna gain pattern.

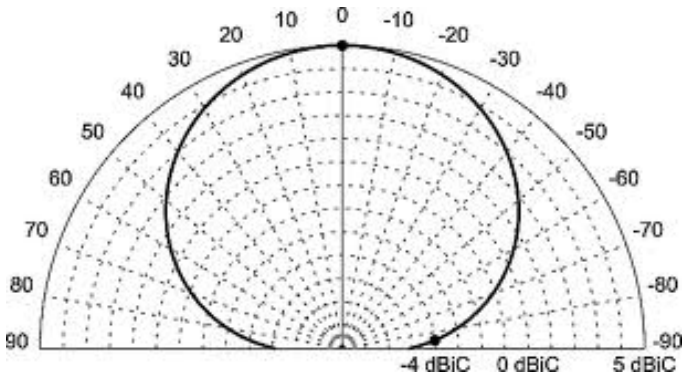

Figure 4-25 Receiver antenna gain pattern[10]

The satellite visibility is decided by the line of sight with respect to the antenna. Note that due to the GPS receiver gain pattern the incoming signal cannot be received below 85 degree from vertical. For the upper antenna, the satellite is visible only when it meets the equation [2, 5]:

$$\text{Elevation}^{\text{sat}}_{\text{upper antenna}} > 5degree \quad \textbf{(4-46)}$$

For the lower antenna, the satellite is visible when meets the equation (4-47):

$$\text{Elevation}^{\text{sat}}_{\text{lower antenna}} < -5degree \quad \textbf{(4-47)}$$

4.5.5 Satellite Visibility Result

The Figure 4-25,4-27,4-29,4-31 show the trajectory of the TORNADO during different flight phase(climb, cruise, turn & descend and landing). They are simulated in the East-North-Up (ENU) frame. The X axis is latitude (degree), the Y axis is longitude(degree), the Z axis is altitude(m).The simulation time is 300s.

With the trajectory model, the satellite visibility can be simulated parallel with the GNSS constellation simulator. The Figure 4-26,4-28,4-30,4-32 show the TORNADO satellite visibility during different flight phase(climb, cruise, turn & descend and landing). They are all simulated in the GPS constellation. The visible satellite number is floating between 6 and 16 during different phases. Usually the number of the visible satellites should at least be 4.

The Figure 4-25 shows the trajectory of the TORNADO during the climb flight phase.

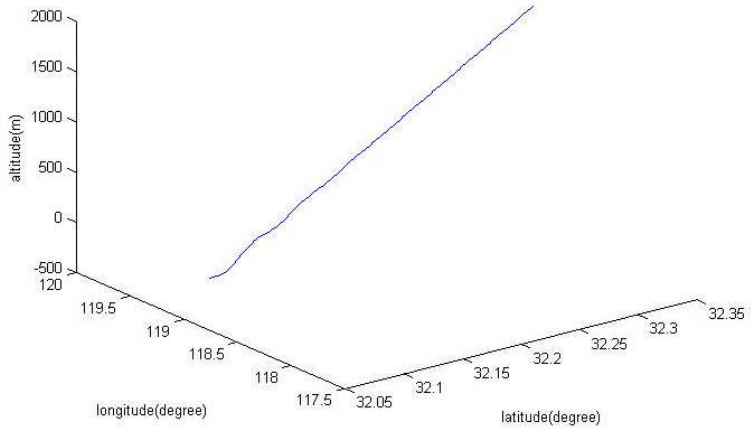

Figure 4-26 Climb trajectory (TORNADO)

The Figure 4-26 shows the TORNADO satellite visibility during the climb phase. There are always 16 satellites in view during the climb phase.

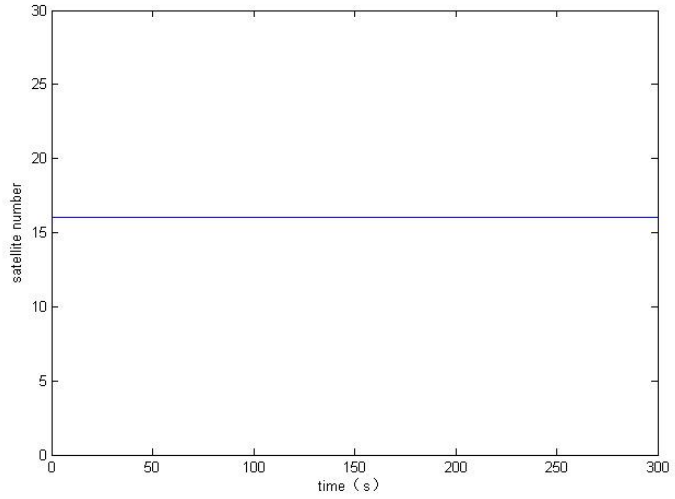

Figure 4-27 Satellite visibility (TORNADO climb phase)

The Figure 4-27 shows the trajectory of the TORNADO during the cruise flight phase.

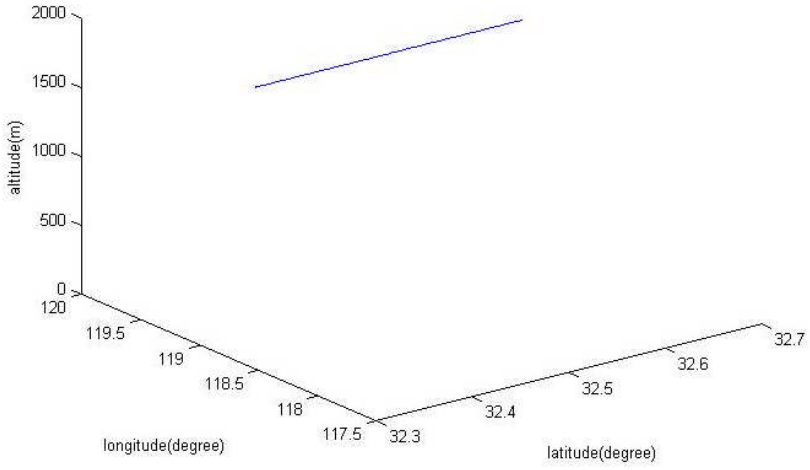

Figure 4-28 Cruise trajectory (TORNADO)

The Figure 4-28 shows the TORNADO GPS satellite visibility during the cruise phase. There are always 16 satellites in view during the cruise phase.

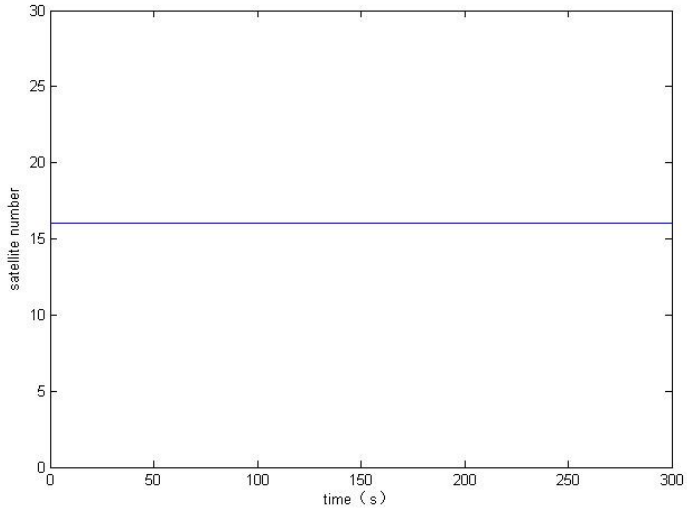

Figure 4-29 Satellite visibility (TORNADO cruise phase)

The Figure 4-27 shows the trajectory of the TORNADO during the turn and descend flight phase.

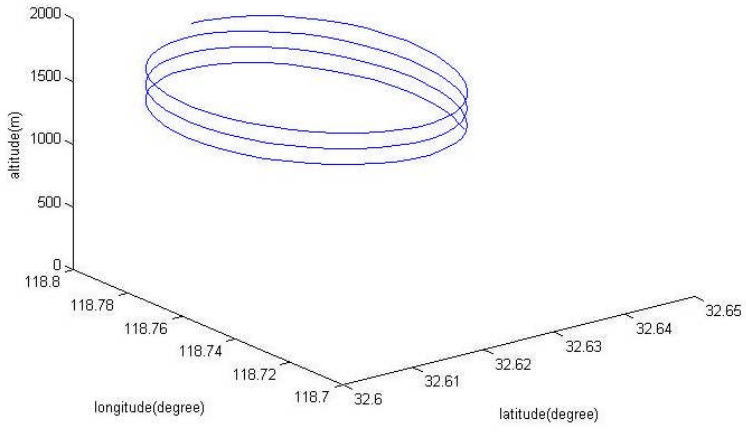

Figure 4-30 Turn and descend trajectory (TORNADO)

The Figure 4-30 shows the TORNADO GPS satellite visibility during the turn and descend phase. The number of satellite in view varies from 7 to 16 during this flight phase.

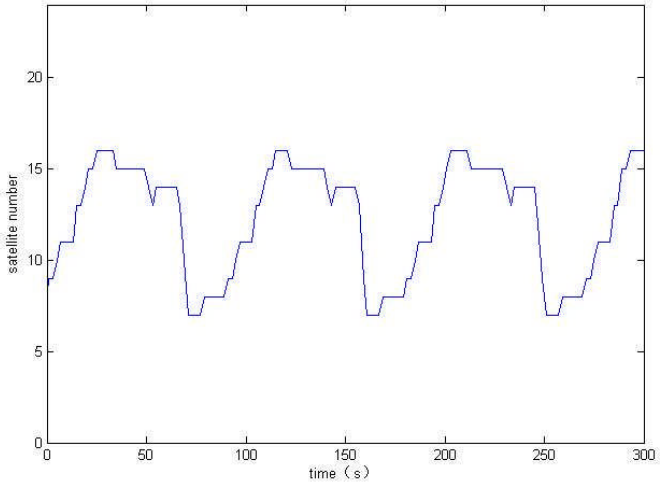

Figure 4-31 Satellite visibility (TORNADO turn&descend phase)

The Figure 4-31 shows the trajectory of the TORNADO during the landing flight phase.

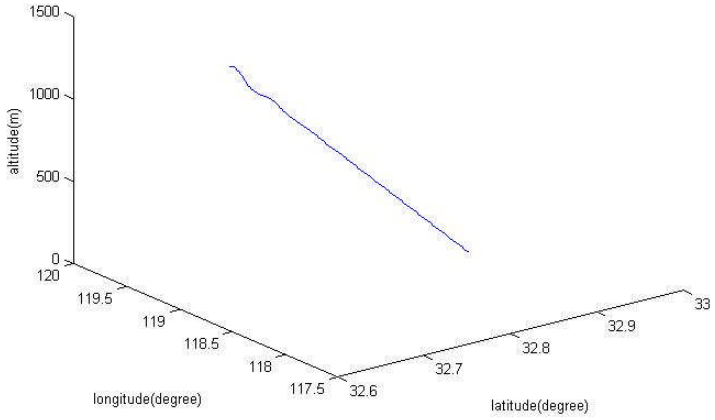

Figure 4-32 Landing trajectory (TORNADO)

The Figure 4-28 shows the TORNADO GPS satellite visibility during the landing phase. There are always 16 satellites in view during the cruise phase.

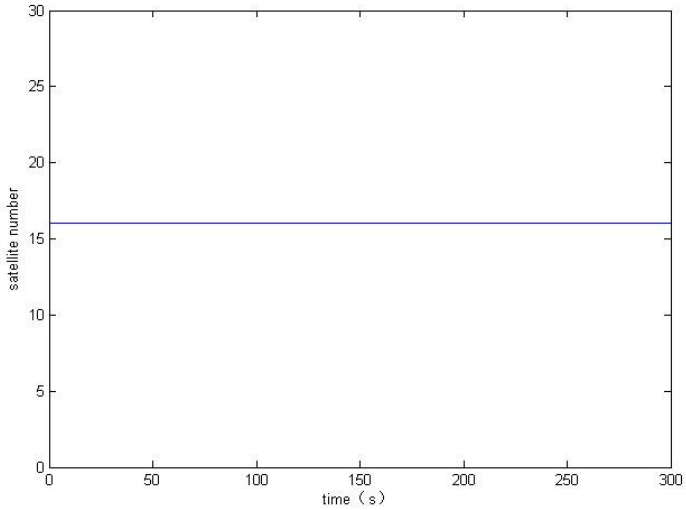

Figure 4-33 Satellite visibility (TORNADO landing phase)

5 FADING

5.1 Introduction

In order to generate the integrity flag, the flag that whether the received GNSS signal power strength is strong enough is very important. It will cause the signal loss when the received signal has low power. And there are some factors make contributions to this fading process. They are known as GNSS antenna gain pattern and the receiver antenna gain pattern, atmospheric effects, inonspheric effects, tropospheric effects and the noise figure.[11] The following Figure 5-1 shows the structure of the fading.

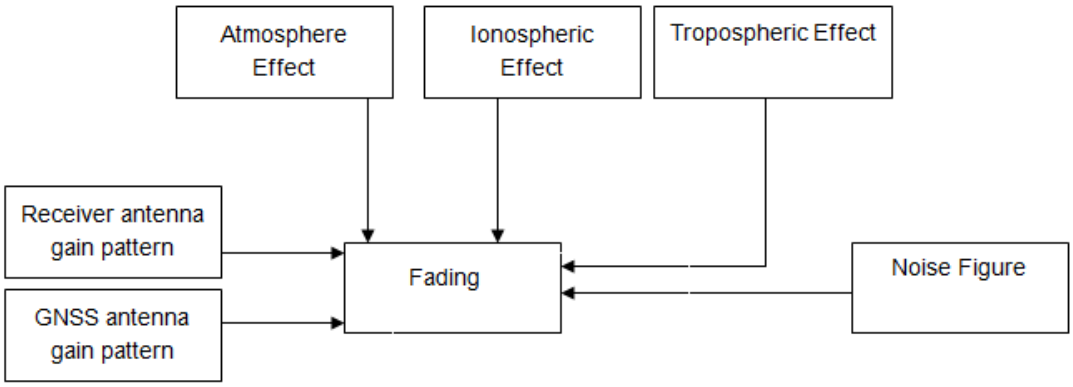

Figure 5-1 Fading structure

In our research the aim is to combine all the factors that make contributions to the fading and do the simulation to generate the fading flag. So in this chapter we bring the SNR (signal to noise ratio) model parallel with the GNSS constellation model and the flight trajectory model to simulate all these fading factors during different flight phases. The SNR model is introduced in the chapter 5.2

The GNSS antenna gain pattern and the receiver antenna gain pattern will influence the signal power. And they are discussed in the following chapter 5.3 and chapter 5.4.

GNSS signal has some perturbations which are known as the inonspheric effects, tropospheric effects and multipath effects.[11] These effects will influence the received signal power and they are discussed in the following chapter 5.5, chapter 5.6, chapter 5.7.The multipath effect is discussed in the chapter 6.

The GNSS system noise figure is also one of the influence on the received signal power. In general, the system noise figure(in dB) is related to system noise temperature(in Kelvin).And the noise figure is discussed in the following chapter 5.8.

The simulation results are presented in the chapter 5.9.

With the simulation results the fading flag is discussed in the chapter 5.9.

5.2 SNR Model

In order to analysis the fading, it is important to simulate the strength of the signal power. In this research the signal-to-noise ratio (SNR) is used to simulate the fading. In practice, the ratio of total carrier power to the noise C/N_0 in dB-Hz is the most generic representation of signal power .The SNR can be induced from some factors below.

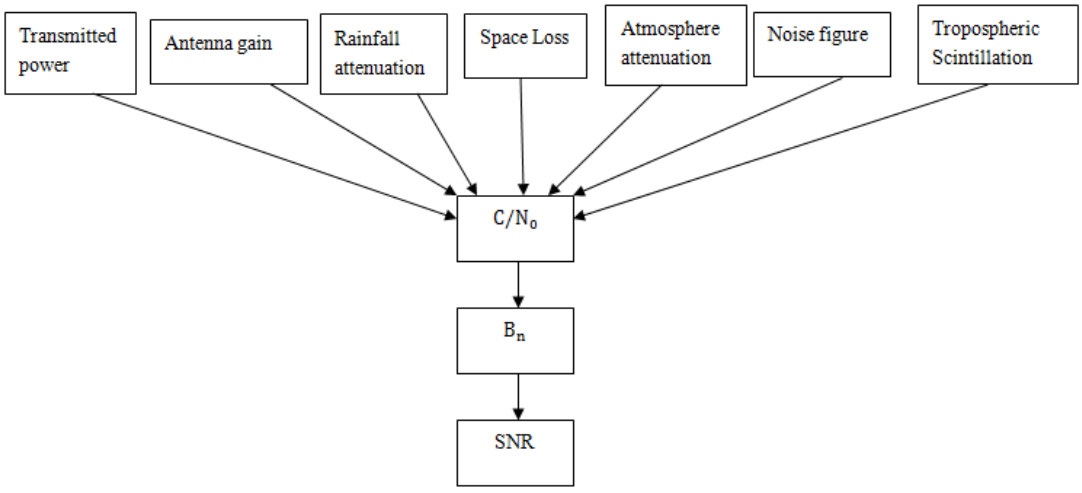

Figure 5-2 SNR structure [2, 5]

The figure 5-2 shows the SNR model structure. An approximation relationship of SNR and C/N_0 can be represented by equation (5-1)[2]

$$\mathrm{SNR(dB)} = \frac{S}{N} = \frac{C}{N_0}(\mathrm{dB-Hz}) - B_n(\mathrm{dB}) \quad \textbf{(5-1)}$$

B_n, Bandwidth of the filter in the receiver to move out of band noise

$$\frac{C}{N_0} = P + G_T + G_R + SL - L_1 - L_2 - \sigma_m - N_F(\mathrm{dB}) \quad \textbf{(5-2)}$$

P-transmitted power

G_T-satellite antenna gain pattern, which will be discussed in the chapter 5.3.

G_R-receiver antenna gain pattern, which will be discussed in the chapter 5.4.

SL-Free Space Loss=(wave length/4πdistance)^2

L_1- The atmospheric attenuation, which will be discussed in the chapter 5.7.1.

L_2- The rainfall attenuation, which will be discussed in the chapter 5.7.2.

σ_m- Tropospheric Scintillation, which will be discussed in the chapter 5.7.3.

N_F-noise figure, which will be discussed in the chapter 5.8.

5.3 Satellite Antenna Gain Pattern

The L-band antenna on board the GPS satellite is designed to radiate the composite L-band signals to the users on and near Earth. It provides a nearly constant signal level to the user receivers over the whole Earth coverage with circular polarization at L1, L2, and L3 frequencies. From the GPS satellite altitude, the view angle from edge-to-edge of Earth is about 27.7 deg. As it can be seen from the following Figure 5-3. [2]

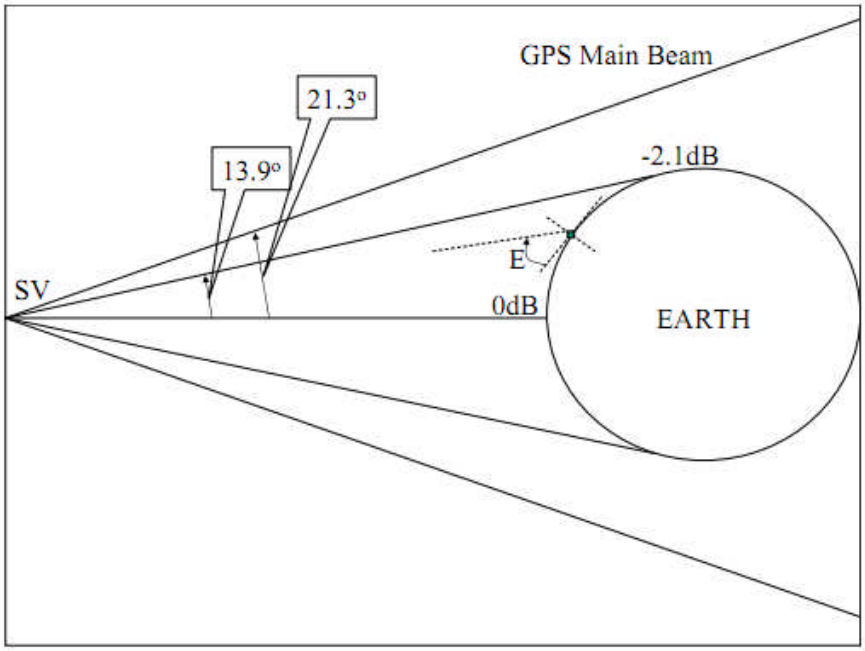

Figure 5-3 GPS Satellite antenna gain pattern [11]

The goal of the antenna is to illuminate the Earth's surface in view of the satellite with almost uniform signal strength. The path loss of the signal is a

function of the distance from the antenna phase centre to the surface of the Earth. The path loss is minimum when the satellite is directly overhead (satellite at 90deg elevation), and is maximum at the edge of Earth coverage (satellite at horizon.)The difference in path loss caused by this variation in path length is about 2.1 dB.

The antenna gain can be simply induced from graph of y=sinx:[2]

$$\mathrm{Gain(dB)} = \mathrm{k} * \mathrm{sinE} + \mathrm{m} \quad \textbf{(5-3)}$$

The GPS satellite antenna gain can be derived [2]

$$\mathrm{G_T(dB)} = 2.5413 * \mathrm{sinE} - 2.5413 \quad \textbf{(5-4)}$$

In equation (5-4) E is the angle between the satellite zenith angle and the receiver, in radians.

5.4 Receiver Antenna Gain Pattern

“The GPS antenna shall accept the GPS navigation signals at both the L1 and L2 frequencies and output them to the GPS antenna electronics.”[12]

The receiver antenna gain pattern is specified as follows:[13]

>.-1 dBic to 75 deg from vertical

>.-2.5 dBic to 80 deg from vertical

>.-4.5 dBic to 85 deg from vertical

>.-7.5 dBic to 90 deg from vertical

The receiver antenna gain also use the simple approximation for antenna gain pattern using the equation (5-3), and the receiver gain pattern is derived in equation(5-5):[2]

$$G_R(dB) = 7.8659 * \sin E - 7.3659 \quad \textbf{(5-5)}$$

5.5 Inonspheric Effects

The major effects the ionosphere can have on GNSS are the following:[14]

1. range error;
2. carrier phase error;
3. Doppler shift ;
4. Faraday rotation of linearly polarized signals;
5. refraction or bending of the radio wave;
6. distortion of pulse waveforms;
7. signal amplitude fading or amplitude scintillation;
8. phase scintillations.

In our research in order to generate the integrity flag , we have to simulate the SNR considering about the 7th effect which is the amplitude scintillation. It is introduced in the chapter 5.5.1.

5.5.1 Amplitude Scintillation

Fading of the amplitude of the received signal, is caused by irregularities of scale size from hundreds of meters to kilometres in the electron density of the ionosphere.

Note that rapid fading of signal on both the GPS frequency. Some of the fades exceeded the average signal-to –noise ratio of the GNSS receiver then in use, which was 20dB.[14]

Fortunately, the strong scintillation effects are all observed in the near-equatorial regions.[14] In this research ,the location of the simulation is set in london where the ionospheric scintillation fading effect is very small. So in this research the ionospheric scintillation effect is ignored.

5.6 Tropospheric Effects

5.6.1 Atmospheric Attenuation

Atmospheric attenuation in the 1-2 GHz frequency band is dominated by oxygen attenuation, but even this effect normally is small. The attenuation is on the order of 0.035dB for a satellite at zenith.[15] However, it can be ten times larger(in dB) at low elevation angles. The effects of water vapour, rain, and nitrogen attenuation at frequencies in the GNSS frequency bands are negligible [16].

Oxygen attenuation A(E) in dB for the 1.5 GHz frequency range is approximately 0.035dB at zenith (E=90deg) and varies with elevation angle E in proportion to the tropospheric path length L(obliquity factor or mapping function). If the troposphere is modelled by a simple uniform spherical shell of height h_m with elevation angle E, as shown in the Figure 5-5.

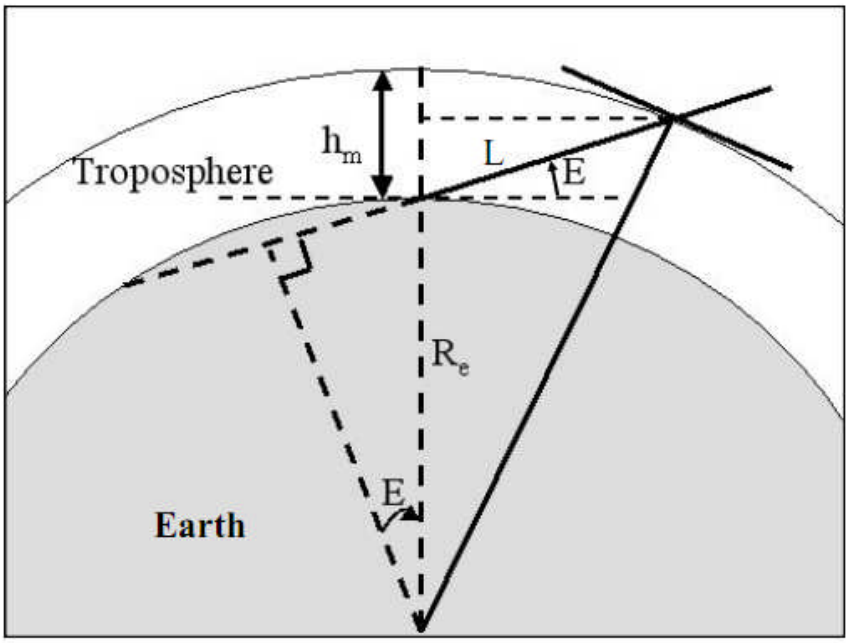

Figure 5-4 Atmospheric Attenuation

Thus, A (E) has the following approximate value [16]:

$$A(E) \cong \frac{2A\left(\frac{\pi}{2}\right)\left(1+\frac{a}{2}\right)}{\sin E + \sqrt{\sin^2 E + 2a + a^2}} = \begin{cases} \frac{2A(90\ \text{deg})}{\sin E + 0.043}\ \text{dB for small E but} > 3\ deg \\ \frac{A(90\text{deg})}{\sin E}\ \text{dB for E} > 10\ deg \end{cases} \quad \textbf{(5-6)}$$

Where $a = \frac{h_m}{R_e} \ll 1$ and h_m is the equivalent height for oxygen, h_m =6km,and R_e is the Earth radius $R_e \cong 6378$km.

5.6.2 Rainfall Attenuation

For a frequency of 2 GHz, the attenuation even for dense, 100 mm/h rainfall, is less than 0.01 dB/km; thus, it has a very small effect. Rainfall attenuation below 2 GHz is even less; thus, rain attenuation is of little consequence in the

frequency bands of interest for GPS, 1.57542 GHz and 1.2276 GHz. The following Figure 5-6 shows the rainfall attenuation vs elevation in degree.[16]

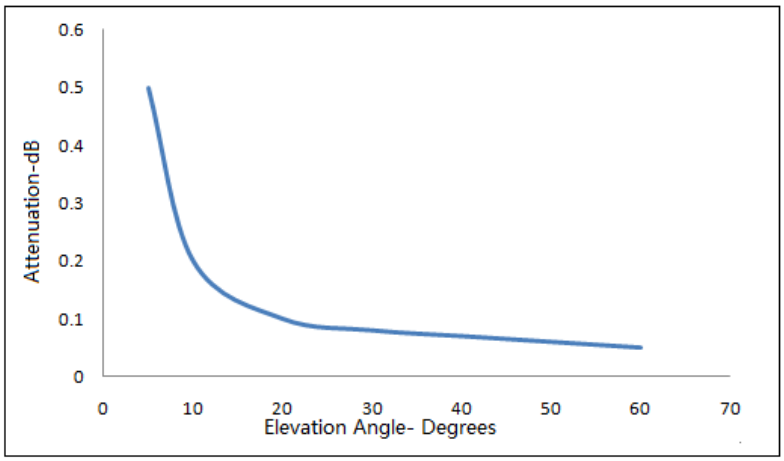

Figure 5-5 Rainfall Attenuation vs elevation in degrees [16]

5.6.3 Tropospheric Scintillation

Tropospheric scintillation is caused by irregularities and turbulence in the atmospheric refractive index primarily in the first few kilometres above the ground. The scintillation effect varies with time and is dependent upon frequency, elevation, angles above 10 deg, the predominant effect is forward scattering caused by atmospheric turbulence. At GPS frequencies, these effects are generally relatively small except for a small fraction of the time and at low elevation angles.

The CCIR(1982) [16] has given an expression for the long-term mean value of scintillation intensity σ_x. For small antennas such as omnidirectional GPS antennas, the CCIR expression for the long-term rms amplitude scintillation varies with frequency and elevation angle as follows [2, 16]:

$$\sigma_m = 0.025 f^{\frac{7}{12}} (\csc E)^{-0.85} \text{dB} \quad \textbf{(5-7)}$$

Where f is in GHz, and the elevation angle is E. For L1=1.57542GHz we have the following [2, 16]

$$\sigma_m = 0.0326 (\csc E)^{-0.85} \text{dB} \quad \textbf{(5-8)}$$

Thus, for low elevation angles and small fractions of time, tropospheric scintillation can be significant, but otherwise it is quite small.

5.7 Noise Figure

The GNSS system noise figure (in dB) is related to system noise temperature (in Kelvin) as follows [2, 17]:

$$NF = 10 \log_{10}(1 + \frac{T_{sys}}{T_0}) \quad \textbf{(5-9)}$$

Where T_0=290K=24.6 dB-K.

The corresponding noise density, in W/Hz, is $N_0 = K_B T_{sys}$; where K_B = -228.6dBW/K-Hz=1.380× 10^{-23}W/K-Hz, is the Boltzmann constant [17].

When the receiver is connected directly to a GPS signal generator or simulator, in which the source temperature is the ambient noise temperature (290K). Normally, adjustments to the signal power must be made to compensate for this. Note that in this case, if the first stage gain is high enough, the noise density is simply as following equation [2, 17]

$N_0 = K_B T_0 NF_1$=-228.6+24.6+NF_1(dB)=-204dBW/Hz+ NF_1(dB) **(5-10)**

Sometimes this equation is erroneously used for “real-world” computations, providing pessimistic analysis results. A source temperature of 75-100 K is typical, depending on the antenna pattern and the measured temperature on earth.[18]

5.8 SNR Simulation Result

According to the SNR model, the simulation is generated in matlab. And the following figures show the different satellite SNR results during TORNADO different flight phases. The Y axis is the signal to noise ratio C/N_0 (dB-Hz). The X axis is the simulation time. It is 300s.

Figure 5-7 shows the signal to noise ratio C/N_0 (dB-Hz) of Prn.1 GPS satellite during TORNADO climb phase.

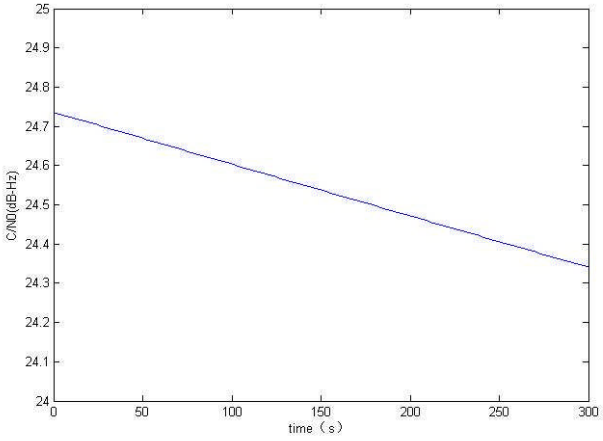

Figure 5-6 Prn.1 GPS satellite C/N_0 (TORNADO climb phase)

Figure 5-8 shows the signal to noise ratio C/N_0 (dB-Hz) of Prn.1 GPS satellite during TORNADO cruise phase.

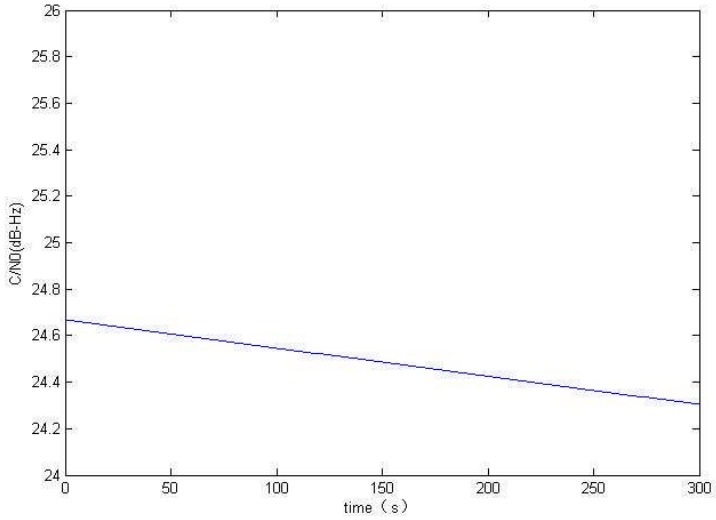

Figure 5-7 Prn.1 GPS satellite SNR (TORNADO cruise phase)

Figure 5-9 shows the signal to noise ratio C/N_0 (dB-Hz) of Prn.1 GPS satellite during TORNADO turn and descend phase.

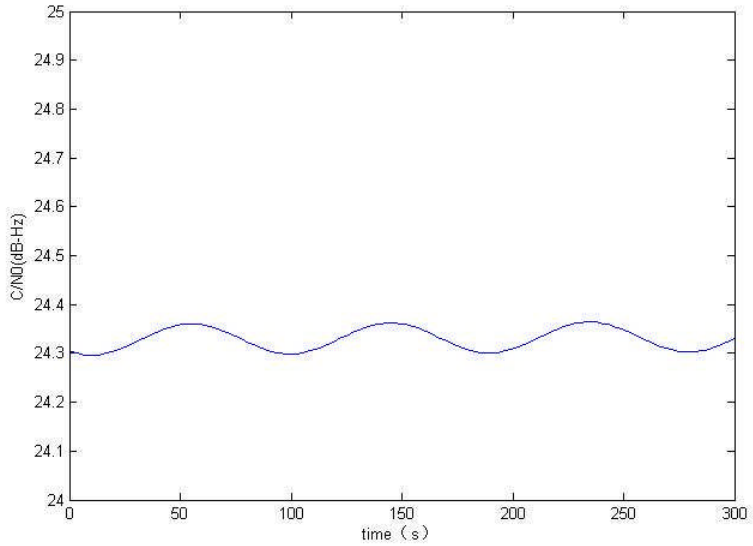

Figure 5-8 Prn.1 GPS satellite SNR (TORNADO turn and descend phase)

Figure 5-10 shows the signal to noise ratio C/N_0 (dB-Hz) of Prn.1 GPS satellite during TORNADO landing phase.

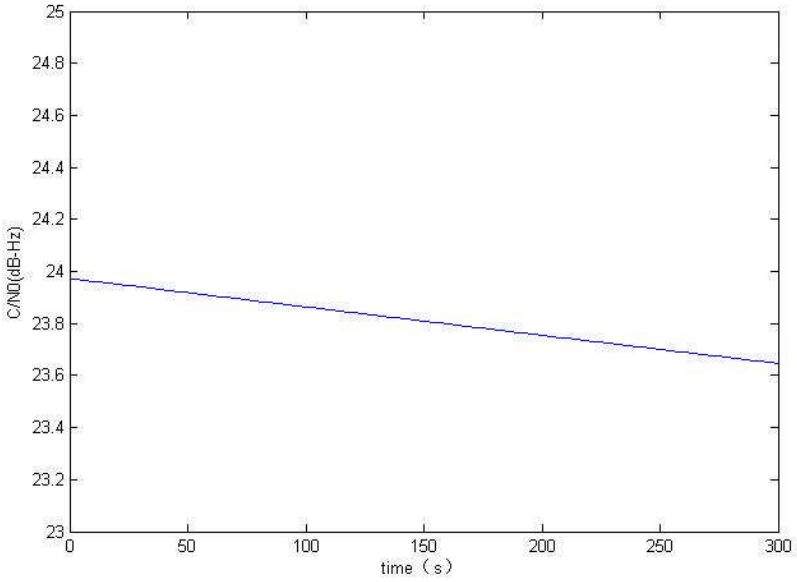

Figure 5-9 Prn.1 GPS satellite SNR (TORNADO landing phase)

6 MULTIPATH

6.1 Introduction

The multipath effect is caused by the interference of multiple reflections with the direct signal transmitted by the satellite, and represents a considerable source of error in the GNSS carrier phase observations.

The level and characteristics of the multipath effect depends on the geometry of the surrounding of the receiver antenna, the reflectivity of the nearby objects and the satellite's elevation angle. In order to built the multipath model, the geometric optics method is brought in. We use the aircraft 3D CATIA model to identify the geometric of the multipath path. In our research we use SNR and geometric ray tracing to analysis the multipath effect [2, 19]

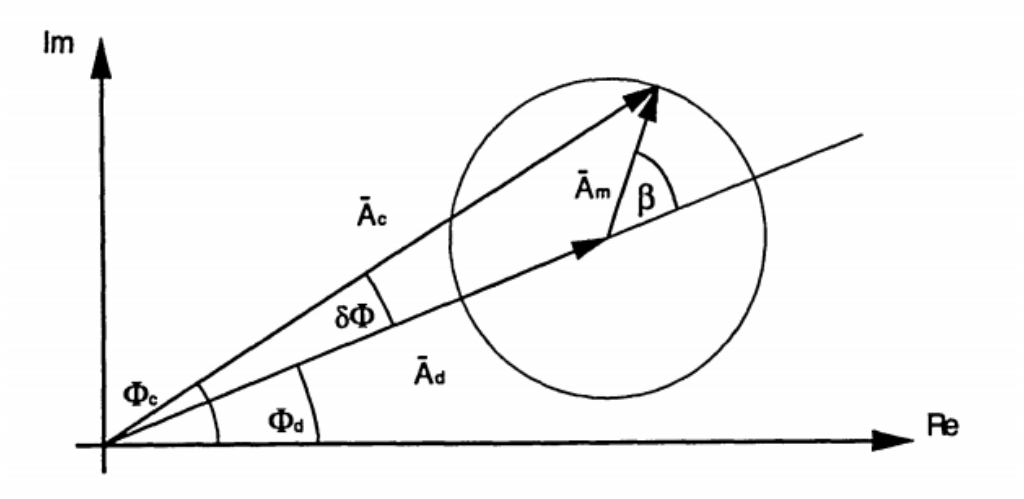

Figure 6-1 Phase of GPS signal [2, 5]

From figure 6-1, SNR or the received signal amplitude and phase error of a reflection signal can be calculated from the amplitudes of direct signal and multipath signal and the multipath signal phase β [2, 20]

$$\mathrm{SNR} = \mathrm{A_c^2} = \mathrm{A_d^2} + \mathrm{A_m^2} + 2\mathrm{A_d}\mathrm{A_m}\cos\beta \quad \textbf{(6-1)}$$

$$\tan(\delta_\phi) = \frac{\mathrm{A_m}\sin\beta}{\mathrm{A_d} + \mathrm{A_m}\cos\beta} \quad \textbf{(6-2)}$$

Where $\mathrm{A_d}$ is thedirect signal amplitude, $\mathrm{A_m}$ is the reflection signal amplitude, β is the phase of the multipath signal.

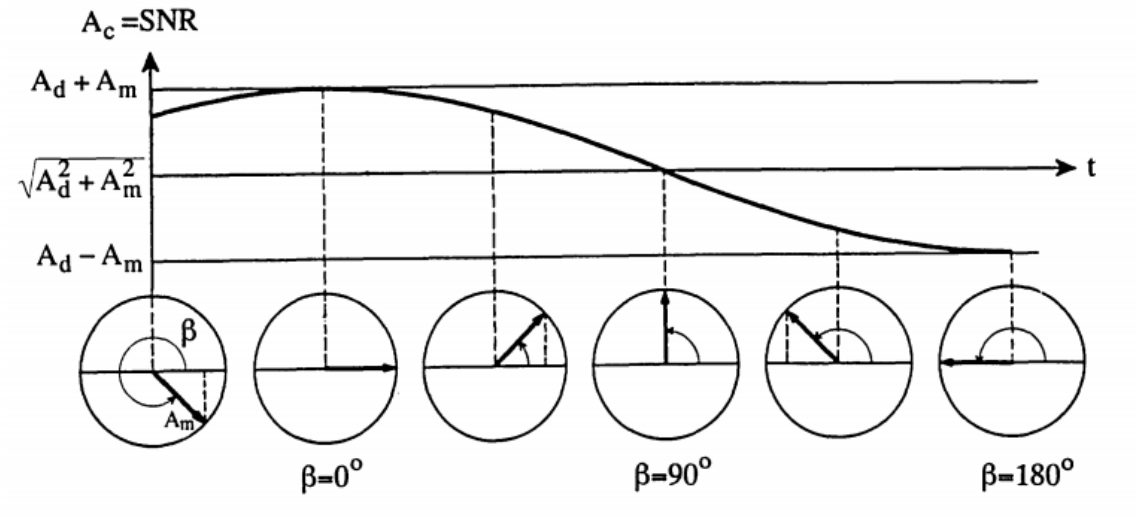

Figure 6-2 Variation of Ac as function of the angle β [2, 5]

The Figure 6.2 shows the multipath phase β and the multipath signal amplitude will influence the received signal. In this research our aim is to build the multipath model to simulate these two factors.

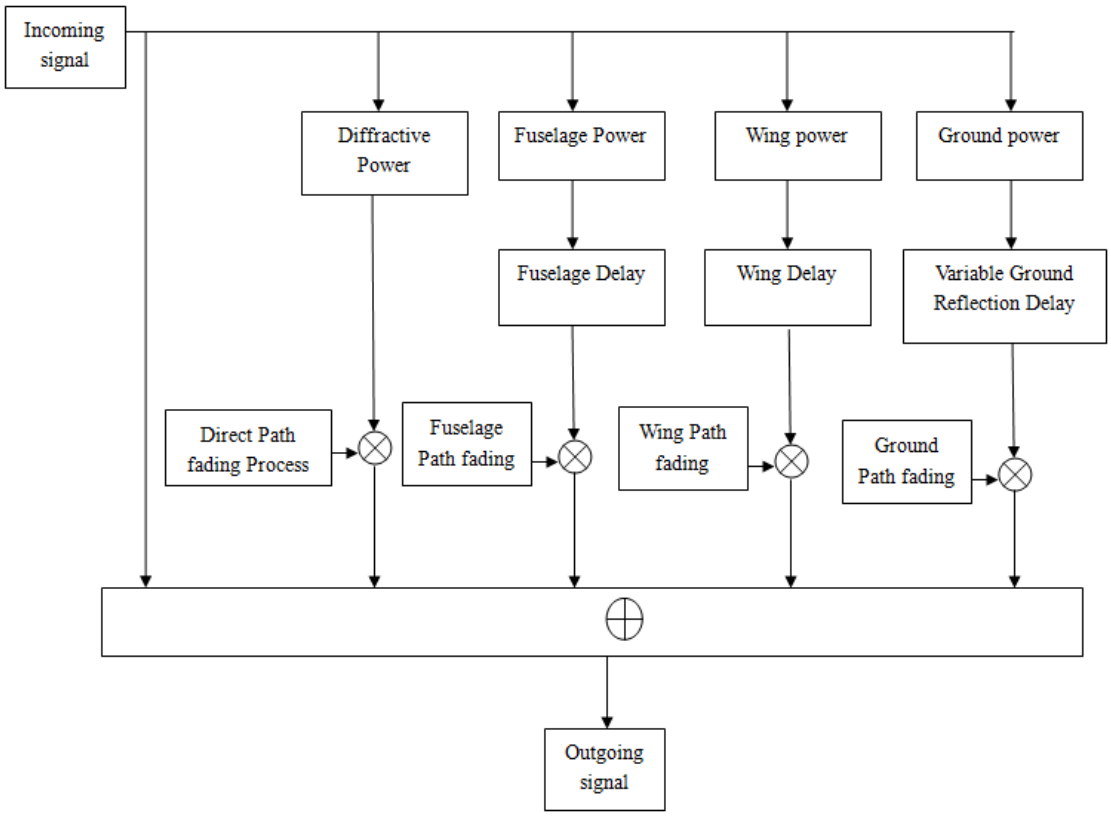

Figure 6-3 Multipath channel model [2, 5]

The Figure 6-3 above shows the multipath channel model. h(t,τ) is the impulse response of the mutipath. Then h(t,τ) is given by [19]

$$h(t,\tau) = 1 + \sum_{i=1}^{3} \sqrt{P_i} * n_i(t) * \delta(t - \tau_i) \quad \textbf{(6-3)}$$

Where P_i is the ith path signal power. The signal $n_i(t)$ is a noise signal, and a power spectral density $N(f)$:[19]

$$N(f) = \begin{cases} 0 & f < -B/2 \\ \frac{1}{B} & -B/2 < f < B/2 \\ 0 & f > B/2 \end{cases} \quad \textbf{(6-4)}$$

Where B is the noise bandwidth. In our research it is considered to be 20Hz.

From the multipath channel model Figure 6-3, the wing reflection, the fuselage reflection and the ground echo are the main paths of the multipath signal. They are discussed in the following chapters.

6.2 Geometric Ray Tracing

Figure 6-4 shows the geometric Ray Tracing theory model. The incoming wave is considered to be located T, a receiver at location R, and the reflection point at S. Location V is a defined point on the reflecting surface and n stands for a unit vector normal to the surface.

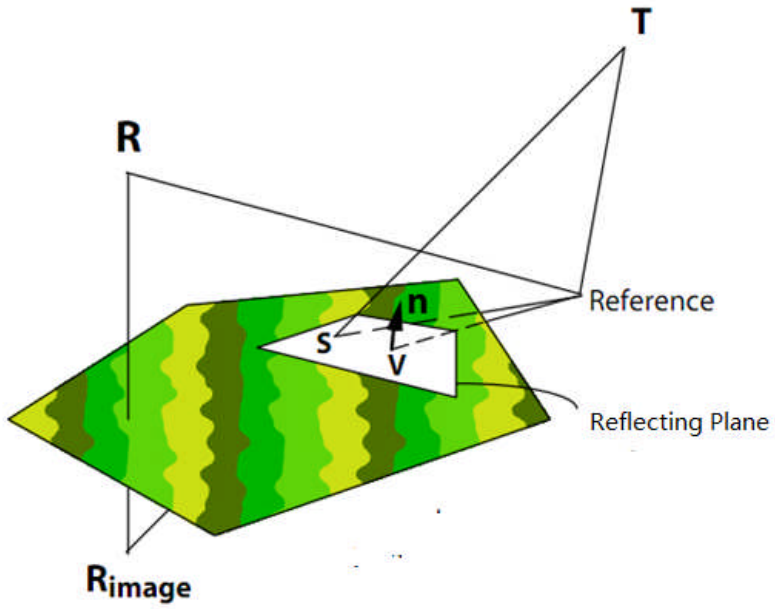

Figure 6-4 Geometric Ray Tracing Model [2, 5]

In geometric ray tracking theory, the reflection point S and the defined point V should satisfy the equation:

$$(\mathbf{S}-\mathbf{V})\times\mathbf{n}=0 \tag{6-5}$$

And the line equation connecting T and$\mathrm{R}_{\mathrm{image}}$:

$$\mathbf{S} = \mathbf{T} + \mathrm{t} \times \left(\mathbf{R_{image}} - \mathbf{T}\right) \tag{6-6}$$

Where t is a parameter between 0 and 1. Then combine the equation (6-5) and (6-6):

$$\mathbf{S} = \mathbf{T} + \frac{\mathbf{n} \times \mathbf{V} - \mathbf{n} \times \mathbf{T}}{\mathbf{n} \times \left(\mathbf{R_{image}} - \mathbf{T}\right)} \left(\mathbf{R_{image}} - \mathbf{T}\right) \tag{6-7}$$

In this research, the point S should be within the region of the aircraft (wing or fuselage), or the reflection signal from this path cannot be received.

The extra path length, L_{mS} , is then:

$$\mathrm{L}_{\mathrm{mS}} = |\mathbf{T} - \mathbf{S}| + |\mathbf{R} - \mathbf{S}| - |\mathbf{T} - \mathbf{R}| \tag{6-8}$$

The extra path is used to calculate the time delay.

6.3 Wing Reflection

6.3.1 Wing Reflection Model

From the geometric ray tracing analysis, the wing reflection model should consider two different cases because of different wing types: upper wing and lower wing.

Most civil aircraft has lower wing. According to the ESA-SDS research[19] , the wing reflect multipath signal can be neglected.

Some military aircraft has upper wing, and their wings also reflect the signal to the antenna. In this research, the TORNADO will be the model to simulate the wing reflection.

In the wing reflection model the wing is assumed to be flat. By Gaussian Doppler Spectrum theory, the power of wing echo spectrum is assumed:[21]

$$P_{Gr(dB)} = 20 * \log_{10}\left(\frac{1}{\sqrt{2\pi\sigma^2}} * e^{-\frac{f^2}{2\sigma^2}}\right) \quad \textbf{(6-9)}$$

Where the deviation σ=3.8Hz.[19]

The wing reflection echo delay can be calculated in the equation (6-10) as function of the elevation.

$$\tau_{wing}(t) = \frac{2 * L * \sin(E)}{C_0} \quad \textbf{(6-10)}$$

Where L is the antenna height from the wing and E is the elevation angle. C_0 is the speed of light.

Also through the analysis of the TORNADO 3D model, there are some limitations of the position of the satellites on the wing reflection model. And Table 6-1 shows the wing reflection model the limitations of satellites azimuth and elevation angles.

Table 6-1 Limitations of azimuth and elevation angles.(wing reflection model)

Azimuth (degrees)	Elevation (degrees)
62~142&118~298	5~23

6.4 Fuselage Reflection

According to the ESA-SDS research [19], the main multipath signal is coming from the fuselage reflection.

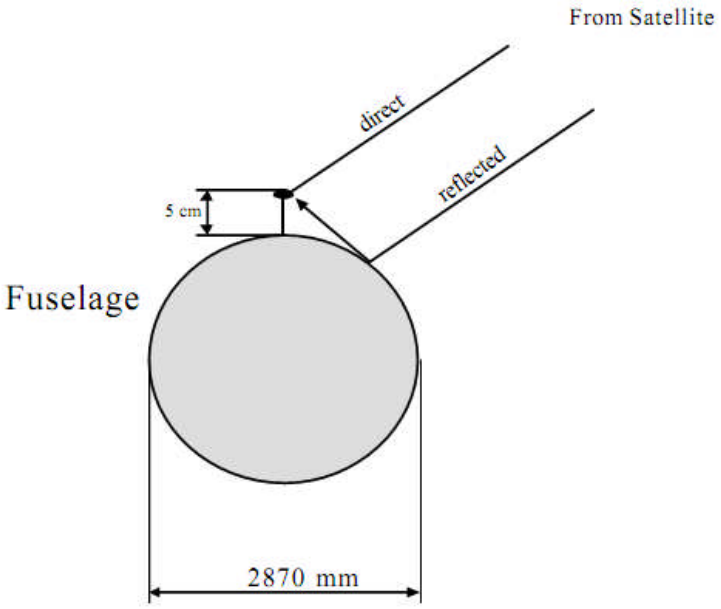

Figure 6-5 Fuselage reflection [2, 19]

In the fuselage reflection model the fuselage is assumed to be a cylinder. The equation (6-5) shows the power of fuselage echo spectrum [21]

$$P_{proc}(dB) = 20 * \log_{10}(k + b_2 * e^{b_3 * |f|}) \quad \textbf{(6-11)}$$

Where b_2 and b_3 are the fuselage coefficients.

The overall power had been calculated by SNR model which determines the constant k.

$$k = -SNR - mean\ [dB] \quad \textbf{(6-12)}$$

ESA-SDS research [19] results show that with the change of the fuselage radius, fuselage coefficients change very little.

For easier implementation of the fuselage reflection a parameter (mean, b2, b3) is fitted [2, 19]

$$\mathrm{mean}(\varepsilon,\varphi) = [\varepsilon^4 \quad \varepsilon^3 \quad \varepsilon^2 \quad \varepsilon \quad 1] * \mathrm{A}_{\mathrm{mean}} * \begin{bmatrix} \varphi^4 \\ \varphi^3 \\ \varphi^2 \\ \varphi \\ 1 \end{bmatrix} \tag{6-13}$$

$$\mathrm{A}_{\mathrm{mean}} = \begin{bmatrix} -2.0057\mathrm{e}-12 & 5.0499\mathrm{e}-10 & -4.6114\mathrm{e}-8 & 1.8053\mathrm{e}-6 & -2.4773\mathrm{e}-5 \\ 2.8598\mathrm{e}-10 & -7.4259\mathrm{e}-8 & 7.0553\mathrm{e}-6 & -2.9116\mathrm{e}-4 & 0.0043 \\ -1.1568\mathrm{e}-8 & 3.2474\mathrm{e}-6 & -3.3846\mathrm{e}-4 & 0.0156 & -0.2698 \\ 3.8681\mathrm{e}-8 & -2.2536\mathrm{e}-5 & 0.0038 & -0.2512 & 6.3140 \\ 1.9434\mathrm{e}-6 & -3.5747\mathrm{e}-4 & 0.0133 & 0.8133 & -28.1329 \end{bmatrix} \tag{6-14}$$

$$\mathrm{A}_{\mathrm{b}_3=} \begin{bmatrix} -1.8398\mathrm{e}-12 & 4.2182\mathrm{e}-10 & -3.3813\mathrm{e}-8 & 1.8055\mathrm{e}-6 & -1.0875\mathrm{e}-5 \\ 2.6665\mathrm{e}-10 & -6.0897\mathrm{e}-8 & 4.8490\mathrm{e}-6 & -1.5346\mathrm{e}-4 & 0.0015 \\ -1.2870\mathrm{e}-8 & 2.9171\mathrm{e}-6 & -2.2947\mathrm{e}-4 & 0.0071 & -0.0629 \\ 2.3542\mathrm{e}-7 & -5.2520\mathrm{e}-5 & 0.0040 & -0.1193 & 0.9153 \\ -1.2058\mathrm{e}-6 & 2.5797\mathrm{e}-4 & -0.0187 & 0.5027 & -4.1128 \end{bmatrix} \tag{6-15}$$

$$\mathrm{A}_{\mathrm{b}_2} = \begin{bmatrix} -3.9148\mathrm{e}-11 & 8.8672\mathrm{e}-9 & -7.0048\mathrm{e}-7 & 2.2069\mathrm{e}-5 & -2.1492\mathrm{e}-4 \\ 6.0699\mathrm{e}-9 & -1.3708\mathrm{e}-6 & 1.0784\mathrm{e}-4 & -0.0034 & 0.0322 \\ -3.2203\mathrm{e}-7 & 7.2344\mathrm{e}-5 & -0.0057 & 0.0071 & -0.0629 \\ 6.7649\mathrm{e}-7 & -0.0015 & 0.1162 & -3.5328 & 31.6814 \\ -4.4741\mathrm{e}-5 & 0.0098 & -0.7383 & 21.9981 & -142.3524 \end{bmatrix} \tag{6-16}$$

Because the antenna is located on the fuselage so the fuselage reflection extra path is very short and considered to be the height of the antenna.$\mathrm{L}_{\mathrm{fuselage}}$=0.05m and the time delay $\tau_{\mathrm{fuselage}} = 1.7 \times 10^{-10}$s.

6.5 Ground Echo

The ground echo would be a dominate multipath signal during the landing. By Gaussian Doppler Spectrum theory, the ground echo power is assumed [5, 21]:

$$\mathrm{P}_{\mathrm{Gr(dB)}} = 20 * \log_{10}\left(\frac{1}{\sqrt{2\pi\sigma^2}} * \mathrm{e}^{-\frac{\mathrm{f}^2}{2\sigma^2}}\right) \tag{6-17}$$

Where the deviation σ=3.8Hz. [16].

The ground echo delay can be calculated in the equation (6-18) as function of the elevation E. It is assumed that the airport or the environment is flat. Also the ground echo model can be expanded to various terrain models.

$$\tau_{\mathrm{ground}}(\mathrm{t}) = \frac{2 * \mathrm{h}(\mathrm{t}) * \sin(\mathrm{E})}{\mathrm{C}_0} \qquad \textbf{(6-18)}$$

Where h(t) is the aircraft altitude varies with time and E is the elevation angle.

6.6 Multipath Simulation Results

According to the Multipath model introduced, the multipath simulation is generated in matlab parallel with the GNSS constellation and flight dynamics model. Figure 6-6, 6-7, 6-8, 6-9, 6-10 and 6-11 show different path(fuselage reflection, wing reflection and ground echo) reflection GPS signal amplitude and time delay during TORNADO turn and descend flight phase.

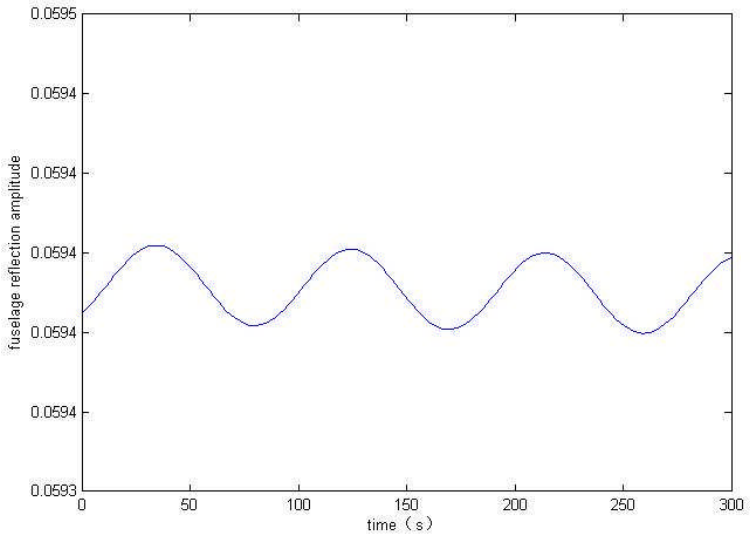

Figure 6-6 Fuselage reflection amplitude

Figure 6-6 shows the fuselage reflection signal amplitude during TORNADO turn and descend phase. The incoming direct signal amplitude is assumed to be 1. The simulation time is 300s.

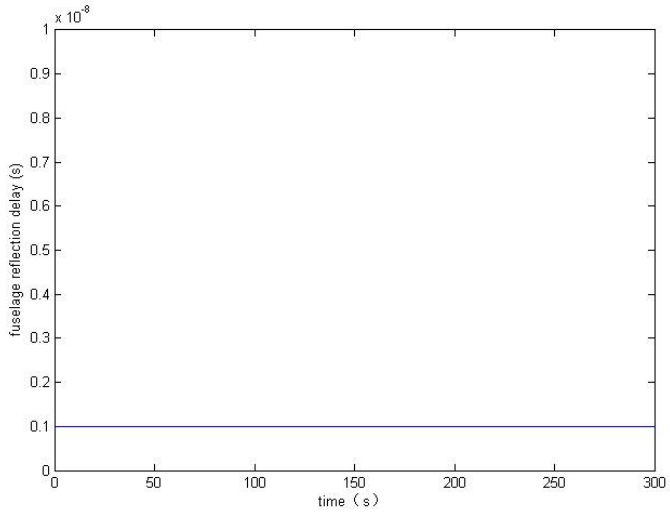

Figure 6-7 Fuselage reflection delay

Figure 6-7shows the fuselage reflection signal time delay during TORNADO turn and descend phase. The simulation time is 300s.

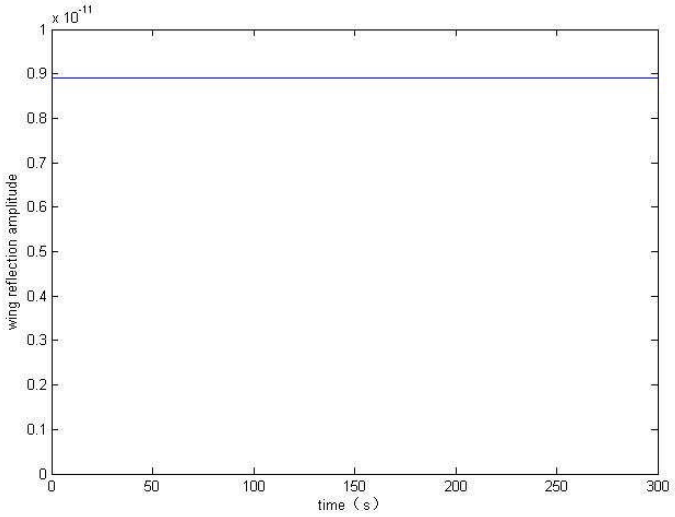

Figure 6-8 Wing reflection amplitude

Figure 6-8 shows the wing reflection signal amplitude during TORNADO turn and descend phase. The incoming direct signal amplitude is assumed to be 1. The simulation time is 300s.

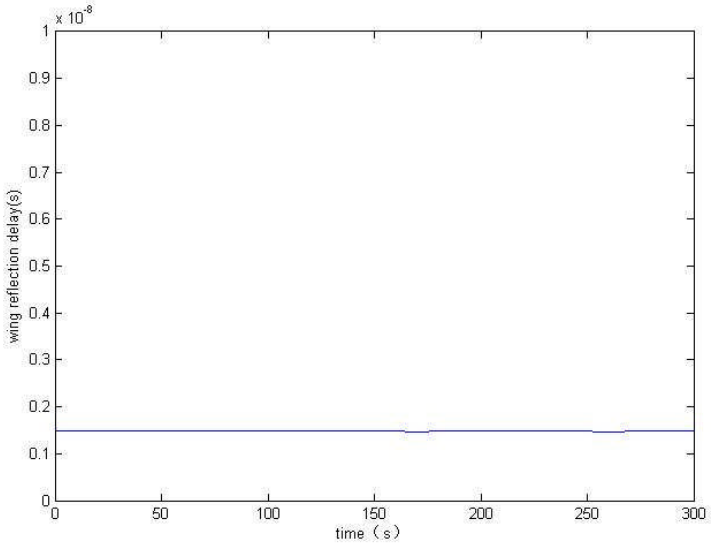

Figure 6-9 Wing reflection time delay

Figure 6-9 shows the wing reflection signal time delay during TORNADO turn and descend phase. The simulation time is 300s.

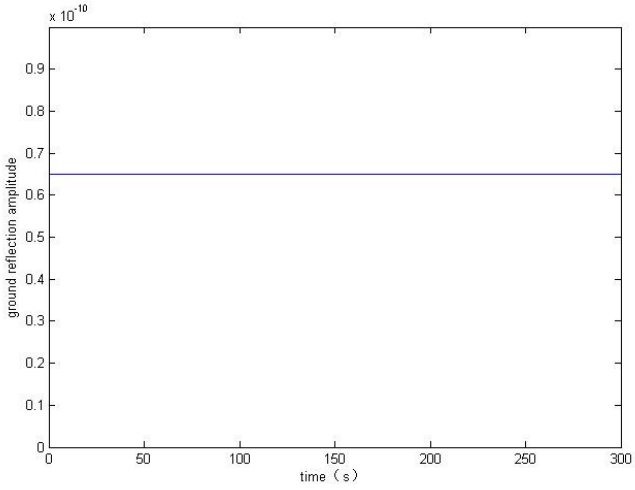

Figure 6-10 Ground echo amplitude

Figure 6-10 shows the ground echo signal amplitude during TORNADO turn and descend phase. The incoming direct signal amplitude is assumed to be 1. The simulation time is 300s.

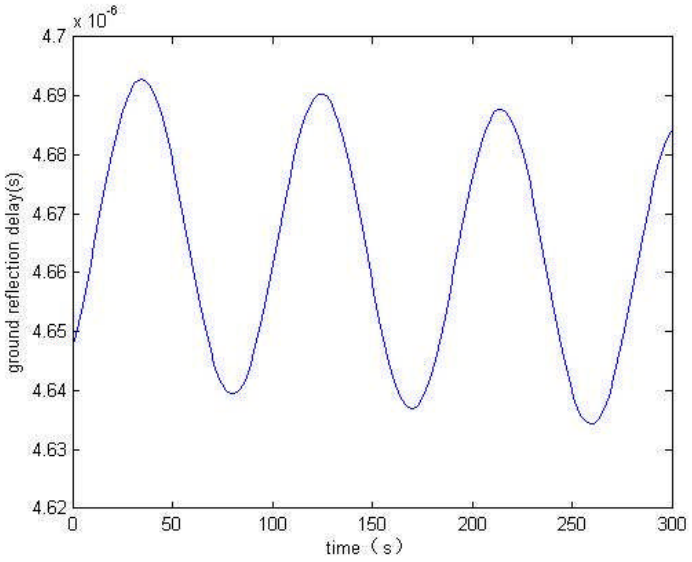

Figure 6-11 Ground echo time delay

Figure 6-11 shows the ground echo signal time delay during TORNADO turn and descend phase. The simulation time is 300s.

According to all the multipath simulation results, we notice that the fuselage reflection is the main contribution to the multipath signal. The effect of reflection signal from wing and ground is very small.

7 DOPPLER SHIFT

7.1 Introduction

The Doppler Shift is the change in frequency of the received signal when an observer moves relative to the source of wave. The received frequency is higher during the approach while it is lower during the recession.

This Doppler shift effects the receiver frequency .So that the Doppler Shift affects the antenna to track the GNSS signal carrier phase and also cause some errors in calculating the pseudo range, SNR and multipath simulation model. In the following Figure 7-1,it shows the Doppler Shift influence on the acquisition time.[1]

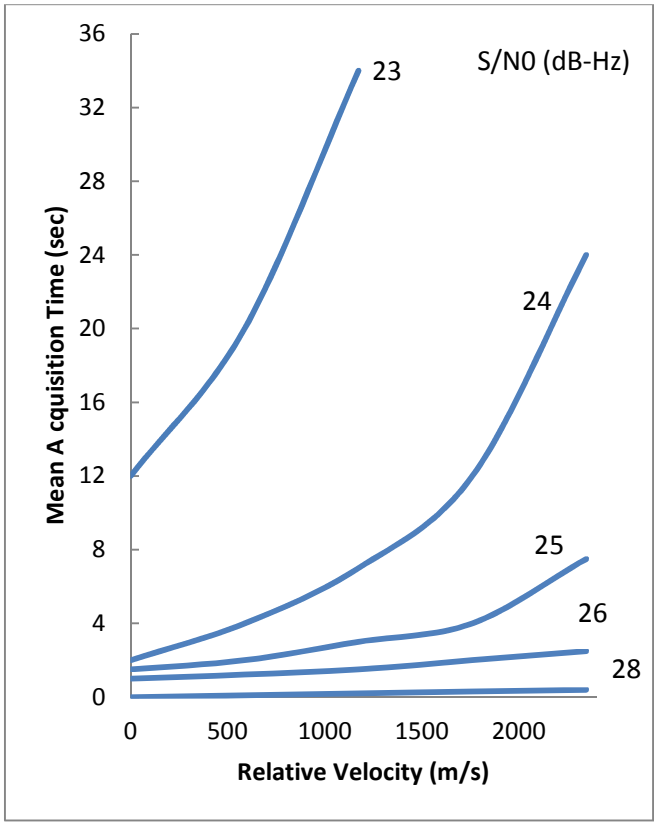

Figure 7-1 Mean Acquisition Time vs. Relative Velocity and SNR [1, 2]

In this chapter our aim is to build a Doppler Shift Model and use it to analyse its effect to the signal track. It will be used to generate the flag represents in which condition the Doppler Shift has critical influence.

7.2 Doppler Shift Model

The Doppler Shift frequency shift is calculated as follows [2, 5]

$$\Delta f_n = \left(\frac{v_i - v_u}{c}\right) \times f \times \cos\alpha_n \qquad \textbf{(7-1)}$$

Where

Δf_n is the nth satellite signal wave frequency shift;

v_i is the satellite velocity vector ;

v_u is the aircraft velocity vector;

c is the speed of light($3*10^8$ $m*s^{-1}$);

f is the GPS frequency;

α_n is the angle between the aircraft velocity and the nth satellite LOS vector;

Note that the Doppler does depend on the observer position through the line-of-sight unit vector.

In this chapter the Doppler shift model is based on the GNSS constellation model, flight trajectory model and the obscuration model. The trajectory model is used to generate the velocity of the aircraft and its position. The GNSS constellation model is used to generate the velocity of satellite and its position.

The obscuration model is used to generate the LOS vector and calculating the angle between aircraft velocity vector and LOS vector.

All the simulation will be done in all 6 flight phases (taxi, climb, cruise, turn and climb, turn and descend, landing) with the whole GNSS constellation simulation.

Also this model will simulate different conditions to generate the flag that when the Doppler shift will affect the receiver capability to track the carrier phase and rapidly reacquire the signal after loss.

7.3 Doppler Shift Simulation Results

According to the Doppler Shift model, the Doppler Shift simulation is generated in matlab parallel with the GNSS constellation and flight dynamics model. Figure 7-2, 7-3, 7-4, 7-5, 7-6 and 7-7 show the received signal of Prn.5 satellite frequency shift caused by Doppler Shift during different TORNADO flight phase(climb, cruise, turn&descend and landing).

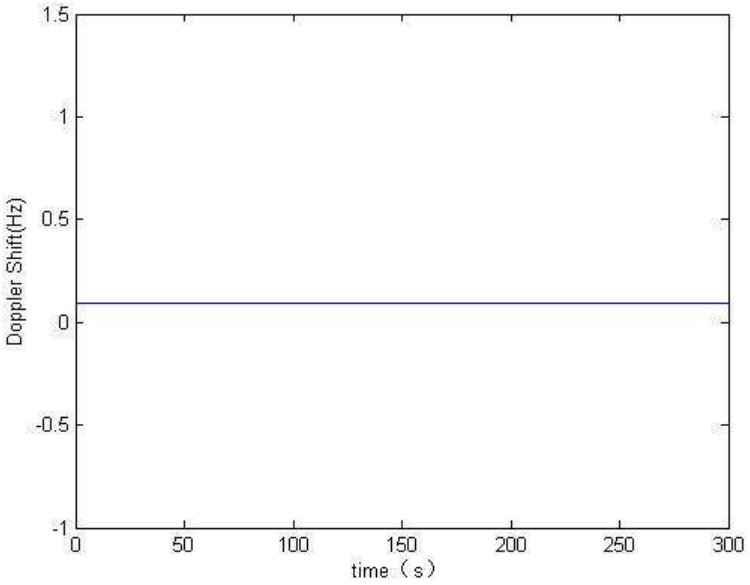

Figure 7-2 Prn.5 Frequency shift (TORNADO in climb phase)

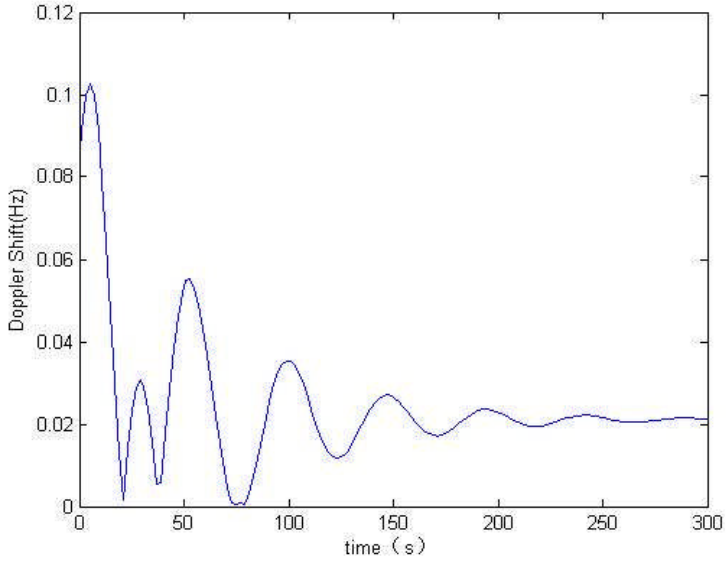

Figure 7-3 Prn.5 Frequency shift (TORNADO in cruise phase)

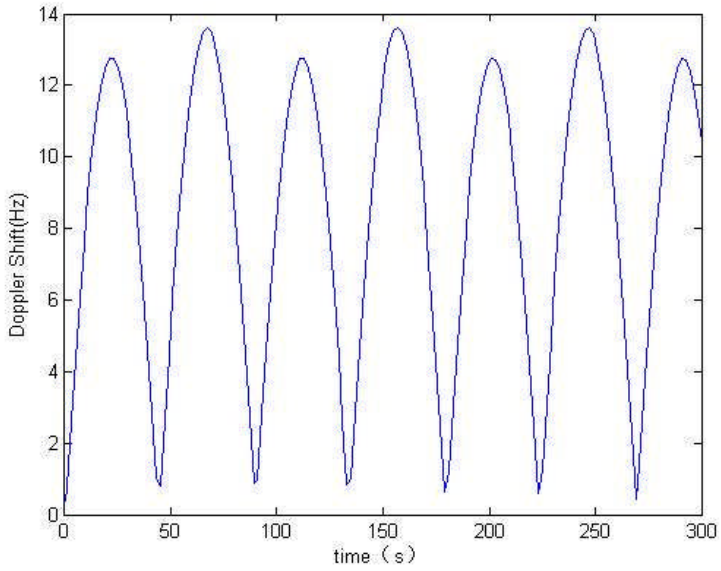

Figure 7-4 Prn.5 Frequency shift (TORNADO in turn&descend phase)

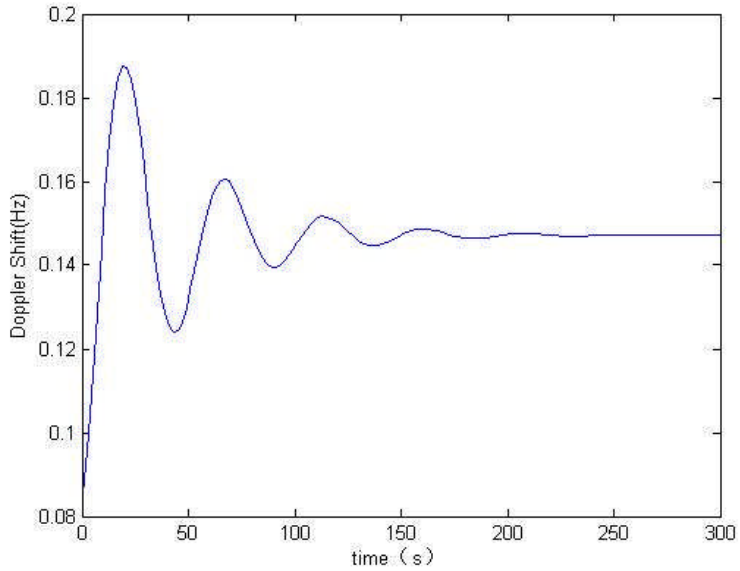

Figure 7-5 Prn.5 Frequency shift (TORNADO in landing phase)

8 GPS REICEIVER TRACKING

As discussed in the former chapters, the multipath effect causes phase error and the Doppler shift causes frequency error. Both of the errors make contribution to the false of signal tracking. In order to generate the integrity flag caused by these errors, some research have to be done with the GPS/GALILEIO receiver tracking technology. It will be introduced in this chapter.

8.1 GPS/GALILEO Receiver

Nowadays most of the GPS receivers are digital. They are consisted of some high level digital components. A typical GPS receiver architecture is shown in Figure 8-1.

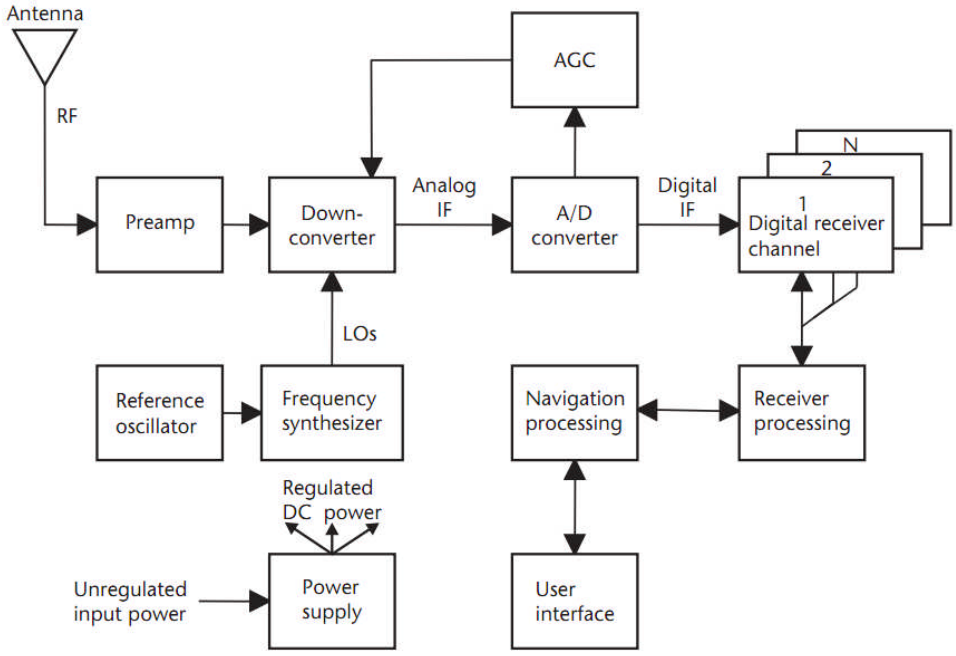

Figure 8-1 Typical GPS receiver architecture [23]

GPS RF(Radio Frequency) signals of all visible satellites are received by a RHCP(Right-Hand Circularly Polarized) antenna. These signals are amplified by

preamp(preamplifier), which can effectively remove the noise figure out of the receiver.

These amplified RF signals then go through a down-converter by using mixed frequencies generated from local oscillators(LOs) into an IF(Intermediate Frequency). The LOs are derived from the reference oscillator by the frequency synthesizer.

Then these IF signals are able to be processed by each of the digital receiver channels.

8.2 Carrier Tracking Loop

The carrier NCO(Numerically controlled oscillator) use discrete sine and cosine functions to synthesize the replica carrier signals which can strip the IF of the carrier to produce in-phase (I) and quadraphase (Q) sampled data.

The I component phase and Q component phase are produced 90^{o} apart, then the signal amplitude can be calculated by the sum of the I and Q while the phase angle can be computed by the arctangent of Q/I.

In the receiver processing operation, the carrier tracking loop is used for controlling the carrier NCO. In PLL (phase lock loop) operation, the carrier tracking loop keeps phase error between the satellite carrier signal phase and the replica carrier phase to be zero. Any change of the direction and the amplitude of the phase can be detected and modified by the PLL.

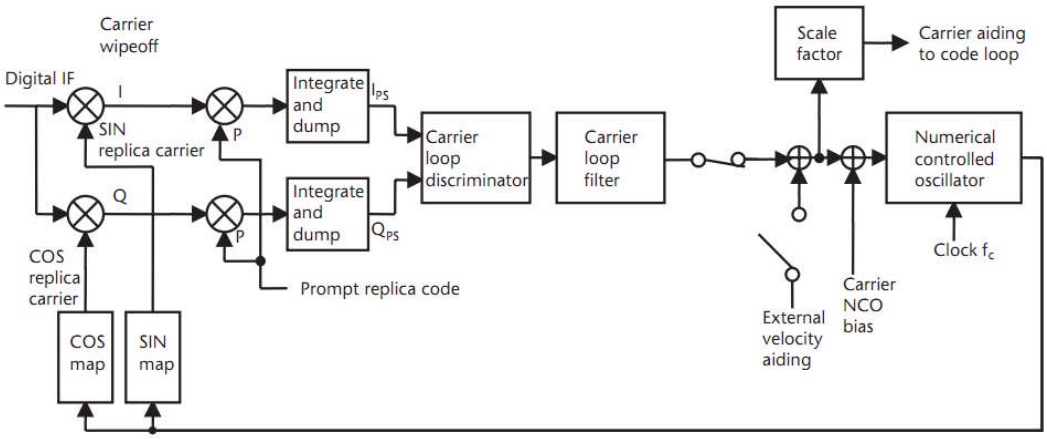

Figure 8-2 GPS receiver carrier tracking loop[23]

Figure 8-1 presents a GPS receiver carrier tracking loop. The receiver carrier tracking loop is consisted of the carrier loop discriminators, carrier predetection integrators and the carrier loop filters.

8.2.1 Carrier Loop Discriminator

The carrier loop discriminator defines the type of tracking loop as a phase lock loop (PLL) or a frequency lock loop (FLL). The PLL and is more accurate, but it is more sensitive to dynamic stress than the FLL. In practice some compromise should be made. The PLL discriminators estimate the phase error as their outputs while the FLL discriminator estimates a frequency error as outputs.

8.2.2 Predetection Integration

Predetection is the signal processing after the IF signal has been converted to baseband by the carrier and code stripping processes, but prior to being passed through a signal discriminator. Usually the predetection time is 20ms during track modes.[23]

8.2.3 Loop Filters

The objective of the loop filter is to reduce noise in order to produce an accurate estimate of the original signal at its output. The loop filter order and noise bandwidth also determine the loop filter's response to signal dynamics. Table 8-3 shows all the information about 3 types of the loop filters.

Table 8-1 Loop Filter Characteristics [23]

Loop Order	Noise Bandwidth B_n (Hz)	Typical Filter Values	Steady State Error
First	$\frac{\omega_0}{4}$	ω_0 $B_n = 0.25\omega_0$	$\frac{dR/dt}{\omega_0}$
Second	$\frac{\omega_0(1+a_2^2)}{4a_2}$	ω_0^2 $a_3\omega_0 = 1.414\omega_0$ $B_n = 0.53\omega_0$	$\frac{d^2R/dt^2}{{\omega_0}^2}$
Third	$\frac{\omega_0(a_3b_3^2 + a_3^2 - b_3)}{4(a_3b_3 - 1)}$	ω_0^3 $a_3\omega_0^2 = 1.1\omega_0^2$ $b_3\omega_0 = 2.4\omega_0$ $B_n = 0.7845\omega_0$	$\frac{d^3R/dt^3}{{\omega_0}^3}$

8.3 Phase Tracking Loop

If there was no 50-Hz data modulation on the GPS signal, the carrier tracking loop discriminator could use a PLL discriminator. It is also possible to implement short-term pure PLL modes by a process called data wipeoff. The GPS receiver typically acquires a complete copy of the full navigation message after 25 iterations of the 5 subframes (12.5 minutes), or the current data can be provided by some external means. The receiver then can compute the navigation message sequence until the GPS control segment uploads a new message or

until the SV changes the message. Until the message changes significantly, the GPS receiver can perform data wipeoff of each bit of the incoming 50-Hz navigation data message and use a pure PLL discriminator. [23] The receiver baseband processing function does this by reversing the sign of the integrated prompt I and Q components in accordance with a consistent algorithm.

Table 8-2 PLL Discriminator[23]

Discriminator Algorithm	Output Phase Error
$\mathrm{ATAN2}(\mathrm{Q_{PS}}, \mathrm{I_{PS}})$	ϕ
$\frac{\mathrm{Q_{PS}}}{\mathrm{A_{ve}}\sqrt{\mathrm{I_{PS}^2} + \mathrm{Q_{PS}^2}}}$	$\sin\phi$

Table 8-1 illustrates the PLL four-quadrant arctangent discriminator algorithm, its output phase error and its characteristics.

8.4 Frequency Tracking Loop

PLLs replicate the exact phase and frequency of the incoming SV (converted to IF) to perform the carrier wipeoff function. FLLs perform the carrier wipeoff process by replicating the approximate frequency, and they typically permit the phase to rotate with respect to the incoming carrier signal.

Table 8-2 summarizes several GPS receiver FLL discriminators, their output frequency errors, and their characteristics.

Table 8-3 FLL Discriminators [23]

Discriminator Algorithm	Output Frequency Error
$\frac{\text{cross}}{(t_2 - t_1)}$ Where: $\text{cross} = I_{PS1} \times Q_{PS2} - I_{PS1} \times Q_{PS2}$	$\frac{\sin[(\phi_2 - \phi_1)]}{t_2 - t_1}$
$\frac{(\text{cross}) \times \text{sign}(\text{dot})}{(t_2 - t_1)}$ Where: $\text{dot} = I_{PS1} \times I_{PS2} + Q_{PS1} \times Q_{PS2}$ $\text{cross} = I_{PS1} \times Q_{PS2} - I_{PS2} \times Q_{PS1}$	$\frac{\sin[2(\phi_2 - \phi_1)]}{t_2 - t_1}$
$\frac{\text{ATAN2}(\text{dot}, \text{cross})}{(t_2 - t_1)}$ Where: $\text{dot} = I_{PS1} \times I_{PS2} + Q_{PS1} \times Q_{PS2}$ $\text{cross} = I_{PS1} \times Q_{PS2} - I_{PS2} \times Q_{PS1}$	$\frac{\phi_2 - \phi_1}{t_2 - t_1}$

8.5 Measurement Errors and Tracking Thresholds

When the GPS measurement errors exceed a certain amount, the receiver will loses lock. So in order to analysis the GPS receiver tracking thresholds to generate the integrity flag, the GPS measurement error are related. Because the code and carrier tracking loops are nonlinear, especially near the threshold regions, only Monte Carlo simulations of the GPS receiver in different dynamic and signal to noise ratio conditions can determine the receiver tracking performance [24]. However, general rules that approximate the measurement errors of the tracking loops can be used based on closed form equations. Numerous sources of measurement errors are in each type of tracking loop.

However, it is sufficient for tracking thresholds to analysis only the dominant error sources.

8.5.1 PLL Tracking Loop Measurement Errors

Phase jitter and dynamic stress error are the main phase errors in a GPS receiver PLL. The receiver tracking threshold is that the 3-sigma jitter must not exceed one-fourth of the phase pull-in range of the PLL discriminator. Only arctangent carrier phase discriminators are considered for the generic receiver design. In the case of a dataless PLL four-quadrant arctangent discriminator whose phase pull-in range is 360º, the 3-sigma rule threshold is therefore 90º. For the case where there is data modulation, the PLL two-quadrant arctangent discriminator must be used and has a pull-in range of 180 º.Therefore, the PLL thresholds are stated as follows [5, 23]:

$$3\sigma_{\mathrm{PLL}} = 3\sigma_{\mathrm{j}} + \theta_{\mathrm{e}} \leq 45^{\circ} \qquad \textbf{(8-1)}$$

σ_j= 1-sigma phase jitter from all sources except dynamic stress error

θ_e= dynamic stress error in the PLL tracking loop

In the P(Y) code and C/A code examples, the presence of data modulation is assumed. Expanding on (8-1), the 1-sigma rule threshold for the PLL tracking loop for the two-quadrant arctangent discriminator is therefore [5, 23]:

$$\sigma_{\mathrm{PLL}} = \sqrt{\sigma_{\mathrm{tPLL}}^2 + \sigma_{\mathrm{v}}^2 + \theta_{\mathrm{A}}^2} + \frac{\theta_{\mathrm{e}}}{3} \leq 15^{\circ} \qquad \textbf{(8-2)}$$

where:

σ_{tPLL} = 1-sigma thermal noise (degrees)

σ_{υ}= Vibration-induced oscillator phase noise (degrees)

θ_A = Allan variance–induced oscillator jitter (degrees)

In our research the 1-sigma rule threshold (equation 8-2) will be considered as the alert threshold for the integrity flag when analysis the phase error.

8.5.1.1 PLL Thermal Noise

Often the PLL thermal noise is often thought to be the only carrier tracking error, since the other sources of PLL jitter may be either transient or negligible. The PLL thermal noise jitter is computed as follows [5, 23]:

$$\sigma_{PLLt} = \frac{360}{2\pi}\sqrt{\frac{B_n}{C/N_0}\left(1+\frac{1}{2TC/N_0}\right)}\ (\text{degrees}) \qquad \textbf{(8-3)}$$

B_n = carrier loop noise bandwidth (Hz)

C/N_0 = carrier to noise power ratio (dB-Hz)

T = predetection integration time (seconds)

λ_L = GPS L-band carrier wavelength (m)

B_n and C/N_0 can be derived from the SNR model introduced in chapter 5.2.

According to the introduction of predetection integration, the mode for our research is tracking .So the predetection integration time is 20ms.

8.5.1.2 Vibration-Induced Oscillator Phase Noise

Vibration-induced oscillator phase noise is a complex analysis problem. In some cases, the expected vibration environment is so severe that the reference oscillator must be mounted using vibration isolators in order for the GPS receiver to successfully operate in PLL. The equation for vibration induced oscillator jitter is [5, 23]:

$$\sigma_{\upsilon} = \frac{360 f_L}{2\pi} \sqrt{\int_{f_{min}}^{f_{max}} S_{\upsilon}^2(f_m) \frac{P(f_m)}{f_m^2} df_m} \ (\text{degrees}) \quad \textbf{(8-4)}$$

where:

f_L = L-band frequency (Hz)

$S_{\upsilon}(f_m)$ = oscillator vibration sensitivity of $\Delta f/f_L$ per g as a function of fm

f_m = random vibration modulation frequency (Hz)

$P(f_m)$ = power curve of the random vibration as a function of f_m (g^2/Hz)

g = the gravity acceleration

Usually the oscillator vibration sensitivity, $S_{\upsilon}(f_m)$ is not variable over the range of the random vibration modulation frequency, then equation 8-5 can be simplified to [5, 23]:

$$\sigma_{\upsilon} = \frac{360 f_L S_{\upsilon}}{2\pi} \sqrt{\int_{f_{min}}^{f_{max}} \frac{P(f_m)}{f_m^2} df_m} \ (\text{degrees}) \quad \textbf{(8-5)}$$

In this research, we assume the random vibration power curve is flat from 20Hz to 2000Hz with amplitude of 0.005g^2/Hz. And the oscillator vibration sensitivity $S_\upsilon(f_m) = 1 \times 10^{-9}$ parts/g [2, 5]

8.5.1.3 Allan Deviation Oscillator Phase Noise

The equations used to determine Allan deviation phase noise are empirical. They are stated in terms of what the requirements are for the short-term stability of the reference oscillator as determined by the Allan variance method of stability measurement. [23] The equation for second –order loop short-term Allan deviation for PLL is [2, 24]:

$$\theta_{A2} = 144 \frac{\sigma_A(\tau) * f_L}{B_n} \text{ (rad)} \quad \textbf{(8-6)}$$

The equation for third–order loop short-term Allan deviation for PLL is [24]:

$$\theta_{A3} = 160 \frac{\sigma_A(\tau) * f_L}{B_n} \text{ (rad)} \quad \textbf{(8-7)}$$

where:

$\sigma_A(\tau)$=Allan deviation-induced jitter (degrees)

f_L= L-band input frequency (Hz)

τ = short-term stability gate time for Allan variance measurement (seconds).

B_n=noise bandwidth.

Usually $\sigma_A(\tau)$ has been determined for the oscillator and it changes very little with gate time τ. In our research, the loop filter is assumed as a third-order with

a noise bandwidth B_n =18Hz and the gate time $\tau = 1/B_n = 56\text{ms}$ .The allan deviation is specified to be $\sigma_A(\tau) = 1 \times 10^{-10}$[2, 5]

8.5.1.4 Dynamic Stress Error

The dynamic stress error is obtained from the steady state error formulas shown in Table 8-3. The dynamic stress error depends on the loop bandwidth and order. In the third-order loop, the dynamic stress error is [2, 23]

$$\theta_{e3} = \frac{d^3R/dt^3}{\omega_0^3} = \frac{d^3R/dt^3}{(\frac{B_n}{0.7845})^3} = 0.4828\frac{\frac{d^3R}{dt^3}}{B_n^3}\ (\text{degrees}) \quad \textbf{(8-8)}$$

Where

d^2R/dt^2= maximum LOS acceleration dynamics ($°/s^2$)

B_n=noise bandwidth

In this research, the third-order loop noise bandwidth is 18Hz and the maximum LOS jerk dynamic stress to the SV is 10g/s=$98\text{m}/s^3$.[14] For L1, $d^3R/dt^3 = (98/s^3) \times (360°/\text{cycle}) \times (1575.42 \times 10^6\ \text{cycles}/s)/c = 185398°/s^3$.

8.5.2 FLL Tracking Loop Measurement Errors

Frequency jitter due to thermal noise and dynamic stress error are the main phase errors in a GPS receiver FLL. The receiver tracking threshold is that the 3-sigma jitter must not exceed one-fourth of the frequency pull-in range of the FLL discriminator. Therefore, the FLL tracking threshold is [2, 23]:

$$3\sigma_{FLL} = 3\sigma_{tFLL} + f_e \le 1/4T\ \ (\text{Hz}) \quad \textbf{(8-9)}$$

where:

$3\sigma_{\mathrm{FLL}}$ = 3-sigma thermal noise frequency jitter

σ_{tFLL}= dynamic stress error in the FLL tracking loop

Equation (8-9) shows that the dynamic stress frequency error is a 3-sigma

effect and is additive to the thermal noise frequency jitter. The reference oscillator vibration and Allan deviation–induced frequency jitter are small-order effects on the FLL and are considered negligible. The 1-sigma frequency jitter threshold would be 1/(12T) = 0.0833/T Hz. And in our research the 1-sigma frequency jitter threshold will be used as the frequency error warning threshold for the integrity flag.

The FLL tracking loop jitter due to thermal noise is:λ_{L} [2, 5]:

$$\sigma_{\mathrm{tFLL}} = \frac{1}{2\pi \mathrm{T}} \sqrt{\frac{4\mathrm{FB_n}}{\mathrm{C/N_0}} \left[1 + \frac{1}{\mathrm{TC/N_0}}\right]} \ (\mathrm{Hz}) \qquad \textbf{(8-10)}$$

Where：

F=1 at high $\mathrm{C/N_0}$=2 near threshold

Note that (8-12) is independent of modulation design and loop order. It is independent of L-band carrier frequency if the error units are expressed in Hz. The dynamic stress error is [2, 5]:

$$\mathrm{f_e} = \frac{\mathrm{d}}{\mathrm{dt}} \left(\frac{1}{360\omega_0^{\mathrm{n}}} \frac{\mathrm{d^n R}}{\mathrm{dt^n}} \right) = \frac{1}{360\omega_0^{\mathrm{n}}} \frac{\mathrm{d^{n+1} R}}{\mathrm{dt^{n+1}}} \ (\mathrm{Hz}) \qquad \textbf{(8-11)}$$

The dynamic stress error differs from the order of loop, all the data in Table 8-2 can be used to calculate the dynamic stress error.

9 INTEGRITY FLAG

Integrity flag includes the ability of a system to provide timely and valid warnings to the pilot [2, 5].

Alert. An annunciation to the pilot to identify that an operating parameter of GNSS system is going to out of tolerance or the following pilot's operation will lead to GNSS fail.

Alert limit. For a given parameter measurement, the tolerance not to be exceeded without issuing an alert.

Time-to-alert. The maximum allowable time elapsed from onset of the GNSS system being out of tolerance until the equipment enunciates the alert.

Warning. An annunciation to the pilot or other aircraft system that the GNSS is not suit for work [2, 5].

This research's integrity flag generation work will focus on a variety of mission-critical and safety-critical applications, including climb, cruise, turn and descend, precision approach and automatic landing.

Based on the previous research on antenna masking, SNR, multipath, Doppler shift and GPS/GALILEO receiver tracking, each of the integrity flag should be generated during all flight phase.

9.1 PDOP Integrity Flag

9.1.1 Horizontal/Vertical Position Error

According to the previous research that the calculation of the position there are some position error caused by clock offset error and ionospheric error and etc. The integrity flag should be generated when these errors exceed a certain threshold because they will affect the accuracy of the navigation. So in this chapter the PDOP(positional dilution of precision) is brought in. DOP(dilution of precision) is defined as the factor mapping the ranging solution to the navigation solution is called dilution of precision (DOP).[26]

From the equation (3-18), we can get the transformation equation (9-1):

$$\rho_i - \rho_{Ti} - c\delta_i^s = \frac{\partial \rho_i}{\partial X}|_{X_0,Y_0,Z_0}\Delta X + \frac{\partial \rho_i}{\partial Y}|_{X_0,Y_0,Z_0}\Delta Y + \frac{\partial \rho_i}{\partial Z}|_{X_0,Y_0,Z_0}\Delta Z - c\delta_R \quad \textbf{(9-1)}$$

Where ρ_i is the ith satellite pseudorange and ρ_{Ti} is the real range from ith satellite to the receiver. X_0, Y_0, Z_0 denote the initial guess position of the receiver. And ΔX, ΔY, ΔZ and δ_R stand for difference between the true solution and initial guess in position and time. Formulate the matrix, A, as [26]:

$$A = \begin{bmatrix} \frac{\partial \rho_1}{\partial X}|_{X_0,Y_0,Z_0} & \frac{\partial \rho_1}{\partial Y}|_{X_0,Y_0,Z_0} & \frac{\partial \rho_1}{\partial Z}|_{X_0,Y_0,Z_0} & -1 \\ \frac{\partial \rho_2}{\partial X}|_{X_0,Y_0,Z_0} & \frac{\partial \rho_2}{\partial Y}|_{X_0,Y_0,Z_0} & \frac{\partial \rho_2}{\partial Z}|_{X_0,Y_0,Z_0} & -1 \\ \frac{\partial \rho_3}{\partial X}|_{X_0,Y_0,Z_0} & \frac{\partial \rho_3}{\partial Y}|_{X_0,Y_0,Z_0} & \frac{\partial \rho_3}{\partial Z}|_{X_0,Y_0,Z_0} & -1 \\ \vdots & \vdots & \vdots & \vdots \\ \frac{\partial \rho_i}{\partial X}|_{X_0,Y_0,Z_0} & \frac{\partial \rho_i}{\partial Y}|_{X_0,Y_0,Z_0} & \frac{\partial \rho_i}{\partial Z}|_{X_0,Y_0,Z_0} & -1 \end{bmatrix} \quad \textbf{(9-2)}$$

DOP is calculated from the design matrix containing the unit vectors A. The Q matrix is calculated from the design matrix as [26]:

$$Q = (A^T A)^{-1} \tag{9-3}$$

The elements of Q are defined as:[26]

$$Q = \begin{bmatrix} \sigma_x^2 & \sigma_{xy}^2 & \sigma_{xz}^2 & \sigma_{xt}^2 \\ \sigma_{xy}^2 & \sigma_y^2 & \sigma_{yz}^2 & \sigma_{yt}^2 \\ \sigma_{xz}^2 & \sigma_{yz}^2 & \sigma_z^2 & \sigma_{zt}^2 \\ \sigma_{xt}^2 & \sigma_{yt}^2 & \sigma_{zt}^2 & \sigma_t^2 \end{bmatrix} \tag{9-4}$$

The Q matrix maps the ranging covariance matrix into the navigation covariance matrix.[26] By using the matrix Q, the pseudorange errors can be converted to the navigation errors. GDOP (Geometrical Dilution of Precision), PDOP (Positional Dilution of Precision), HDOP (Horizontal Dilution of Precision), VDOP (Vertical Dilution of Precision) and TDOP (Time Dilution of Precision) are given respectively by:[26]

$$GDOP = \sqrt{\sigma_x^2 + \sigma_y^2 + \sigma_z^2 + \sigma_t^2} \tag{9-5}$$

$$PDOP = \sqrt{\sigma_x^2 + \sigma_y^2 + \sigma_z^2} \tag{9-6}$$

$$HDOP = \sqrt{\sigma_x^2 + \sigma_y^2} \tag{9-7}$$

$$VDOP = \sqrt{\sigma_z^2} \tag{9-8}$$

$$TDOP = \sqrt{\sigma_t^2} \tag{9-9}$$

Then we can use HDOP and VDOP to calculate the horizontal position error and vertical position error by:

$$Error_{Horizontal} = HDOP \times Error_{Range} \tag{9-10}$$

$$\mathrm{Error}_{\mathrm{Vertical}} = \mathrm{VDOP} \times \mathrm{Error}_{\mathrm{Range}} \quad \textbf{(9-11)}$$

The horizontal position error and vertical position error can then be used to generate the PDOP integrity flag. It will be introduced in the following chapter 9.1.2.

9.1.2 PDOP Integrity Flag

According to the ICAO ANNEX10, the Horizontal Alert Limit, Horizontal Protection Level, Vertical Alert Limit and Vertical Protection Level are defined as the thresholds for the horizontal error and vertical error. In this research, they are used for generating the PDOP integrity flag.

As we introduced in the former chapter, the Horizontal Position Error can be calculated by HDOP and pseudorange error and Vertical Position Error can be calculated by VDOP and pseudorange error. Then the PDOP integrity flag should be generated when:

(1) When the Horizontal Position Error exceeds the HAL or the Vertical Position Error exceeds the VAL, the integrity flag should be generated to provide a alert signal. And the time to alert varies in different landing phases which will be introduced in Table9-1.

(2) When the Horizontal Position Error exceeds the HPL or the Vertical Position Error exceeds the VPL, the integrity flag should be generated to provide a warning signal that the GNSS system is failed.

Notice that the PDOP integrity flag is only suitable for GPS constellation in this research. Because the GALILEO constellation does not use real ephemeris

data, the PDOP cannot be calculated due to the failure of calculating its range error.

According to the ICAO ANNEX10 , Table 9-1 shows the HAL, VAL and time to alert during different landing phases known as: En-route, NPA, APV-I, APV-II, Category I precision approach. They will be used in the integrity flag as thresholds.

Table 9-1 GPS Signal-in–space alert requirements [5, 27]

Typical operation	Horizontal alert limit	Vertical alert limit	Time- to - alert
En-route	7.4 km	N/A	5min
En-route(continental)	3.7km	N/A	15s
En-route ,Terminal	1.85 km	N/A	10s
NPA	556m	N/A	10s
APV-I	40m	50m	6s
APV-II	40m	20m	6s
Category I precision approach	40m	15m-10m	6s

Table 9-2 shows the HPL, VPL and time to alert during different landing phases. They will be used in the integrity flag as thresholds.

Table 9-2 GPS Signal-in–space protection requirements [5, 27]

Typical operation	Accuracy horizontal 95%	Accuracy vertical 95%
En-route	3.7 km	N/A
En-route ,Terminal	0.74km	N/A
NPA	220m	N/A
APV-I	16m	20m
APV-II	16m	8m
Category I precision approach	16m	6m-4m

Our ABAS system is also available for CAT II and CAT III. So it is necessary to generate the HAL, HPL, VAL, VPL and time to alert during CAT-II and CAT-III. They are listed in the Table 9-3 and Table 9-4.

Table 9-3 GPS Signal-in–space (CAT-II&III) alert requirements [28]

Typical operation	Horizontal alert limit	Vertical alert limit	Time- to - alert
Category II precision approach	17.3m	5.3m	1s
Category III precision approach	15.5m	5.3m	1s

Table 9-4 GPS Signal-in–space (CAT-II&III) protection requirements [28]

Typical operation	Horizontal alert limit	Vertical alert limit
Category II precision approach	6.9m	2m
Category III precision approach	6.2m	2m

Figure 9-1 shows in GPS constellation the TORNADO horizontal error during landing phase.

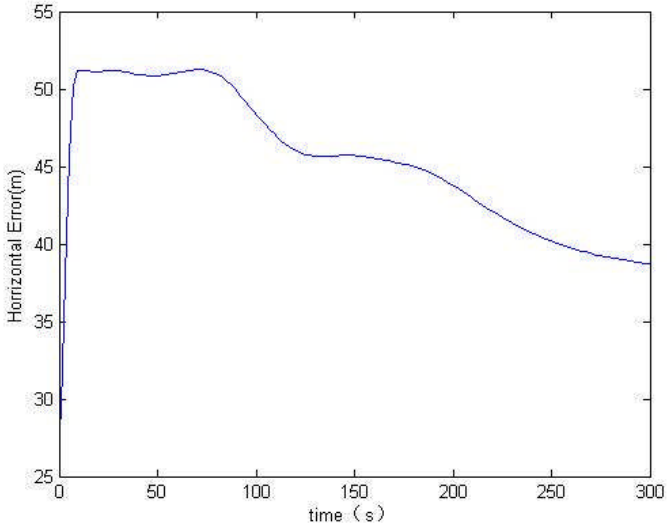

Figure 9-1 Horizontal Error (TORNADO landing phase)

Figure 9-2 shows in GPS constellation the TORNADO vertical error during landing phase.

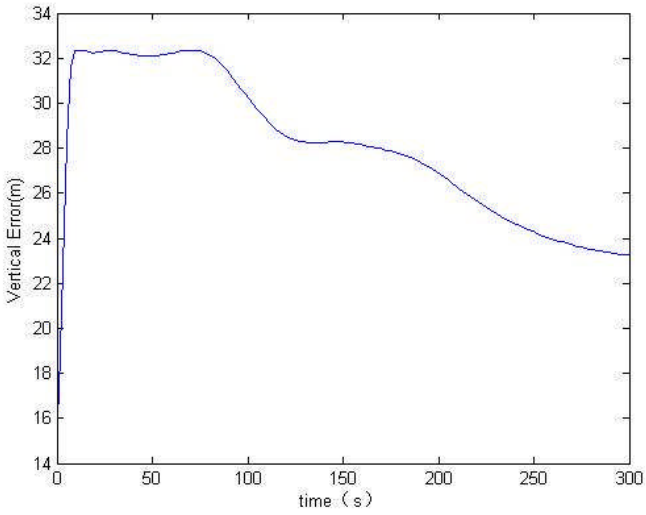

Figure 9-2 Vertical Error (TORNADO landing phase)

According to the PDOP integrity alert flag threshold in Table 9-1 and Table 9-3, the PDOP integrity alert flag during the landing phase is shown in Figure 9-3. “0” means the flag has not been generated.”1” means the flag is generated.

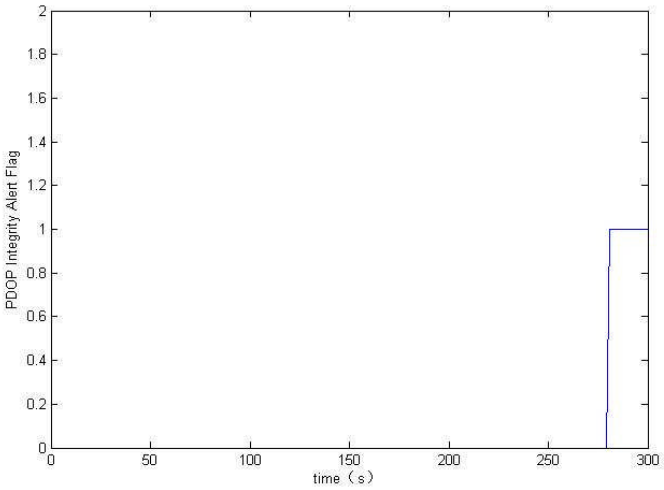

Figure 9-3 PDOP integrity alert flag (TORNADO landing phase)

9.2 Antenna Masking Integrity Flag

In the precision approach and landing phases, the aircraft performs both turn and descend trajectory and descend trajectory. During these flight phases, the pitch angle, roll angle and yaw angle may change all the time. From the previous research we know that the change of the angles will cause antenna masking. So the antenna masking integrity flag should be generated to give the alert and warning during the critical circumstance.

From chapter 4.4 we know that the change of roll angle and pitch angle are the main causes of the antenna masking. Yaw angle effects on the antenna masking can be neglected. So the antenna masking integrity flag should combine all the roll angle and pitch angle effects on antenna masking.

From the previous research results we know that the change of roll angle influence the antenna masking matrix caused by wing while the change of pitch

angle influence the antenna masking matrix caused by fuselage. In other words the total antenna masking matrix can be generated by the sum of both masking matrix.

In order to generate the antenna masking integrity flag, a series of antenna masking matrix are collected. The pitch angle series are collected from -90 degree to 90 degree every five degrees and the roll angle series are collected from -90 degree to 90 degree every five degrees. They are shown in following four different figures. Each line shows the masking limitations of different angles and the blue points stand for certain time satellite position.

Figure 8-1 shows the TORNADO antenna masking integrity flag while pitch angle is from 0 degree to 90 degree and bank angle is from 0degree to 90 degree.

Figure 8-2 shows the TORNADO antenna masking integrity flag while pitch angle is from 0 degree to 90 degree and bank angle is from -90 degree to 0 degree.

Figure 8-3 shows the TORNADO antenna masking integrity flag while pitch angle is from -90 degree to 0 degree and bank angle is from 0degree to 90 degree.

Figure 8-4 shows the TORNADO antenna masking integrity flag while pitch angle is from -90 degree to 0 degree and bank angle is from -90degree to 0 degree.

During the aircraft flight its certain pitch angle and roll angle are included in one of these figures. With the certain pitch angle and roll angle the antenna masking matrix at this time can be generated from the following figures. The antenna masking integrity flag works with the satellite position. It works in this way:

(1) Combine certain time's antenna masking matrix and the satellite position, if the following procedure(for example, increase the roll angle) will cause the loss of satellites and lead to less than 4 satellites in the visible area, then the antenna masking integrity flag should be generated to give the alert signal to the pilot to avoid the following procedure. And the time to alert is 1 second.

(2) Combine certain time's antenna masking matrix and the satellite position, if there are less than 4 satellites in the visible area, then the antenna masking integrity flag should be generated to give the warning signal to the pilot that the GNSS is failed.

The simulation of the antenna masking integrity flag should use database technology to combine the data shown in Figure 8-1 to 8-4 with the real aircraft status. But in this research the antenna masking integrity flag simulation works in a simplified way:

(1) When the satellite elevation angle due to the antenna frame is less than 10 degree, the antenna masking integrity flag should be generated to give the alert signal that such satellite may lose soon.

(2) When the satellite elevation angle due to the antenna frame is less than 5 degree, the antenna masking integrity flag should be generated to give the warning signal to the pilot that such satellite is lost.

Notice that the antenna masking integrity flag is for a certain satellite signal instead of the whole system. So it will work as a sub integrity flag.

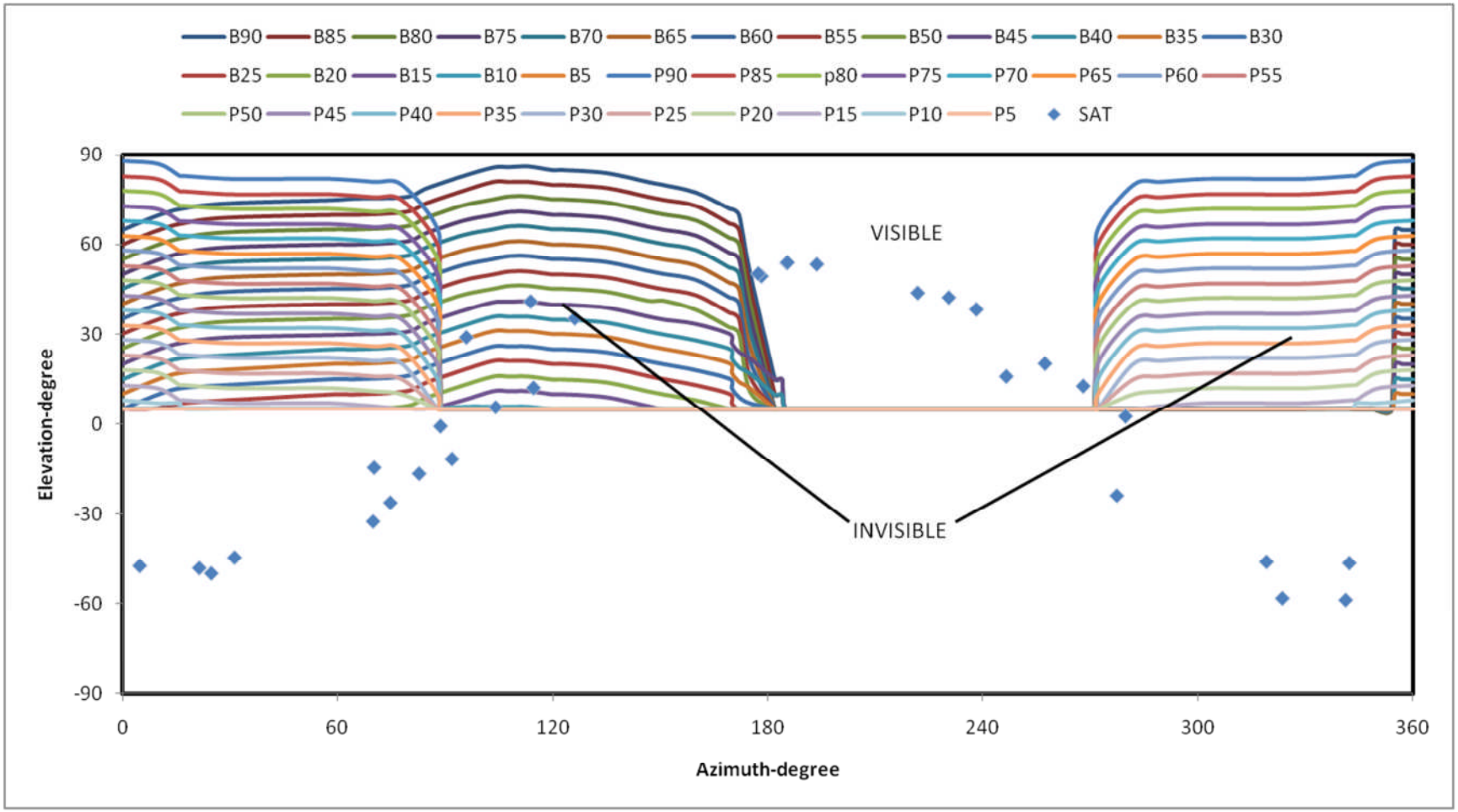

Figure 9-4 TORNADO Antenna masking integrity flag (pitch angle:0-90 degree, bank angle: 0-90 degree) [2]

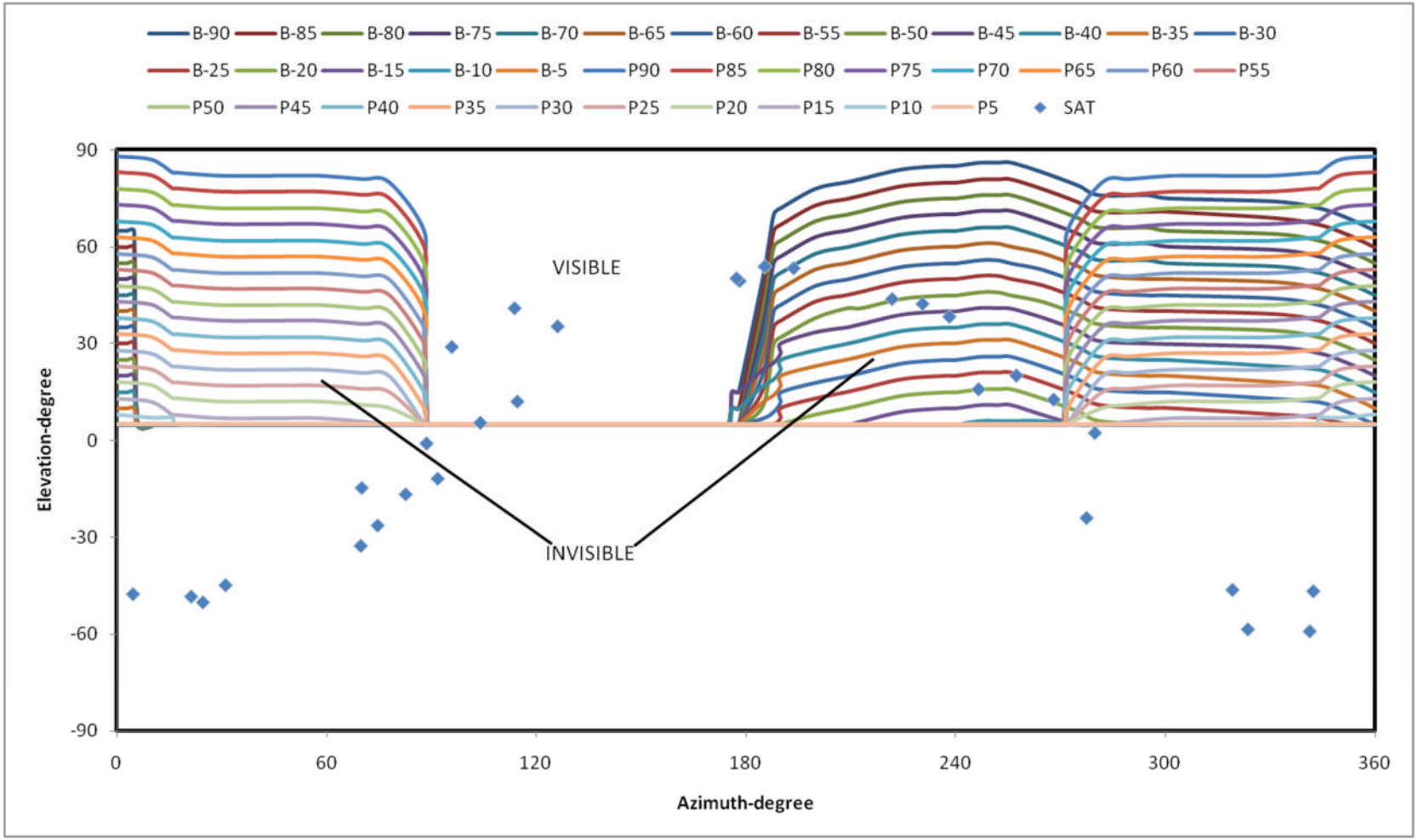

Figure 9-5 TORNADO Antenna masking integrity flag (pitch angle:0 ~ 90 degree, bank angle: -90 ~ 0 degree) [2]

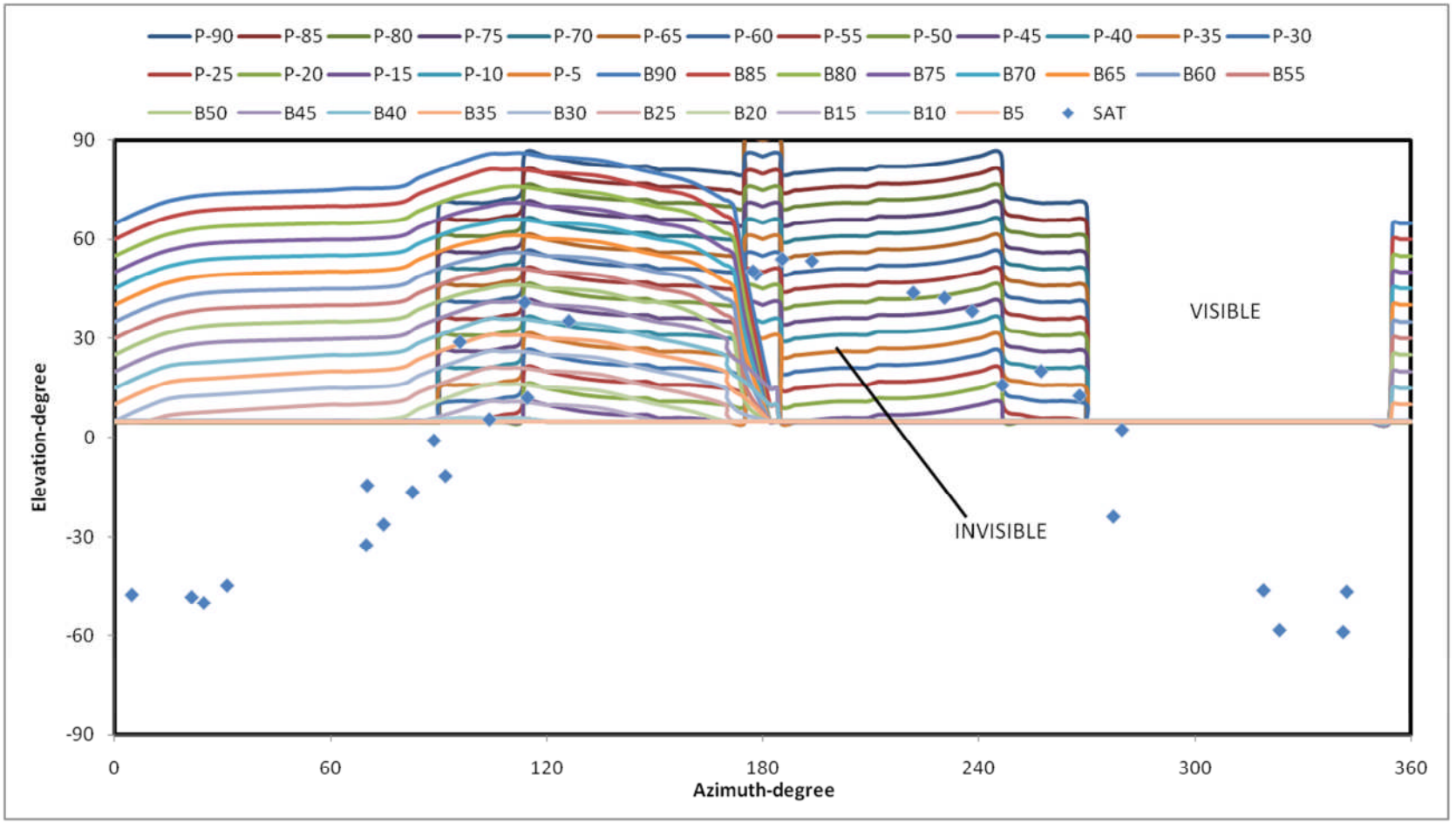

Figure 9-6 TORNADO Antenna masking integrity flag (pitch angle:-90~0 degree, bank angle: 0~90 degree) [2]

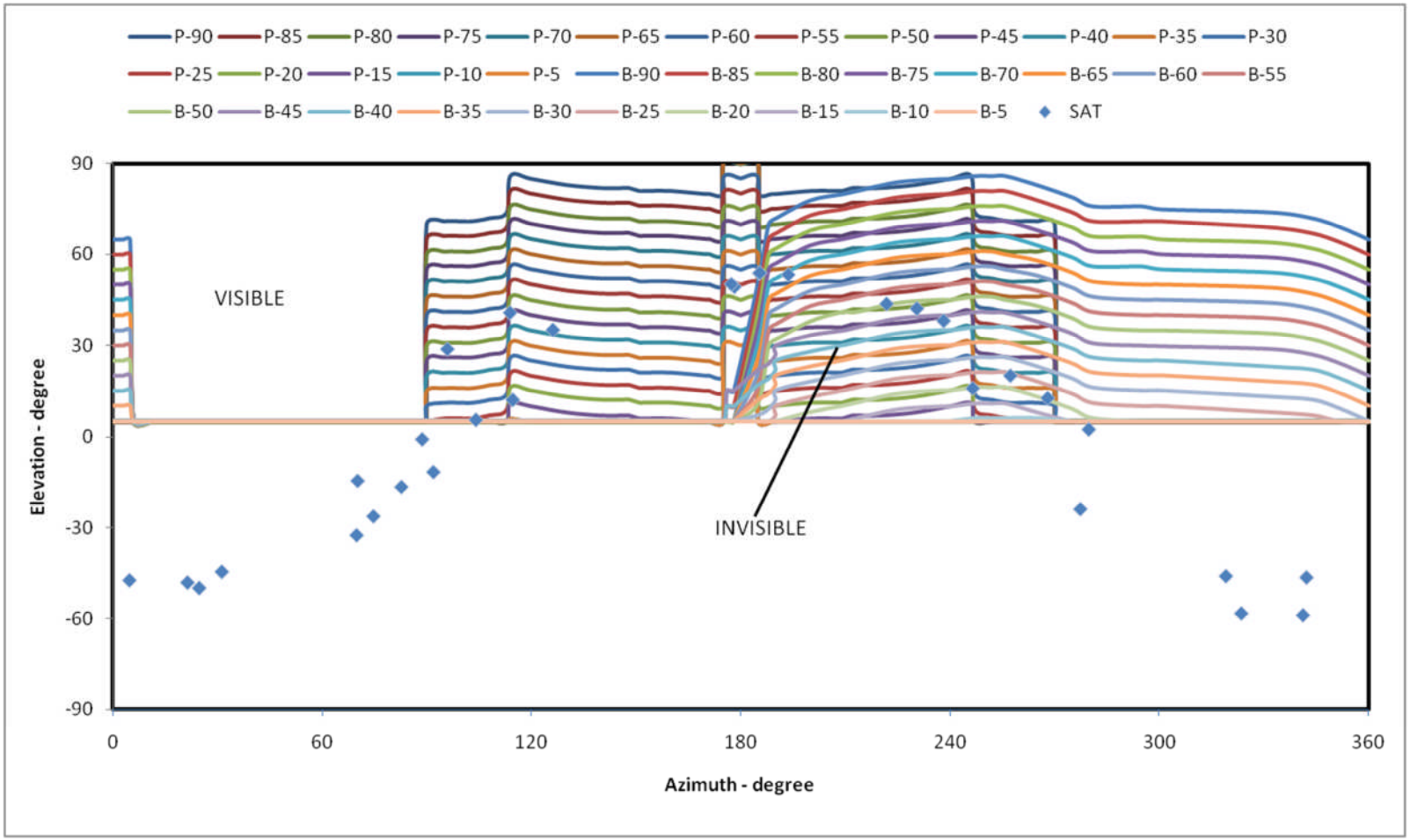

Figure 9-7 TORNADO Antenna masking integrity flag (pitch angle:-90~0 degree, bank angle: -90~0 degree) [2]

9.3 SNR Integrity Flag

9.3.1 Code Lock Detectors

If the GNSS signal is being tracked, we must know it is being, or not being, tracked. Lock detectors are required to perform this function. Code lock detection is very similar to estimating C/N_0 , inferring that the receiver is operating on or near the correlation peak. Knowledge of code lock is obviously the same as the knowledge of received signal power. Usually the required C/N_0 values are more than 25 dB-Hz.[29] This threshold will be used to generate the SNR integrity flag.

9.3.2 Processing Gain

The receiver's code-correlation process is to raise the signal out of the noise. In spread spectrum system Processing Gain(G_p) is a common term. It is defined as the ratio of the spread (or RF) bandwidth to the unspread (or baseband) bandwidth. It is usually presented in decibels (dB).[30]

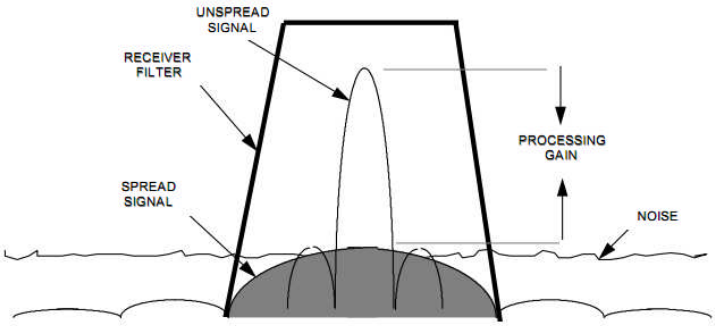

Figure 9-8 Processing gain concept at receiver[30]

Fig 9-5 shows the processing gain concept at receiver. By using Processing gain, the signal is amplified without amplifying the noise at the same time. The post-correlation signal to noise ratio can be calculated by [2, 30]

$$(\mathrm{S/N})_{\mathrm{post-correlation}} = (\mathrm{S/N})_{\mathrm{pre-correlation}} + \mathrm{G_p} \quad \textbf{(9-12)}$$

The GNSS receivers processing gain ($\mathrm{G_P}$) is defined as a ratio between the chipping period and the data bit period. In GPS receiver the C/A code chipping rate is 1.023MHz. When the receiver C/A code is aligned with transmitted code the signal power at the bandpass output is now squished into approximately 100hz of bandwidth.[30]

Calculation of the processing gain is given by equation (8-2) [2, 30]

$$\mathrm{G_P} = \frac{\mathrm{T_D}}{\mathrm{T_C}} = 10\log\left(\frac{{}^{C}/_{A}\ code\ chipping\ rate * 2}{data\ period}\right) dB = 10log(\frac{2*1.023Mhz}{100Hz}) \quad \textbf{(9-13)}$$

For the C/A- code signal, this works out to be about 43dB.

Usually the receiver had a cut off value at 10dB, which means that if the value is less then this the satellite signal level is too low for using in calculations [2]:

$$\mathrm{S/N_{post-correlation}} = \mathrm{S/N_{pre-correlation}} + \mathrm{G_p} < 10dB \quad \textbf{(9-14)}$$

The equation (9-14) will be used as an alert and warning threshold when generating the SNR integrity flag.

9.3.3 Fading integrity flag

According to the analysis in code lock and processing gain, the fading integrity flag should be generated when:

(1) When the C/N_0 is less than 26dB-Hz or the difference value between the SNR and processing gain is less than 11dB,the integrity flag should be generated to provide the alert signal to pilot or other system. And the time to alert is 1 second.

(2) When the C/N_0 is less than 25dB-Hz or the difference value between the SNR and processing gain is less than 10dB, the integrity flag should be generated to provide the warning signal to pilot or other systems that the GNSS signal tracking is failed.

Notice that the SNR integrity flag is for a certain satellite signal instead of the whole system. So it will work as a sub integrity flag.

Figure 9-9 shows the received Prn.14 signal SNR during turn and descend phase.

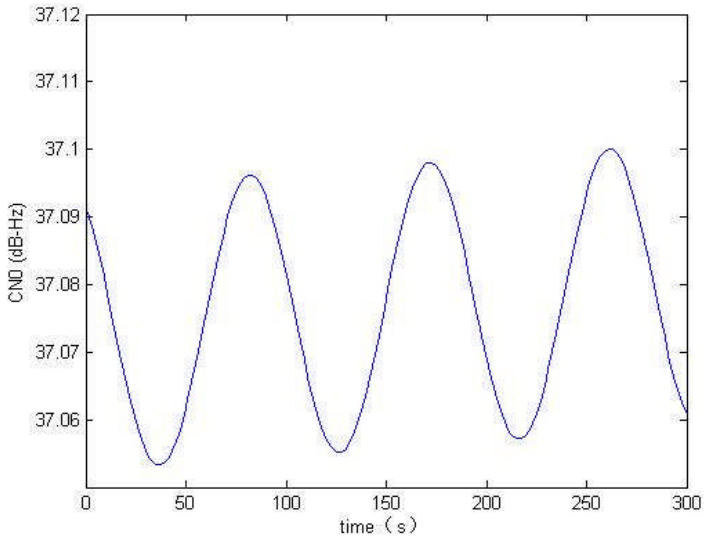

Figure 9-9 Prn.14 SNR (TORNADO turn &descend phase)

Figure 9-10 shows the received Prn.18 signal SNR during turn and descend phase.

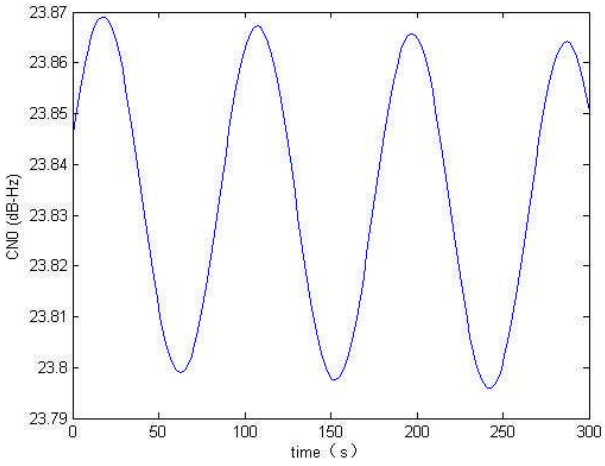

Figure 9-10 Prn.18 SNR (TORNADO turn &descend phase)

According to the SNR integrity alert flag threshold in chapter 9.3.3, the Prn.14 and Prn.18 SNR integrity alert flag during the landing phase are shown in Figure 9-3. “0” means the flag has not been generated.”1” means the flag is generated.

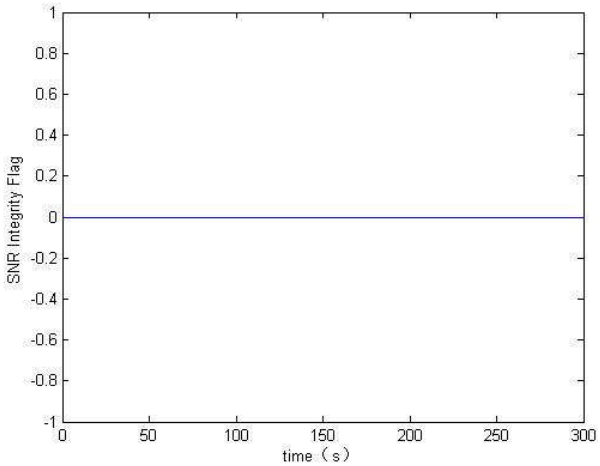

Figure 9-11 Prn.14 SNR integrity alert flag (TORNADO turn &descend phase)

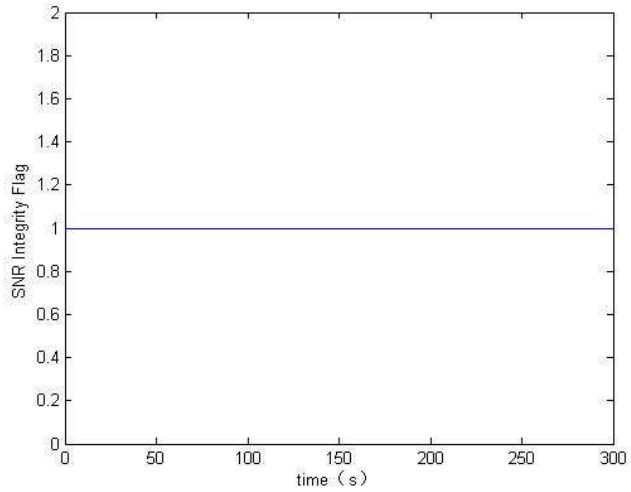

Figure 9-12 Prn.18 SNR integrity alert flag (TORNADO turn &descend phase)

9.4 Multipath Integrity Flag

9.4.1 Multipath Phase Error

According to the previous research on multipath, the total received signal is consisted of direct signal and reflected signals from each path. The total received signal as [31]:

$$R(t) = A \times \exp\big(j(wt - w\tau + \phi)\big) + \sum_{k=1}^{N} A_k \times \exp(j(wt - w\tau_k + \phi + \phi_k)) \quad \textbf{(9-15)}$$

Where the sum R(t) is received signal, and A and A_k are the amplitudes of the direct signal and the reflection signal from each path k. τ and τ_k are the corresponding time delay; ϕ_k is the phase error brought in by the reflection signal coming from path k.

Considering about all reflection path, an extra multipath phase error is given by[31]:

$$\delta\phi = \arctan\left(\frac{\sum_{k=1}^{N}\frac{A_k}{A}\sin(w\tau_k + \phi_k)}{1 + \sum_{k=1}^{N}\frac{A_k}{A}\sin(w\tau_k + \phi_k)}\right) \quad \textbf{(9-16)}$$

Usually $A_k/A<<1$ for all k, the equation then can be expanded as:

$$\delta\phi = \sum_{k=1}^{N}\frac{Ak}{A}\sin(w\tau_k + \phi_k) \quad \textbf{(9-17)}$$

From the previous research the multipath signal power A_k and the time delay τ_k can be generated. So in our research the multipath phase error can be generated and it will work out by comparing with the alert and warning threshold of phase error when the multipath integrity flag is being generated. It will be introduced in the following chapter 9.4.3.

9.4.2 Phase Lock Loop

According to the research on the phase tracing technology in chapter 8.5.1. The phase lock loop performance can be generated by equation (8-2).

Fig 9-13 shows the phase lock loop performance. [32] The performance is compared to that of the theoretical performance. Note that the at low signal-to-noise ratio (below 23 dB-Hz C/N_0) the loop broke lock. When the tracking phase error is over 0.1 cycles, it may cause the loss of lock. This error will be used as a threshold when generate the multipath integrity flag.

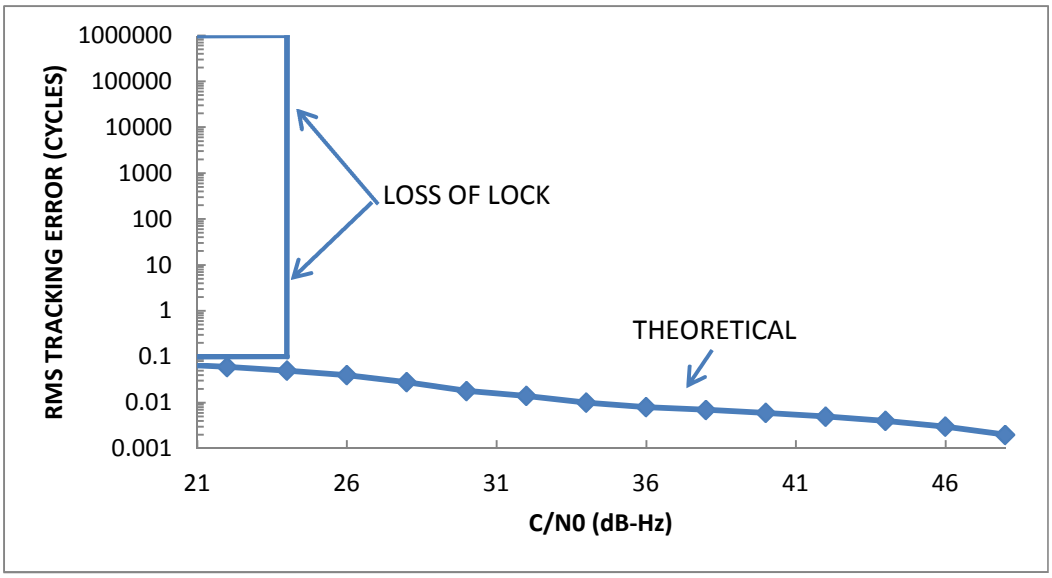

Figure 9-13 Typical phase lock loop performance [32]

9.4.3 Multipath integrity flag

According to the analysis in phase tracking, the Multipath integrity flag should be generated when [2, 5]:

When the multipath phase error exceeds 0.04 cycles or the PLL error (equation 8-2) exceeds 0.04 cycles, the integrity flag should be generated to provide the alert signal. And the time to alert is 1 second.

When the phase error exceeds 0.1 cycles, the integrity flag should be generated to provide the warning signal to pilot or other system that the GNSS signal tracking is failed.

Notice that the multipath integrity flag is for a certain satellite signal instead of the whole system. So it will work as a sub integrity flag.

Figure 9-14 shows the Prn.14 satellite signal PLL tracking error during turn and descend phase in GPS constellation.

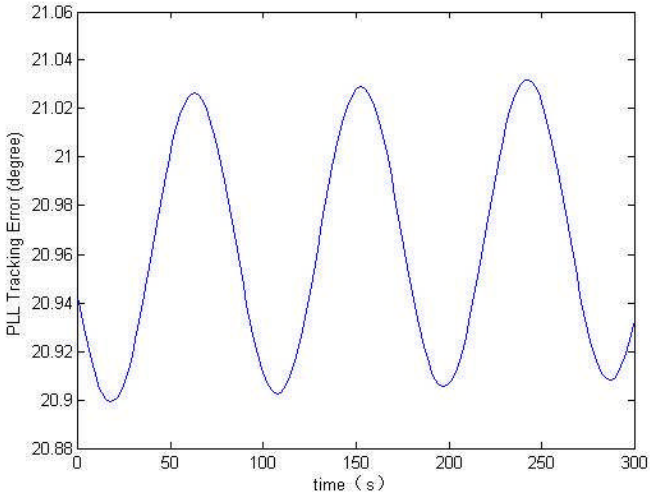

Figure 9-14 Prn.14 PLL Tracking Error (TORNADO turn &descend phase)

Figure 9-15 shows the Prn.14 satellite signal multipath phase error during turn and descend phase in GPS constellation.

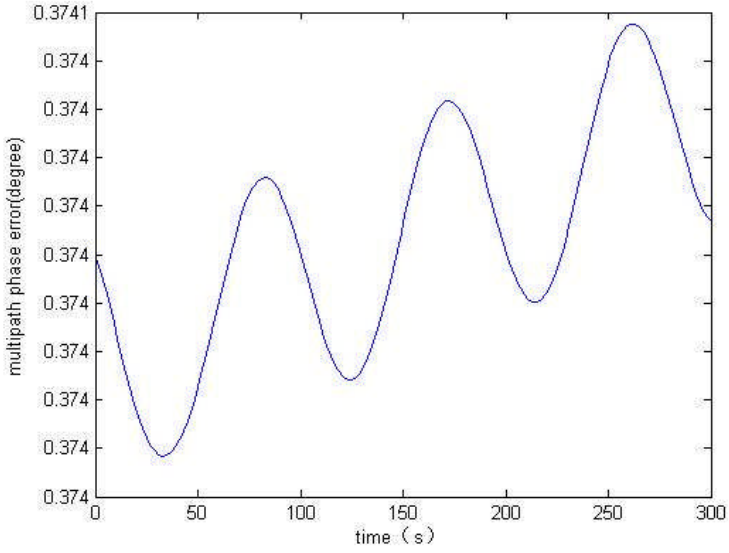

Figure 9-15 Prn.14 multipath phase error (TORNADO turn &descend phase)

According to the Multipath integrity alert flag threshold in chapter 9.1.3, the Prn.14 multipath integrity alert flag during the turn and descend phase is shown

in Figure 9-16. “0” means the flag has not been generated.”1” means the flag is generated.

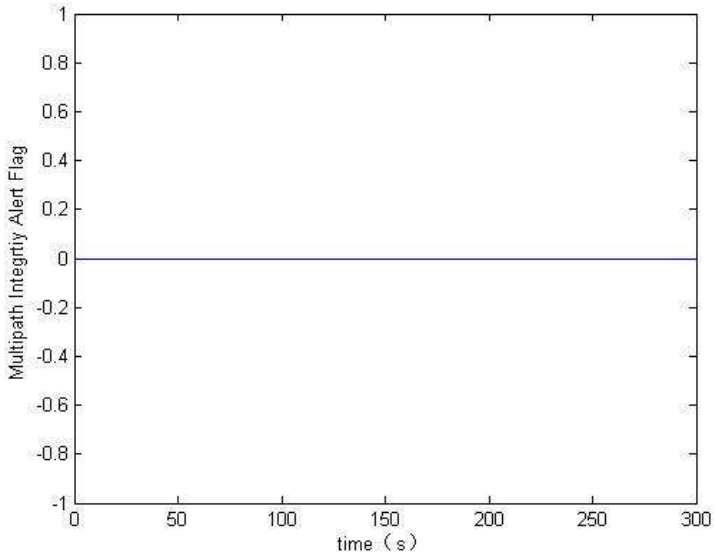

Figure 9-16 Prn.14 multipath integrity alert flag (TORNADO turn&descend phase)

9.5 Doppler Shift Integrity Flag

9.5.1 Frequency tracking

As we discussed in the previous chapter, the Doppler shift leads to the frequency shift and this may lead to the loss of carrier tracking. So in our research the GNSS receiver carrier tracking technology will be used to generate the Doppler shift integrity flag.

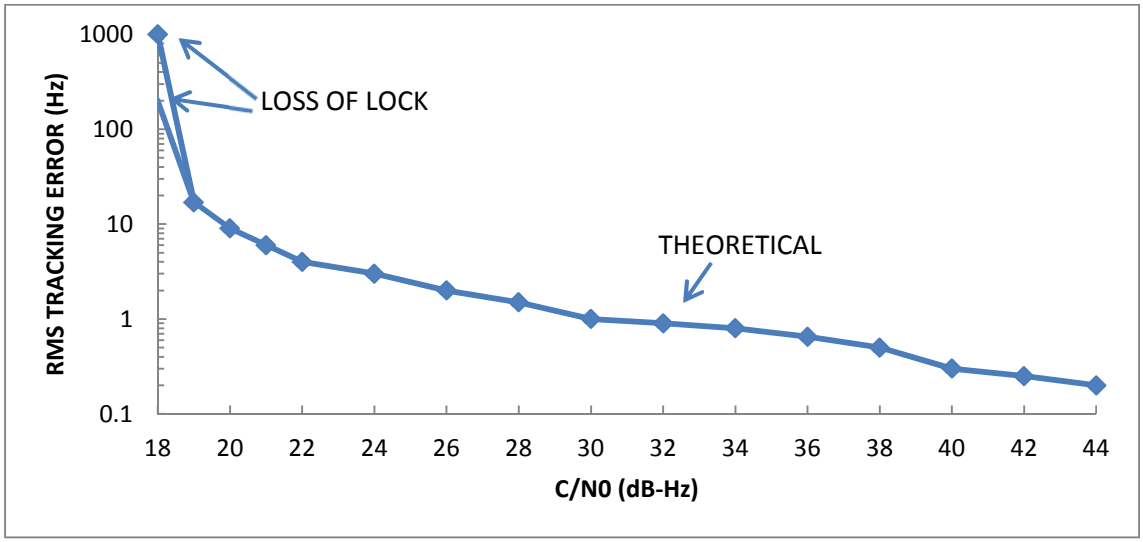

Figure 9-17 Medium bandwidth automatic frequency loop performance [33]

Fig 9-17 shows typical frequency errors for a medium bandwidth frequency loop. [33] According to the research on the phase tracing technology in chapter 8.5.2. The frequency lock loop performance can be generated by equation (8-9). The performance is compared to that of the theoretical performance. Note that at low signal-to-noise ratio the loop broke lock. When the tracking frequency error exceeds 17Hz, it may cause the loss of lock. This will be work as a alert threshold for frequency error when generating the Doppler shift integrity flag.

9.5.2 False lock

False lock(25-Hz offset) is detected with a continuously failing parity, because data demodulation results in an apparent bit transition every 20ms.[34] False lock can also be detected by a discrepancy between carrier and code Doppler. It should be considered as a warning threshold comparing with the code Doppler frequency error while generating the Doppler shift integrity flag.

9.5.3 Doppler shift integrity flag

According to the analysis in frequency tracking and false lock, the Doppler shift integrity flag should be generated when [2, 5]:

When the frequency shift is above 17Hz or the FLL error exceeds a certain threshold (equation 8-9), the integrity flag should be generated to provide the alert signal. And the time to alert is 1 second.

When the frequency shift is above 25Hz, the integrity flag should be generated to provide the warning signal to pilot or other systems that the signal tracking is failed.

Notice that the Doppler Shift integrity flag is for a certain satellite signal instead of the whole system. So it will work as a sub integrity flag.

Figure 9-18 shows the PRN.14 satellite signal Doppler shift error during the turn and descend phase.

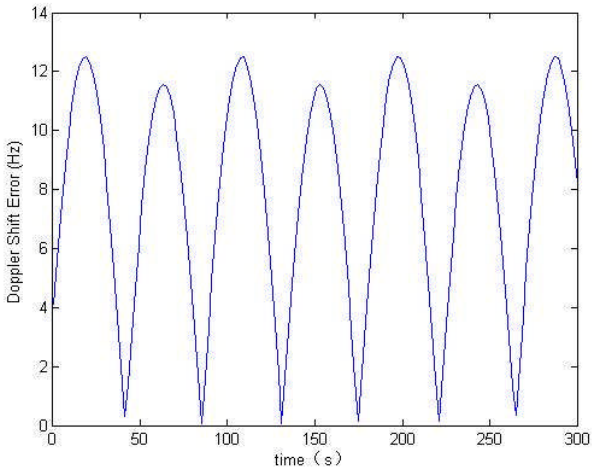

Figure 9-18 Prn.14 Doppler Shift error(TORNADO turn&descend phase)

According to the Doppler Shift integrity alert flag threshold in chapter 9.2.2, the Prn.14 Doppler Shift integrity alert flag during the turn and descend phase is shown in Figure 9-19. “0” means the flag has not been generated. ”1” means the flag is generated.

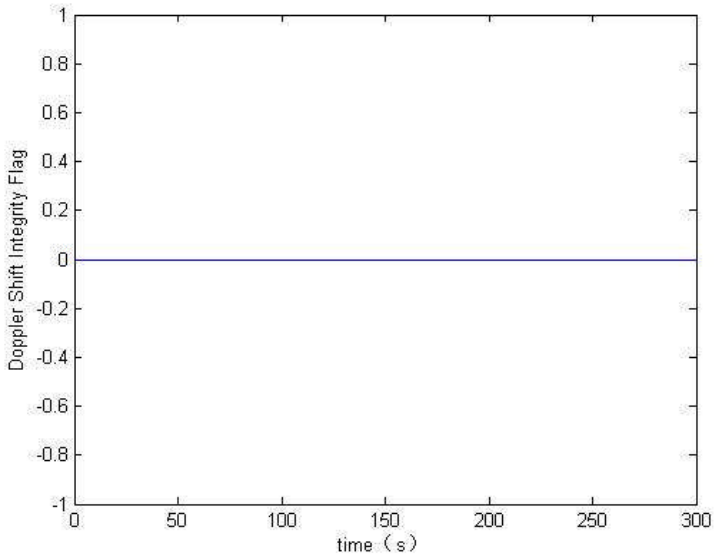

Figure 9-19 Prn.14 Doppler Shift integrity alert flag(TORNADO turn&descend phase)

10 INTEGRITY FLAG SIMULATION

The integrity flag simulation is done combined all the models discussed in the former chapters. All simulations are generated in several conditions and all the results are shown in this chapter.

First, there are two cases of aircraft: TORNADO and A320. The overall simulation time is 25 minutes. Two types of aircraft perform the same trajectory: climb flight phase (0~5min), cruise flight phase (5~10min), turn and descend flight phase (10~5min), cruise flight phase (15~20min) and landing flight phase(20~25min). The simulation will be performed using both cases so that the integrity flag simulation results can show the integrity flag application difference between the civil aircraft and military aircraft.

There are also three cases of satellite constellation: GPS only, GALILEO only and GPS combined GALILEO. The simulation will be performed in all three different constellations. Then some analysis about how the satellite constellation affects our integrity flag can be done after comparing the integrity flag simulation results in different constellation.

During 25 minutes simulation, the masking integrity flag, PDOP integrity flag, SNR integrity flag, Multipath integrity flag and Doppler Shift integrity flag will each be generated. The simulation result shows when the alert flag and warning flag will be generated and their duration.

As introduced in the former chapter 9, the SNR integrity flag, the multipath integrity flag and the Doppler Shift integrity flag is for a certain received satellite

signal. At last all these different sub-integrity flag should be combined together as the final integrity flag and this flag is the one will be used for the whole system we designed.

10.1 TORNADO Integrity Flag Simulation Results

Table 10-1 shows the TORNADO integrity flag simulation results in GPS constellation. It shows the time when the integrity flag is generated and the number of satellite signal which caused the generation of flag. And the "-" means the flag has not been generated.

Table 10-1 GPS Integrity flag simulation results (TORNADO)

Phase	1	2	3	4	5
Trajectory	Climb	Cruise	Turn& descend	Cruise	landing
Duration	5min	5min	5min	5min	5min
Satellites in view	16 Prn.1,3,6,7,9,11,12,13,14,15,22,23,26,27,30,31	16 Prn.1,3,6,7,9,11,12,13,14,15,22,23,26,27,30,31	16 Prn.1,3,6,7,9,11,12,13,14,15,22,23,26,27,30,31	16 Prn.1,3,6,7,9,11,12,13,14,15,22,23,26,27,30,31	16 Prn.1,3,6,7,9,11,12,13,14,15,22,23,26,27,30,31
Integrity alert flag	-	-	600~608s 672~ 698s 762~788s 852~878s	-	1484~1500s
Integrity warning flag	-	-	674s~692s 764~782s 854s~872s	-	1490~1500s
PDOP alert flag	-	-	-	-	1484~1500s
PDOP warning flag	-	-	-	-	1490~1500s

Table 10-1 GPS Integrity flag simulation results (TORNADO) (continued)

Phase	1	2	3	4	5
Trajectory	Climb	Cruise	Turn& descend	Cruise	landing
Duration	5min	5min	5min	5min	5min
Obscuration alert flag	0~300s Prn.30	300~600s Prn.30	Prn.3,6,11,12,13,14,15,22,23,26	900~1200s (Prn.30)	1200~1500s Prn.30
Obscuration warning flag	-	-	Prn.3,6,11,12,13,14,15,22,23,26	-	Prn.30 1210~1236s 1254~1500s
SNR alert flag	0~300s Prn.1,3,9,11,12,13,30	300~600s Prn.1,3,9,11,12,13,30	600~900s Prn.1,3,12,13,30	900~1200s Prn.1,3,9,11,12,13,30	1200~1500s Prn.1,3,9,11,12,13,30
SNR warning flag	0~300s Prn.1,3,11,12,13,30 0~50s Prn.9	300~600s Prn.1,3,11,12,13,30	600~900s Prn.1,3,12,13,30	900~1200s Prn.1,3,11,12,13,30	1200~1500s Prn.1,3,11,12,13,30
Multipath alert flag	0~300s Prn.1,3,7,9,11,12,13,30	300~600s Prn.1,3,7,9,11,12,13,30	600~900s Prn.1,3,7,9,11,12,13,30	900~1200s Prn.1,3,7,9,11,12,13,30	1200~1500s Prn.1,3,11,12,13,30
Multipath warning flag	0~300s Prn.1,3,7,9,11,12,13,30	300~600s Prn.1,3,7,9,11,12,13,30	600~900s Prn.1,3,7,9,11,12,13,30	900~1200s Prn.1,3,7,9,11,12,13,30	1200~1500s Prn.1,3,11,12,13,30
Doppler alert flag	0~300s Prn.1,3,7,9,11,12,13, 30	300~600s Prn.1,3,7,9,11,12,13,30	600~900s Prn.1,3,7,9,11,12,13,30	900~1200s Prn.1,3,7,9,11,12,13,30	1200~1500s Prn.1,3,11,12,13,30
Doppler warning flag	0~300s Prn.1,3,7,9,11,12,13,30	300~600s Prn.1,3,7,9,11,12,13,30	600~900s Prn.1,3,7,9,11,12,13,30	900~1200s Prn.1,3,7,9,11,12,13,30	1200~1500s Prn.1,3,11,12,13,30

Table 10-2 shows the details of the GPS obscuration integrity flag during turn and descend phase.

Table 10-2 GPS Obscuration Integrity flag simulation results (TORNADO)

Phase	3
Trajectory	Turn& descend
Duration	5 min
Obscuration alert flag	Prn.3 (634~666s, 724~756s, 812~846s, 898~900s) Prn.6 (644~666s, 734~756s, 824~846s) Prn.11 (634~676s, 724~766s, 814~856s) Prn.12 (644~672s, 734~762s, 824~852s) Prn.13 (600~604s, 674~694s, 764~784s, 854~874) Prn.14 (674~694s, 764~784s, 852~878s) Prn.15 (664~676s, 754~764s, 844~854s) Prn.22 (600-618s, 668~708s, 758~798s) Prn.23(600~624s, 670~704s, 760~804s, 850~894s) Prn.26(600~620s, 672~710s, 760~800s, 850~890s) Prn.30(630~676s, 718~766s, 808~856s, 892~900s) Prn.31 (672~690s, 762~780s, 852~870s)
Obscuration warning flag	Prn.3 (636~664s, 726~754s, 816~844s) Prn.6 (646~662s, 736~752s, 826~842s) Prn.11 (636~674s, 726~764s, 816~854s) Prn.12 (646~670s, 736~760s, 826~846s) Prn.13 (678~690s, 766~780s, 856~868) Prn.14 (676~694s, 762~786s, 850~882s) Prn.15 (666~678s, 752~766s, 842~856s) Prn.22 (602-616s, 670~706s, 760~798s) Prn.23(602~626s, 672~702s, 762~800s, 852~892s) Prn.26(602~622s, 672~710s, 762~798s,852~894s) Prn.30 (632~674s,720~764s,810~854s, 894~900s) Prn.31 (674~688s, 764~778s, 854~870s)

From Table 10-1 it is shown that there are 16 satellites in view in initial. They are Prn. 1, 3, 6, 7, 9, 11, 12, 13, 14, 15, 22, 23, 26, 27, 30, 31.Due to the

antenna masking ,fading ,multipath effect, Doppler Shift and GPS receiver tracking, some satellites lost during the fight. And at the same time the designed integrity flag is generated.

It is shown in Table 10-1 that during the simulation time 600s-608s, 672s-698s,762s-788s, 852-878s and 1484~1500s the integrity alert flag is generated. That means during these time the GNSS is going to fail if no actions are taken. Phase A1(600s-608s),phase B1(672s-698s), phase C1(762s-788s), phase D1(852-878s) and phase E1(1484~1500s) are defined as alert phases.

It is also shown in Table 10-1 that during the simulation time 674s~692s, 764~782s, 854s~872s and 1490~1500s the integrity warning flag is generated. That means during these time less than 4 received satellite signals are available for navigation. Correspondingly they are defined as phase B2(674s~692s), phase C2(672s-698s), phase D2(762s-788s) and phase E2(1484~1500s).

It is shown in the Table 10-1 the SNR integrity flag of satellite (Prn. 1, 3, 9, 11, 12, 13, 30) are generated through the whole simulation. That means these satellites signals are too weak for calculation due to the fading. The multipath and Doppler Shift integrity flag of satellite (Prn.1, 3, 7, 9,11,12,13,

30) are generated during the whole simulation. That means these satellite signals are failed to track. Mainly because these satellites tracking errors exceed the PLL/FLL integrity flag’s tracking threshold.

Note that phase A1, B1, B2, C1 and C2 are all contained in the turn and descend phase. The reason for that is during military aircraft flight phase, the

aircraft usually has big pitch angle and roll angle and instant change of status. This will cause the loss of satellite and the failure of signal tracking. It is illustrated in Table 10-2 which shows during turn and descend phase the generation of each satellite obscuration integrity flag. It shows clear at what time which satellite is going to lost or already lost.

Note that in A1 phase the integrity flag generates the alert signal, but in fact there are no such warning integrity flag generated later. That means it is a false alert. The integrity alert flag in B1and C1 both are generated 2s earlier than the integrity flag in B2 and C2. It satisfy the threshold of time to alert which is 1s.That means before the GNSS failed, the integrity flag gives sufficient time for the pilot.

From the Table 10-1 it is shown that the PDOP integrity flag is generated during the landing phase. The reason is that the horizontal and vertical errors exceed the PDOP integrity flag threshold during CAT-I, CAT-II and CAT-III. That is also the cause of integrity alert flag generation in phase D1 and integrity warning flag generation in phase D2. Also note that the integrity alert flag is generated 6s before the integrity warning flag. It is longer than the time to alert of the PDOP integrity flag threshold in Table 9-1, 9-2, 9-3 and 9-4.

Table 10-2 shows the TORNADO integrity flag simulation results in GALILEO constellation. It shows the time when the integrity flag is generated and the number of satellite signal which caused the generation of flag.. And the “-”

means the flag has not been generated and “NA” means not available in this simulation.

Table 10-3 GALILEO Integrity flag simulation results (TORNADO)

Phase	1	2	3	4	5
Trajectory	Climb	Cruise	Turn& descend	Cruise	landing
Duration	5min	5min	5min	5min	5min
Satellites in view	16 Prn.1,3,4,5,7,10,13,14,15,19,20,21,23,25,26,27	16 Prn.1,3,4,5,7,10,13,14,15,19,20,21,23,25,26,27	16 Prn.1,3,4,5,7,10,13,14,15,19,20,21,23,25,26,27	16 Prn.1,3,4,5,7,10,13,14,15,19,20,21,23,25,26,27	16 Prn.1,3,4,5,7,10,13,14,15,19,20,21,23,25,26,27
Integrity alert flag	-	-	600~616s 672~ 706s 762~796s 850~884s	-	-
Integrity warning flag	-	-	600s~608s 674~700s 764s~788s 852~878	-	-
PDOP alert flag	NA	NA	NA	NA	NA
PDOP warning flag	NA	NA	NA	NA	NA

Table 10-3 GALILEO Integrity flag simulation results (TORNADO) (continued)

Phase	1	2	3	4	5
Trajectory	Climb	Cruise	Turn& descend	Cruise	landing
Duration	5min	5min	5min	5min	5min
Obscuration alert flag	0~300s Prn.14	300~600s Prn.13,14	Prn.1,3,5,10,13,14,19,20,21,23,25,27	900~1200s Prn.13,14	1200~1500s Prn.13,14
Obscuration warning flag	-	-	Prn.3,5,10,13,14,19,20,21,23,25,27	-	-
SNR alert flag	0~300s Prn.1,7,10,14,15,20.21,23,26	300~600s Prn.1,7,10,14,15,20.21,23,26	600~900s Prn.1,7,10,14,15,20.21,23,26	900~1200s Prn.1,7,10,14,15,20.21,23,26	1200~1500s Prn.1,7,10,14,15,20.21,23,26
SNR warning flag	0~300s Prn.1,7,10,14,15,20.21,23,26	300~600 Prn.1,7,10,14,15,20.21,23,26	600~900s Prn.1,7,10,14,15,20.21,23,26	900~1200s Prn.1,7,10,14,15,20.21,23,26	1200~1500s Prn.1,7,10,14,15,20.21,23,26
Multipath alert flag	0~300s Prn.1,7,10,14,15,20.21,23,26	300~600s Prn.1,7,10,14,15,20.21,23,26,27	600~900s Prn.1,7,10,14,15,20.21,23,26	900~1200s Prn.1,7,10,14,15,20,21,23,26,27	1200~1500s Prn.1,7,10,14,15,20.21,23,26,27
Multipath warning flag	0~300s Prn.1,7,10,14,15,20.21,23,26	300~600s Prn.1,7,10,14,15,20.21,23,26,27	600~900s Prn.1,7,10,14,15,20.21,23,26	900~1200s Prn.1,7,10,14,15,20.21,23,26,27	1200~1500s Prn.1,7,10,14,15,20.21,23,26,27
Doppler alert flag	0~300s Prn.1,7,10,14,15,20.21,23,26	300~600s Prn.1,7,10,14,15,20.21,23,26,27	600~900s Prn.1,7,10,14,15,20.21,23,26	900~1200s Prn.1,7,10,14,15,20.21,23,26,27	1200~1500s Prn.1,7,10,14,15,20.21,23,26,27
Doppler warning flag	0~300s Prn.1,7,10,14,15,20.21,23,26	300~600s Prn.1,7,10,14,15,20.21,23,26,27	600~900s Prn.1,7,10,14,15,20.21,23,26	900~1200s Prn.1,7,10,14,15,20.21,23,26,27	1200~1500s Prn.1,7,10,14,15,20.21,23,26,27

Table 10-2 shows the details of the obscuration integrity flag during turn and descend phase.

Table 10-4 GALILEO Obscuration Integrity flag simulation results (TORNADO)

Phase	3
Trajectory	Turn& descend
Duration	5 min
Obscuration alert flag	Prn.1 (654~666s, 742~756s, 832~844s) Prn.3 (668~686s, 756~774s, 846~864s) Prn.5 (648~664s, 738~754s, 828~844s) Prn.10 (600~618s,672~708s,762~798s,852~888s) Prn.13 (600~624s,668~714s,758~804s,848~894s) Prn.14 (600~628s,670~716s,760~806s,850~896s) Prn.19 (600~618s,672~708s,762~798s,850~888s) Prn.20 (600~612s,672~700s,762~790s,852~880s) Prn.21(636~672s,726~760s,816~850s) Prn.23(600~622s, 668~712s, 758~802s, 848~892s) Prn.25(600~610s, 672~700s, 762~790s, 850~880s) Prn.27 (600~606s, 672~696s, 760~786,850~876s)
Obscuration warning flag	Prn.3 (672~680s, 752~770s, 852~860s) Prn.5 (654~656s, 744~746s, 834~846s) Prn.10 (602~616s,674~70s,764~800s,854~890s) Prn.13 (602~620s,670~710s,760~806s,850~892s) Prn.14 (602~626s,672~710s,762~804s,852~894s) Prn.19 (602~614s,674~700s,764~796s,852~886s) Prn.20 (602~610s,674~698s,764~788s,854~876s) Prn.21(638~670s,728~758s,820~848s) Prn.23(602~620s, 670~710s, 760~800s, 850~890s) Prn.25(602~608s, 674~698s, 764~788s, 852~878s) Prn.27 (602~604s, 674~694s, 762~784,852~874s)

Table 10-4 shows the similar results in GALILEO constellation with the results in GPS constellation. The integrity alert flag and integrity warning flag both are generated during the turn and descend flight phase. The duration times of the

flag are longer. As introduced before, the GALILEO constellation is WALKER Constellation. Due to lack of GALILEO ephemeris data the PDOP integrity flag cannot be generated.

Table 10-3 shows the TORNADO integrity flag simulation results in GPS combined GALILEO constellation. It shows the time when the integrity flag is generated. Each of sub-the integrity flag for each satellite as SNR integrity flag is already shown in Table 10-1,10-2,10-3 and 10-4. And the "-" means the flag has not been generated.

Table 10-5 GPS&GALILEO Integrity flag simulation results (TORNADO)

Phase	1	2	3	4	5
Trajectory	Climb	Cruise	Turn& descend	Cruise	landing
Duration	5min	5min	5min	5min	5min
Integrity alert flag	-	-	600~608 672~698 762~788s 852~878s	-	1484~1500s
Integrity warning flag	-	-	674s~692s 764~782s 854~872s	-	1490~1500s

Table 10-5 shows that in GPS combined with GALILEO constellation the Integrity alert flag is generated in turn and descend phase and landing phase. Comparing this result with GPS only and GALILEO only simulation, the duration of the integrity alert flag and integrity warning flag are shorter. It illustrates that the aircraft using GPS combined with GALILEO navigation system has better performance in safety.

10.2 A320 Integrity Flag Simulation Results

Table 10-6 shows the A320 integrity flag simulation results in GPS constellation. It shows the time when the integrity flag is generated. And the “-” means the flag has not been generated.

Table 10-6 GPS Integrity flag simulation results (A320)

Phase	1	2	3	4	5
Trajectory	Climb	Cruise	Turn& descend	Cruise	landing
Duration	5min	5min	5min	5min	5min
Satellites in view	16 Prn.1,3,6,7,9,11,12,13,14,15,22,23,26,27,30,31	16 Prn.1,3,6,7,9,11,12,13,14,15,22,23,26,27,30,31	16 Prn.1,3,6,7,9,11,12,13,14,15,22,23,26,27,30,31	16 Prn.1,3,6,7,9,11,12,13,14,15,22,23,26,27,30,31	16 Prn.1,3,6,7,9,11,12,13,14,15,22,23,26,27,30,31
Integrity alert flag	-	-	-	-	1484~1500s
Integrity warning flag	-	-	-	-	1492~1500s
PDOP alert flag	-	-	-	-	1484~1500s
PDOP warning flag	-	-	-	-	1492~1500s
Obscuration alert flag	0~300s Prn.30	300~600s Prn.30	Prn.1,11,12,22,23,26,30	900~1200s Prn.30	1200~1500s Prn.30
Obscuration warning flag	-	-	Prn.11,12,22,23,26,30	-	Prn.30 1216~1244s 1292~1306s

Table 10-6 GPS Integrity flag simulation results (A320) (continued)

Phase	1	2	3	4	5
Trajectory	Climb	Cruise	Turn& descend	Cruise	landing
Duration	5min	5min	5min	5min	5min
SNR alert flag	0~300s Prn.1,3,9,11,12,13,30	300~600s Prn.1,3,9,11,12,13,30	600~900s Prn.1,3,9,11,12,13,30	900~1200s Prn.1,3,9,11,12,13,30	1200~1500s Prn.1,3,9,11,12,13,30
SNR warning flag	0~300s Prn.1,3,12,13,30	300~600s Prn.1,3, 12,13,30	600~900s Prn.1,3,12, 13,30	900~1200s Prn.1,3, 12,13,30	1200~1500s Prn.1,3, 12,13,30
Multipath alert flag	0~300s Prn.1,3,7,9, 11,12,13, 30	300~600s Prn.1,3,7,9, 11,12,13, 30	600~900s Prn.1,3,7,9,11,12,13,30	900~1200s Prn.1,3,7,9,11,12,13, 30	1200~1500s Prn.1,3,7,9, 11,12,13, 30
Multipath warning flag	0~300s Prn.1,3,7,9, 11,12,13, 30	300~600s Prn.1,3,7,9, 11,12,13, 30	600~900s Prn.1,3,7,9,11,12,13,30	900~1200s Prn.1,3,7,9,11,12,13, 30	1200~1500s Prn.1,3,7,9, 11,12,13, 30
Doppler alert flag	0~300s Prn.1,3,7,9, 11,12,13, 30	300~600s Prn.1,3,7,9, 11,12,13, 30	600~900s Prn.1,3,7,9,11,12,13,30	900~1200s Prn.1,3,7,9,11,12,13, 30	1200~1500s Prn.1,3,7,9, 11,12,13, 30
Doppler warning flag	0~300s Prn.1,3,7,9, 11,12,13, 30	300~600s Prn.1,3,7,9, 11,12,13, 30	600~900s Prn.1,3,7,9,11,12,13,30	900~1200s Prn.1,3,7,9,11,12,13, 30	1200~1500s Prn.1,3,7,9, 11,12,13, 30

Table 10-7 shows the details of the GPS obscuration integrity flag during A320 turn and descend phase.

Table 10-7 GPS Obscuration Integrity flag simulation results (A320)

Phase	3
Trajectory	Turn& descend
Duration	5 min
Obscuration alert flag	Prn.1 (704~764s) Prn.11 (700~812) Prn.12 (750~774s) Prn.22(600~648s, 794~894s) Prn.23(600~662s,798~900s) Prn.26 (600~646s, 806~896s) Prn.30 (676~814s)
Obscuration warning flag	Prn.11 (704~802) Prn.22(600~638s, 800~886s) Prn.23(600~654s,608~900s) Prn.26 (600~636s, 816~884s) Prn.30 (684~806s)

Table 10-6 shows that the A320 integrity flag is only generated in landing phase because of the PDOP integrity flag. The reason is the same with the simulation on TORNADO.

During turn and descend phase, the integrity flag is not generated. The reason is that A320 has lower bank angle during the turn and descend phae. There are fewer satellites lost due to the masking during the turn and descend phase. This can be seen in Table 10-7. The number of obscuration alert flag and obscuration warning flag are fewer than those in Table 10-2. And the duration of each flag is much shorter.

Table 10-5 shows the A320 integrity flag simulation results in GALILEO constellation. The “-” means the flag has not been generated and “NA” means not available in this simulation.

Table 10-8 GALILEO Integrity flag simulation results (A320)

Phase	1	2	3	4	5
Trajectory	Climb	Cruise	Turn& descend	Cruise	landing
Duration	5min	5min	5min	5min	5min
Satellites in view	16 Prn.1,3,4,5,7,10,13,14,15,19,20,21,23,25,26,27	16 Prn.1,3,4,5,7,10,13,14,15,19,20,21,23,25,26,27	16 Prn.1,3,4,5,7,10,13,14,15,19,20,21,23,25,26,27	16 Prn.1,3,4,5,7,10,13,14,15,19,20,21,23,25,26,27	16 Prn.1,3,4,5,7,10,13,14,15,19,20,21,23,25,26,27
Integrity alert flag	-	-	0~30s 218~278s	-	NA
Integrity warning flag	-	-	-	-	NA
PDOP alert flag	NA	NA	NA	NA	NA
PDOP warning flag	NA	NA	NA	NA	NA
Obscuration alert flag	0~300s Prn.14	300~600s Prn.13,14	Prn.10,13,14,19,21,23,25	900~1200s Prn.13,14	1200~1500s Prn.13,14
Obscuration warning flag	-	-	Prn.10,13,14,19,21,23,25	-	-
SNR alert flag	0~300s Prn.1,7,10,14,15,20.21,23,26	300~600s Prn.1,7,10,14,15,20.21,23,26	600~900s Prn.1,7,10,14,15,20.21,23,26	900~1200s Prn.1,7,10,14,15,20.21,23,26	1200~1500s Prn.1,7,10,14,15,20.21,23,26
SNR warning flag	0~300s Prn.1,7,10,14,15,20.21,23,26	300~600 Prn.1,7,10,14,15,20.21,23,26	600~900s Prn.1,7,10,14,15,20.21,23,26	900~1200s Prn.1,7,10,14,15,20.21,23,26	1200~1500s Prn.1,7,10,14,15,20.21,23,26

Table 10-8 GALILEO Integrity flag simulation results (A320) (continued)

Phase	1	2	3	4	5
Trajectory	Climb	Cruise	Turn& descend	Cruise	landing
Duration	5min	5min	5min	5min	5min
Multipath alert flag	0~300s Prn.1,7,10, 14,15,20.2 1,23,26	300~600s Prn.1,7,10, 14,15,20.2 1,23,26,27	600~900s Prn.1,7,10, 14,15,20.2 1,23,26	900~1200s Prn.1,7,10, 14,15,20,2 1,23,26,27	1200~1500s Prn.1,7,10,1 4,15,20.21,2 3,26,27
Multipath warning flag	0~300s Prn.1,7,10, 14,15,20.2 1,23,26	300~600s Prn.1,7,10, 14,15,20.2 1,23,26,27	600~900s Prn.1,7,10, 14,15,20.2 1,23,26	900~1200s Prn.1,7,10, 14,15,20.2 1,23,26,27	1200~1500s Prn.1,7,10,1 4,15,20.21,2 3,26,27
Doppler alert flag	0~300s Prn.1,7,10, 14,15,20.2 1,23,26	300~600s Prn.1,7,10, 14,15,20.2 1,23,26,27	600~900s Prn.1,7,10, 14,15,20.2 1,23,26	900~1200s Prn.1,7,10, 14,15,20.2 1,23,26,27	1200~1500s Prn.1,7,10,1 4,15,20.21,2 3,26,27
Doppler warning flag	0~300s Prn.1,7,10, 14,15,20.2 1,23,26	300~600s Prn.1,7,10, 14,15,20.2 1,23,26,27	600~900s Prn.1,7,10, 14,15,20.2 1,23,26	900~1200s Prn.1,7,10, 14,15,20.2 1,23,26,27	1200~1500s Prn.1,7,10,1 4,15,20.21,2 3,26,27

Table 10-7 shows the details of the GALILEO obscuration integrity flag during A320 turn and descend phase.

Table 10-9 GALILEO Obscuration Integrity flag simulation results (A320)

Phase	3
Trajectory	Turn& descend
Duration	5 min
Obscuration alert flag	Prn.10 (600~640s,810~888s) Prn.13 (600~664s,790~900s) Prn.14 (600~680s,788~900s) Prn.19(808~892s, 794~894s) Prn.21(714~786s) Prn.23 (600~658s, 792~900s) Prn.25 (830~844s)

Table 10-9 GALILEO Obscuration Integrity flag simulation results (A320)

Phase	3
Trajectory	Turn& descend
Duration	5 min
Obscuration warning flag	Prn.10 (600~628s,822~874s) Prn.13 (600~654s,798~900s) Prn.14 (600~668s,796~900s) Prn.19(818~886s, 818~898s) Prn.21(724~780s) Prn.23 (610~656s, 798~900s) Prn.25 (836~840s)

Table 10-8 shows the similar results in GALILEO constellation with the results in GPS constellation. The only difference is that between 0~30s and 218~278s the integrity alert flag are generated. But there are no integrity warning flag generated after. That means these alert signals are false alert.

Table 10-10 shows the A320 integrity flag simulation results in GPS combined with GALILEO constellation. It shows the time when the integrity flag is generated. Each of sub-the integrity flag for each satellite as SNR integrity flag is already shown in Table 10-6,10-7,10-8 and 10-9. And the “-” means the flag has not been generated.

Table 10-10 GPS&GALILEO Integrity flag simulation results (A320)

Phase	1	2	3	4	5
Trajectory	Climb	Cruise	Turn& descend	Cruise	landing
Duration	5min	5min	5min	5min	5min
Integrity alert flag	-	-	-	-	1484~1500s
Integrity warning flag	-	-	-	-	1492~1500s

Table 10-10 shows that in GPS combined with GALILEO constellation, the integrity flag is generated only in landing phase. It is the same result as in GPS only simulation. But the fact in reality may be different because in this research the GALILEO constellation model use WALKER constellation, it fails to calculate the PDOP. In other way, the GALILEO navigation system may improve the performance to avoid the integrity flag in landing phase in reality.

11 CONCLUSION

1. This research project contributed to the design of an avionics based integrity augmentation system for GNSS applications. This system is capable of generating integrity flag to provide the alert signal and warning signal to the pilot when GNSS critical safety situation occurs.

2. According to the simulation results, after the integrity alert flag is generated, the time to alert this thesis brought up is sufficient for the pilot before the integrity warning flag is generated.

3. The integrity flag generator is simulated in different constellation as GPS only, GALILEO only and GPS combined with GALILEO. In this research the GPS constellation simulation makes use of the real ephemeris data while GALILEO constellation simulation uses WALKER constellation model.

4. In this research the integrity flag generator is simulated on both military aircraft (TORNADO) and civil aircraft (A320). In both cases a series flight phase(taxi, climb, cruise, turn and descend and landing) are simulated using real data. The integrity flag can be generated when the satellite loss caused by aircraft obscuration and manoeuvre occurs.

5. In this research the PDOP model is simulated. The integrity flag can be generated when the horizontal error or vertical error exceeds the threshold.

6. In this research the multipath model is simulated. The integrity flag can be generated when multipath effect causes the failure of tracking GNSS signal.

7. In this research the SNR model is simulated. The integrity flag can be generated when fading effect causes the failure of tracking GNSS signal.

8. In this research the Doppler Shift model is simulated. The integrity flag can be generated when Doppler Shift effect causes the failure of tracking GNSS signal.

9. In this research the integrity flag is generated when the GNSS receiver PLL and FLL tracking error exceeds the threshold.

12 FUTURE WORK

1. Improve the GNSS constellation simulator with adding the GLONASS constellation simulator.
2. Improve the integrity flag generator because the GLONASS receiver technology is different from the GPS and GALILEO.
3. Improve the flight dynamic model to 6DOF. Also take more types of aircraft into consideration as a platform for the ABAS.
4. Use database technology to deal with the masking data shown in Figure 8-1,8-2, 8-3 and 8-4. Using the integrity flag combined with the instant aircraft status data such as pitch angle and roll angle can alert the pilot to avoid the procedure may cause loss of satellites.
5. Investigate the possibility of using high integrity software (e.g., ADA) for the design and development of the GNSS ABAS system.

REFERENCES

[1] R. Sabatini. “Differential Global Positioning System (DGPS) for Flight Testing”. NATO Research and Technology Organization (RTO) – Systems Concepts and Integration Panel (SCI). AGARDograph Series RTO-AG-160 Volume 21. Oct 2008.

[2] R. Sabatini. “A Novel Avionics Based Integrity Augmentation System – A Research Tutorial”. Cranfield University – Dept. of Aerospace Engineering (Lecture Notes), 2012

[3] B.W. Parkinson and J.J. Spilker Jr. “Global Positioning System: Theory and Applications”. Volume I. Progress in Astronautics and Aeronautics, Vol. 163.AIAA,1996 page121-176.

[4] Alexander Steingass. “The High Resolution Aeronautical Multipath Navigation Channel”. German Aerospace Center DLR, 2004

[5] R. Sabatini, T. Moore and C. Hill. “A Novel Avionics Based GNSS Integrity Augmentation System for Manned and Unmanned Aerial Vehicles.” Paper accepted for presentation at the European Navigation Conference 2012, held in Gdansk (Poland). 2012.

[6] AIRCRAFT DRAWINGS. “www.aircraftdrawindsdownload.com”.

[7] TORNADO WIKIPEDIA. “Http://en.wikipedia.org/wiki/Tornado_fighter ”.

[8] AIRBUS. “AIRBUS 320 WEIGHT AND BALANCE MANUAL”

[9] B.L. Stevens and F. L. Lewis. “Aircraft Control and Simulation”. Toronto: John Wiley& Sons,1992.

[10] Charles S. Carrano. “Impacts of the December 2006 solar radio bursts on the performance of GPS”. 2009 Boston College, Institute for Scientific Research, Chestnut Hill, Massachusetts, USA. RADIO SCIENCE, VOL. 44, RS0A25, 12 PP, 2009.

[11] B.W. Parkinson and J.J. Spilker Jr. “Global Positioning System: Theory and Applications”. Volume I. Progress in Astronautics and Aeronautics, Vol. 163.AIAA,1996, pp. 478-480.

[12] Anon. “GP1010 Global Positioning Receiver Front End.” Gec Plessey Semiconductors Data Sheet DS3076-2.4, Oct.1992

[13] Anon. Sensor Systems GPS Antennas Data Sheet, Dec. 1992.

[14] B.W. Parkinson and J.J. Spilker Jr. “Global Positioning System: Theory and Applications”. Volume I. Progress in Astronautics and Aeronautics, Vol. 163.AIAA, 1996, pp. 485-584.

[15] Boithias l. “Radio Wave Propagation”. McGraw Hill, New York, 1982

[16] B.W. Parkinson and J.J. Spilker Jr. “Global Positioning System: Theory and Applications”. Volume I. Progress in Astronautics and Aeronautics, Vol. 163.AIAA,1996, pp. 517-523.

[17] B.W. Parkinson and J.J. Spilker Jr. “Global Positioning System: Theory and Applications”. Volume I. Progress in Astronautics and Aeronautics, Vol. 163.AIAA,1996, pp. 344.

[18] Phillip Martin Corbell. “Design and validation of an accurate GPS signal and receiver truth model for comparing advanced receivers processing techniques”. Master’s thesis, March 2000.

[19] Alexander Steingass. “The High Resolution Aeronautical Multipath Navigation Channel”. German Aerospace Center DLR, 2007

[20] Michael S.Braasch. “On the characterization of multipath errors in satellite-based precision approach and landing systems”. College of Engineering and Technology, Ohio University, June 1992

[21] Cyril-Daniel Iskander . “A MATLABR -based Object-Oriented Approach to Multipath Fading Channel Simulation ” . Cyril-Daniel Iskander 7945 Avenue de Cornouailles, Quebec, QC, Canada, G1H 3V9, 2006

[22] B.W. Parkinson and J.J. Spilker Jr. “Global Positioning System: Theory and Applications”. Volume I. Progress in Astronautics and Aeronautics, Vol. 163.AIAA,1996, pp. 411

[23] Phillip W. Ward. John W. Betz and Christopher J. Hegarty. “Understanding GPS principles and application 2nd Edition”. 2004, pp. 153-200.

[24] Ward, P. “Using a GPS Receiver Monte Carlo Simulator to Predict RF Interference Performance”. Proc. of 10th International Technical Meeting

of The Satellite Division of The Institute of Navigation, Kansas City, MO, September 1997, pp.1473–1482.

[25] Fuchser, T. D. “Oscillator Stability for Carrier Phase Lock”. Internal Memorandum G(S)-60233, Texas Instruments Incorporated, February 6, 1976.

[26] B.W. Parkinson and J.J. Spilker Jr. Global Positioning System: Theory and Applications Volume I. Progress in Astronautics and Aeronautics, Vol. 163.AIAA,1996, pp. 469-477

[27] Annex 10 to the Convention on International Civil Aviation. “Aeronautical Telecommunications”. Volume 1 Radio Navigation Aids. ICAO

[28] UK CAA PAPER. “GPS Integrity and Potential Impact on Aviation Safety”. CAA, 2003

[29] B.W. Parkinson and J.J. Spilker Jr. “Global Positioning System: Theory and Applications”. Volume I. Progress in Astronautics and Aeronautics, Vol. 163.AIAA,1996, pp. 390

[30] Phillip Martin Corbell. “Design And Validation of an Accurate GPS Signal and Receiver Truth Model for Comparing Advanced Receiver Processing Techniques” Second Lieutenant, United States Air Force. March, 2000

[31] Sung H. Byun, George A. Hajj, and Lawrence E. Young. “Development and Application of GPS Signal Multipath Simulator” Jet Propulsion Laboratory, California Institute of Technology, Pasadena, California, USA, 2000

[32] B.W. Parkinson and J.J. Spilker Jr. “Global Positioning System: Theory and Applications”. Volume I. Progress in Astronautics and Aeronautics, Vol. 163.AIAA,1996, pp. 389

[33] B.W. Parkinson and J.J. Spilker Jr. “Global Positioning System: Theory and Applications”. Volume I. Progress in Astronautics and Aeronautics, Vol. 163.AIAA,1996, pp. 382

[34] B.W. Parkinson and J.J. Spilker Jr. “Global Positioning System: Theory and Applications”. Volume I. Progress in Astronautics and Aeronautics, Vol. 163.AIAA,1996, pp. 392